N° d'ordre 2007-XXX, Année 2007

Thèse

ACTIVE CONTROL AND SENSOR NOISE FILTERING DUALITY APPLICATION TO ADVANCED LIGO SUSPENSIONS

présentée devant
L'Institut National des Sciences Appliquées de Lyon

pour obtenir
le grade de docteur

Ecole doctorale : MEGA

Spécialité : Génie Mécanique

par

Laurent RUET

Soutenue le 11 Janvier 2007 devant la Commission d'examen :

Professeur Willy CHARON	Rapporteur	L3M, UTBM, Belfort
Docteur HDR Johan DER HAGOPIAN	Co-Directeur de thèse	LAMCOS-DCS, INSA de Lyon
Professeur Régis DUFOUR	Examinateur	LAMCOS-DCS,INSA de Lyon
Professeur Luc GAUDILLER	Co-Directeur de thèse	LAMCOS-DCS, INSA de Lyon
Professeur Jean-Claude GOLINVAL	Rapporteur	LTAS-VIS, Univ Liège, Belgique
Docteur HDR Jean-Marie MACKOWSKI	Examinateur	LMA, Université Lyon I
Docteur Richard MITTLEMAN	Examinateur	MIT Boston USA, LIGO Project

**Cette thèse a été préparée au LAboratoire de Mécanique des COntacts et des Structures (LAMCOS) – Equipe DCS (Dynamique et Contrôle des Structures)
UMR CNRS 5514 - INSA de Lyon**

ACKNOWLEDGMENTS

I would first of all like to thank my MIT supervisors Richard Mittleman and David Ottaway for the patience, help and encouragement they have given me over the last three years. They helped me through difference of culture and language during all these years. I would also like to thank Myron McInnis and Ken Mason for the amazing help they have given me throughout my time to set up the experiments, most of the measurements and installations wouldn't have been possible without their patience and dedication.

My thanks also go to David Shoemaker, who enabled me to work in this laboratory, and gave me his support during these three years and every time my visit needed to be extended. I also want to thank Marie Woods and Danielle Noonan for their patience and help with the immigration process, the housing, the trips and all the things that made my visit here such a great experience.

I would also like to thanks the LIGO community and especially the suspension group. Many thanks to Calum Torrie, Norna Robertson, Janeen Romie, Mark Barton, Denis Coyne, jay Heefner for the hours they spent answering my emails and questions on the phone, or during the very nice visits I have made in their laboratory in Caltech or Stanford. The seismic group Joseph Giaime, Brian Lantz, Hua Wensheng also deserves big thanks for their help on related projects and advices all along these years.

Of course I have to mention The LASTI laboratory and all the people who provided me their help and support, thanks to Peter Fritschel and Gregg Harry to help me to understand LIGO and the noise issues better, thanks to Nergis Mavalvala and Thomas Corbitt for their help on the optical part of my experiment. And of course thanks to the Friday's beer crew and their weekly enthusiasm.

In France, I would like to thank Luc Gaudiller and Johan Der Hagopian who in spite of the distance gave me their support and help during these years. Regis Dufour and Riccardo Desalvo also deserve big thanks to help me to get in contact with LIGO MIT, I wouldn't write these lines if they hadn't support me during those first months.
On a personal front I would like to thank my Mum, Dad and My sister Caroline. They all supported me and encouraged me to come and stay here, in spite of the distance and the separation. They gave me so much through these years of studies, and who knows if I could have survived here without the tons of chocolate they sent me. I also want to thank all my friends here and the Boston's French community.

RESUME

Einstein a prévu l'existence des ondes gravitationnelles dans sa théorie de relativité générale de 1916. Ces ondes sont produites par l'accélération d'objets massifs dans l'espace tel que les étoiles à neutron, ou les trous noirs. Ces ondes étirent et compriment l'espace-temps et peuvent être détectées en mesurant la contrainte qu'elles produisent. Cependant, la contrainte discernable est extrêmement petite ; détecter des ondes gravitationnelles sur terre reviendrait à mesurer la variation de distance entre la terre et le soleil équivalente au diamètre d'un d'atome. Les détecteurs actuels essayent de détecter cette contrainte en utilisant les interféromètres optiques pour mesurer le mouvement relatif de quatre masses séparées de 4km. Pour atteindre une sensibilité si importante, il est nécessaire d'isoler les masses des sources de bruits telles que le bruit sismique.

Le détecteur avancé d'ondes gravitationnelles Américain, appelé Advanced LIGO, emploiera un système complexe se composant de trois étages de systèmes d'isolation sismique. Les deux premiers étages utilisent le contrôle actif de vibration pour réduire le bruit sismique aux plus basses fréquences. Le dernier étage est une suspension qui peut être soit un triple ou un quadruple pendule. La dernière masse de ces pendules est la masse test (miroir) dont la position est mesurée par l'interféromètre. Le rôle de ces pendules est de fournir le filtrage passif du bruit sismique et de limiter l'effet du bruit thermique. À 10 hertz, le déplacement de la masse test du pendule sera inférieur à $10^{-19} m/\sqrt{Hz}$, ce qui est environ 10000 fois moins que le diamètre d'un proton dans un atome.

Afin que le détecteur fonctionne correctement, la distance relative entre les miroirs doit être maintenue inférieure à $10^{-11} m$ sur la distance totale de 4km. Par conséquent, les résonances de corps rigide des pendules doivent être atténuées en utilisant les boucles d'avertissement actives numériques. Cependant, à ce niveau de sensibilité, le contrôle actif a un coût puisque le bruit de mesure n'est pas négligeable. Pour Advanced LIGO, le bruit de mesure sera jusqu'à 100 fois plus élevé que le bruit sismique à l'endroit où les suspensions sont attachées au système d'isolation sismique. Ce bruit de mesure sera traité dans la boucle d'avertissement et re-injecté dans le pendule, ajoutant du bruit dans les hautes fréquences.

Dans cette thèse, nous démontrerons qu'il est possible de concevoir des systèmes avancés de contrôle actif qui tirent profit de notre connaissance fine de la dynamique du pendule afin de réduire au minimum l'injection du bruit de mesure. Nous emploierons le contrôle modal indépendant pour atténuer chaque mode du pendule séparément et pour réduire la transmission de bruit de mesure. Nous couplerons ce contrôle modal à un observateur modal

qui peut être employé pour reconstruire les degrés de liberté que nous ne pouvons pas mesurer : ici l'état modal. Nous transformerons ensuite cet observateur en estimateur en filtrant les mesures bruitées.

Afin de valider nos modèles et simulations, la boucle de contrôle actif sera testée sur un triple pendule en fonctionnement. Pour mesurer le déplacement extrêmement petit de la dernière masse du pendule, nous emploierons un laser résonnant à l'intérieur d'une cavité optique constituée par deux triples pendules. Cette technique que nous avons proposé est souvent employée dans d'autres domaines de la physique mais rarement employée pour mesurer des vibrations mécaniques et s'avérera très efficace. Les résultats du modèle et les mesures seront comparés pour vérifier la validité de nos simulations et mettre en évidence les qualités de prédiction du contrôle modal et de la finesse du modèle.

ABSTRACT

Einstein, in his 1916 Theory of General Relativity, predicted the existence of gravitational waves. These waves are generated by the acceleration of massive objects in space such as neutron stars, or black holes. These waves stretch and compress space-time and can be detected by measuring the strain that is produced. However, the detectable strain is extremely small; detecting gravity waves on earth is as hard as measuring a variation of the distance between the earth and the sun of about one atom diameter. The current detectors attempt to detect this strain by using optical interferometers to sense the relative motion of four isolated test masses separated by 4km. To reach such an extraordinary sensitivity, it is necessary to isolate the test masses from noises sources such as the seismic noise.

The Advanced American GW detector, named Advanced LIGO, will use a complex system consisting of three stages of seismic isolation systems. The first two stages use active vibration control to reduce the seismic noise at lower frequencies. The last stage is a suspension that is made either of a triple or a quadruple pendulum. The last mass of these pendulums is the test mass whose position is sensed by the interferometer. The role of these pendulums is to provide passive filtering of the seismic noise as well as limiting the effect of thermal noise. At 10 Hz, the displacement of the test mass of the pendulum will be lower than $10^{-19} m/\sqrt{Hz}$, which is about 10^{-4} the diameter of a proton.

In order for the detector to function correctly, the relative distance between the test masses needs to be controlled to the $10^{-11} m$ level over 4km. Hence, the pendulum rigid-body resonances must be damped using digital active control loops. However, at that level of sensitivity, using active control has a cost since the sensor noise is not negligible. In advanced LIGO, the sensor noise is expected to be up to a 100 times higher than the seismic noise at the point where the suspension attaches to the active two stage seismic isolation system. This sensor noise will be processed in the control loop and re-injected into the pendulum, adding displacement noise at high frequencies.

In this thesis, we will demonstrate that it is possible to design advanced control loop topologies that take advantage of our good knowledge of the pendulum's dynamics in order to minimize the sensor noise injection. We will use Independent Modal State Control to damp each mode of the pendulum separately and reduce the sensor noise transmission. We will couple this modal control with a modal observer that can be used to reconstruct the states that we cannot measure. We will turn this observer into an estimator by helping the filtering of the noisy measurements.

In order to validate our models and simulations, the new control loop will be tested on a working triple pendulum. In order to measure the very small displacement of the test mass, we will use a laser beam resonating inside the optical cavity formed by two triple pendulums. This technique that we suggested is often used in other domains of physics but is rarely used to measure mechanical vibrations and will prove to be very effective. The results of the model and the measurements will be compared to check the validity of our simulations.

CONTENTS

LIST OF FIGURES

LIST OF TABLES

1 INTRODUCTION

1.1 ASTROPHYSICS BACKGROUND, THE NATURE AND SOURCES OF GRAVITATIONNAL WAVES

The existence of gravitational waves was first predicted by Einstein in 1916 [1] to provide a causal explanation to the gravitational force exerted by an accelerating mass. By expressing gravitational force with the wave equation, it ceases to act instantaneously, as suggested earlier by Newton, and instead travels at the speed of light.

In the 1960’s, a world-wide interest in detecting gravitational waves started as a results of the suggestion by Weber that they could be detected [2].

In 1993, Hulse & Taylor were awarded the Nobel Prize for their indirect observation of gravitational waves [3]. Through careful study of the orbital decay in a neutron star binary system, Hulse & Taylor found the decay rate to be in excellent agreement with the predicted energy lost to gravitational radiation.

Today there is a number of collaboration around the word working towards the challenging goal of the direct detection of gravitational waves. The detection of such waves is important for several reasons. First it will allow some of the predictions of General Relativity to be tested. Secondly, it will provide new information on astrophysical events in the universe, for example the collapse of stars or interactions of black holes. Because gravitational waves pass through most matter undisturbed, observing the waves enables to look directly at the source of the event, thereby opening a new field in astronomy.

1.1.1 The nature of gravitational waves

It is useful to compare gravitational waves to electromagnetic waves. While electromagnetic waves are produced by the acceleration of charges, gravitational waves are produced by the acceleration of mass.

Gravitational waves are differential planar strain waves, meaning that an object subjected to a gravitational wave is alternatingly stretched in one axis while compressed in the orthogonal axis (see figure below).There are both a plus, h+, and cross, hx, polarization.

The effect of the strain on a ring of test particles is shown in figure 1.1. If the wave is incident perpendicular to the plane of the page, the ring is stretched in one direction and compressed in the other

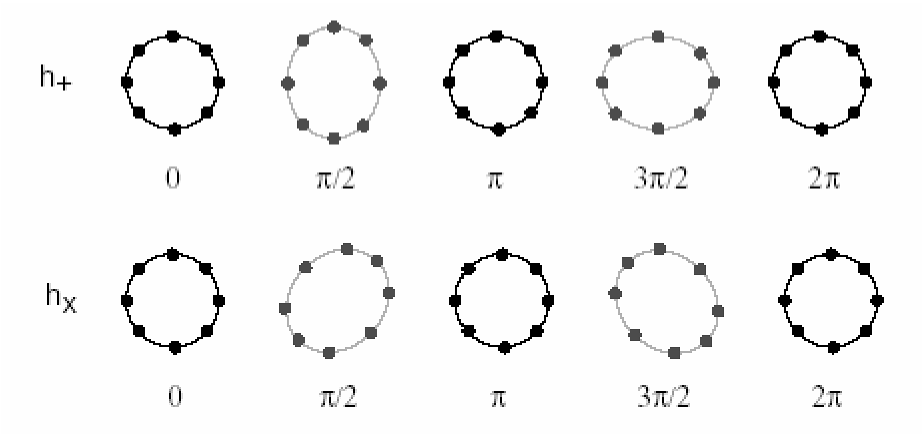

Figure 1.1: Effect of the strain on a ring of particles

The strain produced by a gravitational wave is tiny, for example, for a pair of orbiting objects, the strain is given by : $h \approx (r_{s1} r_{s2}) / (r_0 R)$.

Where r_{s1} and r_{s2} are the Schwarzschild radii of the masses involved $\left(r_s = 2GM / c^2\right)$ and r_0 is the separation of the two objects.

The variables are described below

- G is the gravitational constant
- R is the distance to the source
- M is the mass of each object
- c is the speed of light

The ratio of G^2 / c^4 is so small that the only measurable sources of gravitational waves are produced by masses on the order of at least a solar mass.

1.1.2 Gravitational Wave Sources

Advanced terrestrial gravitational waves detectors are expected to be sensitive to gravitational waves in the frequency range of a few tens of Hz to a few KH wave detectors. This frequency range is limited due to various sources of noise (see section 1.2.2).
Possible sources of detectable waves are summarized in the following section.

a) Supernovae

A supernovae occurs when a star collapse, triggering a stellar explosion. If the collapse is perfectly symmetrical, no gravitational waves will be produced. However, if the collapse is asymmetric, due to a significant amount of angular momentum in the core of the star, then there is a possibility that strong gravitational waves will be produced.

The strain amplitude, as measured on earth, that is produced by such an event is given by [4]

- $$h \approx 5.10^{-22}\left(\frac{E}{10^{-3}M_{\phi}c^{2}}\right)^{\frac{1}{2}}\left(\frac{15Mpc}{r}\right)\left(\frac{1kHz}{f}\right)\left(\frac{1ms}{\tau}\right)^{\frac{1}{2}} \qquad 1.1$$

Where

- E is the total energy radiated
- M_{ϕ} is the mass of our sun
- c is the speed of light
- f is the frequency of the gravitational signal
- τ is the time taken for the collapse to occur
- r is the distance to the source

The event rate, out to the Virgo cluster at a distance of about 15 Mega Parsec $\left(\approx 4.5.10^{23}\,m\right)$, has been estimated as several per month.

b) Coalescing binaries

A compact binary system consists of two high density collapsed stars (neutron stars or black holes) orbiting about their common center of mass. The orbital period and distance between the stars decays due to the loss of energy in the form of gravitational waves. As the two stars approach each other, the amplitude and frequency of the GW emitted increases. A few seconds before the two stars coalesce; the amplitude and frequency reach values that could be detectable by current ground based detectors for sources located as far as the Virgo Super Cluster (15 MPc).

Schutz [5] approximates the strain amplitude as

- $$h \approx 1.10^{-23}\left(\frac{100Mpc}{r}\right)\left(\frac{M_b}{1.2M_\phi}\right)^{\frac{5}{3}}\left(\frac{f}{200Hz}\right)^{\frac{2}{3}} \qquad 1.2$$

Where

- M_b is called the mass parameter of the binary
- M_ϕ is the mass of our sun
- c is the speed of light
- f is the frequency of the gravitational signal
- r is the distance to the source

The event rate, out of a distance of a 200Mpc, has been estimated as about 3 (+/-10) per year.

c) Pulsars

Rotating neutron stars and white dwarfs are possible sources of continuous periodic gravitational waves. For example, a pulsar, if not axisymetric, can emit gravitational waves. A pulsar emits gravitational waves at twice its rotational frequency. An estimate of the amplitude for such a source is [6]

- $$h \approx 2.10^{-26}\left(\frac{f_{rot}}{1kHz}\right)^2\left(\frac{10kpc}{r}\right)\left(\frac{\varepsilon}{10^{-6}}\right) \qquad 1.3$$

Where

- f_{rot} is the rotational frequency of the pulsar
- ε is the equatorial ellipticity (a measure of how non-axisymetrical the star is)
- r is the distance to the source

A typical pulsar that could be detected by LIGO is the Crab Pulsar at a distance of about 1.8kpc and with an ellipticity of about 7.10^{-4}. This pulsar is expected to emit gravitational waves at about 60hz with an upper limit of the signal around $h \approx 10^{-24}$.

d) Stochastic background

It is expected that a random background of gravitational waves exist, as the result of the superposition of signals from many sources. This may contains information about the creation of universe. The stochastic background will be difficult to distinguish from other sources of noise in one detector. However, such a signal will be coherent between two different detectors. Therefore, by cross-correlating the data from several detectors, it should be possible to extract the stochastic background from the other noises associated with each detector.

The strain produced by this background radiation is expected to be small and in the order of magnitude of $h \approx 10^{-25}$. Since the signal can be measured for very long period of times, it is possible to increase the signal to noise ratio by integrating the data over a long observation time.

1.2 TECHNICAL BACKGROUND, LIGO AND THE DETECTION OF GRAVITATIONNAL WAVES

In spite of the extraordinarily small strain that can be expected on earth, several methods have been proposed to detect gravitational radiation for astrophysical observation. These include bar detectors [7] which consist of a large suspended mass whose longitudinal flexible mode is at a frequency of about 1 kHz for which there are anticipated gravitational radiation sources. However, in more recent times, most research effort has been directed toward laser interferometric detectors, and at this time, several countries have commissioned detectors of this type.

Rainer Weiss first proposed a practical interferometric detection scheme in the 1970's [8][9]. However, the first to embark on the path toward building a interferometric detector was a British-German group known as GEO [10]. This group is responsible for the GEO600 detector in Hanover, Germany. Subsequent to this, several countries have constructed detectors: the Japanese built a detector with impressive sensitivity for its size called TAMA [11], there is an Italian/French effort known as VIRGO [12]. LIGO is both larger and more sensitive than any other existing detector, but for each of these, the mechanism for detection remains fundamentally the same.

1.2.1 Laser interferometry

A simple laser interferometer gravitational wave detector is, in principle, a Michelson interferometer whose mirrors are suspended as pendulums.

The figure 1.2 shows such an interferometer. Light from the laser is incident on a beamsplitter where the light beam is partially reflected and partially transmitted into the two arms each of the same length. The light is then reflected from a mirror at each end of the arms back to the beamsplitter. The combined interference pattern is then detected at the photodetector. A gravitational wave would cause a change in the interference pattern due to the relative motion of the mirrors. The mirrors are suspended under vacuum to isolate them from noise sources such as air pressure or ground vibrations.

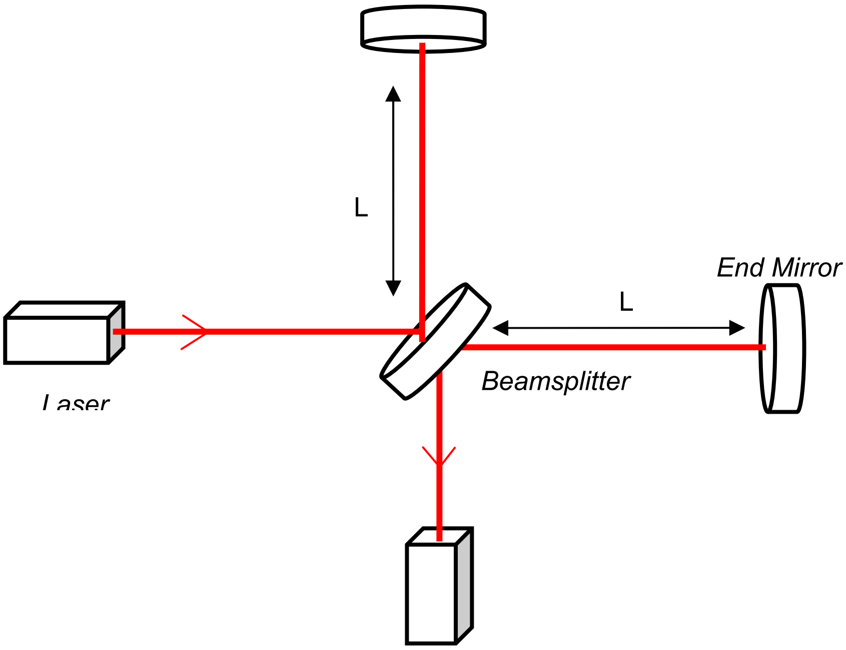

Figure 1.2: Michelson interferometer

The maximum sensitivity is achieved when the light is stored in the arms for approximately half the period of the gravitational wave. A gravitational wave of frequency 1kHz would correspond to an arm length of about 75km, which is unfortunately impractical to build on earth. It is however possible to build a 4km interferometer and increase the distance that light travels by making it travel up and down the arms several times. This increases the effective arm length and hence, the storage time for the light.

This method uses 2 Fabry-Perot cavities to increase the distance the light travels in the arms. The figure 1.3 shows the interferometer. Each cavity consists of one partially and one fully reflecting mirror, with the reflecting beams lying on top of each other.

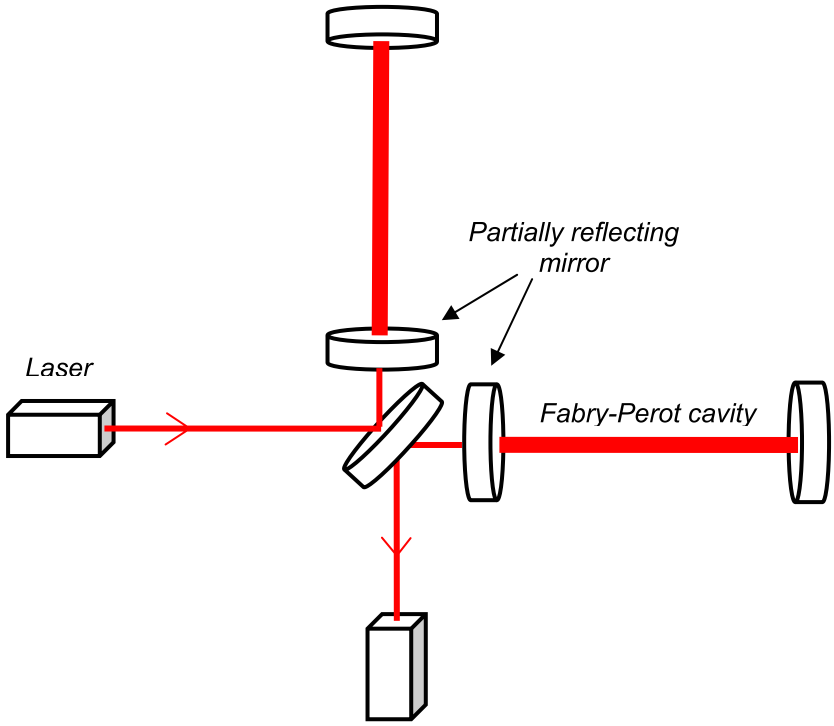

Figure 1.3: Michelson interferometer with Fabry-Perot resonant cavities

The cavity is at resonance and the amount of energy in the cavity is at a maximum if the length of the cavity is tuned to fit an integral number of half wavelengths of the laser light. The cavity is held at resonance using a servo control, under this condition, the differential displacement the arm can measure is increased by a factor of F/π , where F is the finesse of the cavity and depends of the reflectivity of the mirrors, it reaches a value of several hundreds for LIGO mirrors.

1.2.2 Initial LIGO, Laser Interferometer for Gravitational Wave detection

Several laser interferometers have been built around the world to detect gravitational waves. The most sensitive of these detectors are the LIGO interferometer located in the United States. There are two installations of LIGO: one in Hanford (LHO), Washington and another in Livingston (LLO), Louisiana. Both of these observatories are now operational. The current configuration of each observatory is commonly known as Initial LIGO with the expectation of an Advanced LIGO configuration by approximately 2015.

The LIGO observatories consist of two 4 km long beam tubes orientated orthogonally to one another. Each beam tube contains one arm of a Michelson interferometer with a Fabry-Perot resonant cavity. The end mirrors of the Fabry-Perot cavity are contained in Beam Splitter Chambers (BSC) at either end of each 4 km long beam tube. The BSC at the Corner Station houses the beam splitter and the surrounding Horizontal Access Modules (HAM) contains a variety of support optics for the main interferometer (see figure 1.4).

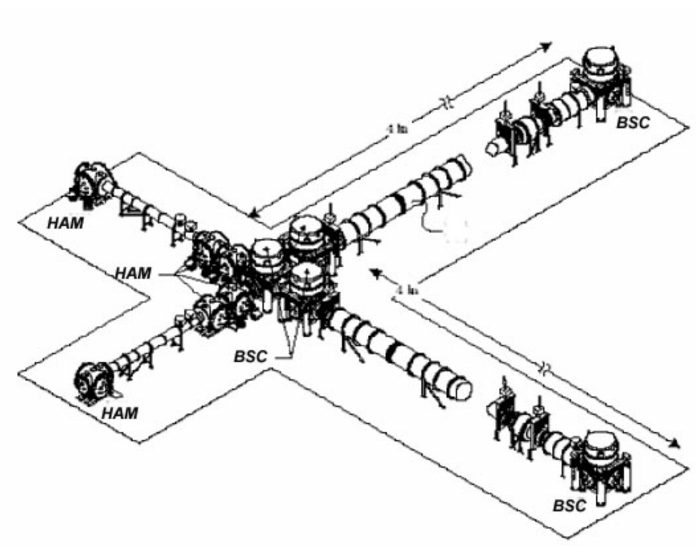

Figure 1.4: LIGO layout

Figure 1.5: LIGO Hanford Laboratory

Figure 1.6: LIGO Livingston Laboratory

1.2.3 Noise sources

The design sensitivity of the initial-LIGO interferometers is limited by 3 sources of noise. The figure 1.7 shows the displacement sensitivity of initial LIGO and the 3 limiting sources of noise. The seismic, thermal and shot noise are then described.

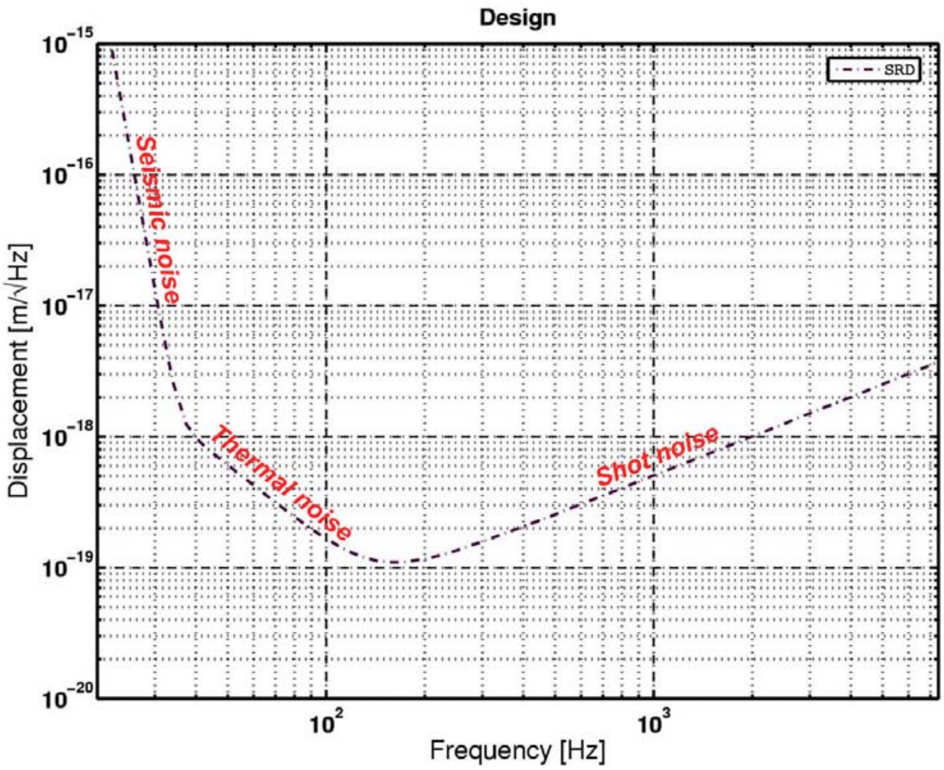

Figure 1.7: Noise sources for LIGO

a) Shot noise

Photon noise, also called shot noise, is due to the statistical fluctuation in the number of photon detected at the output of the interferometer. The signal detected at the output will have an uncertainty due to Poisson counting statistics. This uncertainty gives rise to noise at the photodetector that will limit the sensitivity of the instrument. It is possible to improve the shot noise sensitivity by increasing the level of input power. However, as the laser power increases, the radiation pressure noise, caused by fluctuations in the number of photon reflecting off the mirrors, increases. Ideally, the laser power is optimized to minimize the effect of those two noises.

b) Thermal noise

The random motion of atoms in the test mass mirrors and their suspensions generates thermal noise. The first form of thermal noise was discovered by Robert Brown around 1828 [13], it is only later that Einstein [14] understood the phenomena by showing that the molecular impacts create a dissipation of energy and create noise displacement.

This noise depends on the temperature of the atoms. The sources of thermal noise include the pendulum modes of the suspended masses, the violin modes of the wires and the internal modes of the mirrors. The maximum thermal noise occurs at the resonance frequencies; however, it is the shape of the thermal noise spectrum as a function of the frequency that is important for GW interferometers. The power spectrum of a system's fluctuation motion due to thermal noise is given by the fluctuation-dissipation theorem [15]:

- $$x_{therm}^2(f) = \frac{k_b T}{\pi^2 f^2} \Re\big(Y(f)\big) \qquad 1.4$$

Where

- f is the frequency
- k_b is the Boltzmann's constant
- T is the temperature
- $\Re\big(Y(f)\big)$ is the real part of the admittance given by $\dfrac{\dot{x}}{F_{ext}}$

In order to check the influence f the quality factor on the thermal noise, the complex form of Hooke's Law is used

- $$F = -k(1 + i\alpha) \qquad 1.5$$

Where the quality factor Q (a measure of how small the dissipation is) is related to α by $Q = \alpha^{-1}$. In the case where $\alpha = 0$, we retrieve the usual Hooke's law with no delay. In practice, the quality factor will often depends on the frequency, but for the purpose of this explanation, we will assume it is a constant.

From this, the motion of a mass can be written

- $F_{ext} = m\ddot{x} + kx + i\alpha x$ 1.6
- $\frac{F_{ext}}{\dot{x}} = \left(2\pi fm - \frac{k}{2\pi}\right)i + \frac{k\alpha}{2\pi f}$ 1.7

From there, we get the power spectrum of the thermal noise motion from the Fluctuation-dissipation theorem:

- $x^2_{therm}(f) = \frac{4k_bTk\alpha}{2\pi f\left[\left(k - m(2\pi f)^2\right)^2 + k^2\alpha^2\right]} = \frac{4k_bT{\omega_0}^2\alpha}{\omega m\left[\left({\omega_0}^2 - \omega^2\right) + {\omega_0}^4\alpha^4\right]}$ 1.8

As we see on this equation, the maximum thermal motion occurs at the resonance frequency. By designing very high Q, low α suspensions, it is possible to keep this noise contained to a very narrow bandwidth around the resonance. These resonances can then be filtered in the output data.

c) Seismic noise

Ground motion induced vibrations can disrupt the operation of the interferometer and add noise at the low end of the gravitational wave detection band. The sources and magnitude of seismic disturbances vary with frequency [16].

Overall, the root-mean-square (rms) of the ambient ground motion at the LIGO sites is approximately $1\mu m$. Much of the spectral contribution to this rms motion comes from the microseismic peak in the 0.1-0.3 Hz band. The microseismic peak results from coastal ocean water waves exciting surface waves along the Earth's crust. Another notable disturbance source is human activity which contributes largely between 1 and 10 Hz. This is particularly a problem at the Louisiana site, where commercial logging in the surrounding forest causes a factor of about 10 increase in motion during the daytime.

At very low frequencies, the surface of the Earth undergoes a tidal motion on the order of $200\mu m$ peak to peak caused by attraction to the sun and the moon. Seasonal temperature variations may also introduce annual length variations as large as 1 mm.

1.2.4 From initial LIGO to Advanced LIGO

As the initial LIGO interferometers start to put new limits on gravitational wave signals, Advanced LIGO [17] [18] has been proposed to improve the sensitivity by more than a factor of 10. This new detector, which will be installed at the LIGO Observatories, will replace the present detector once it has reached its goal of a year of observation. It is anticipated that Advanced LIGO will transform gravitational wave science into a real observational tool. It is predicted that this new instrument will potentially see gravitational wave signatures possibly as once a day with excellent signal to noise. The improvement of sensitivity will allow the same science product of one-year of observation of initial LIGO to be equaled in just several hours. The improvement of the detector requires nearly every aspect of the detector to be improved or replaced with the notable exception of the vacuum envelope.

The goal is to push the sensitivity to its fundamental limits, thus, most of the sensitivity will be limited by the quantum noise due to the high power laser. The seismic noise will be pushed at the limit of the gravity gradient at the sites by using multiple stage isolation system and multiple pendulums to filter the high frequency noise. Finally the thermal noise will be reduced by using fused silica fibers instead of steel wires for the pendulums. The noise curve for advanced LIGO is shown in figure 1.8.

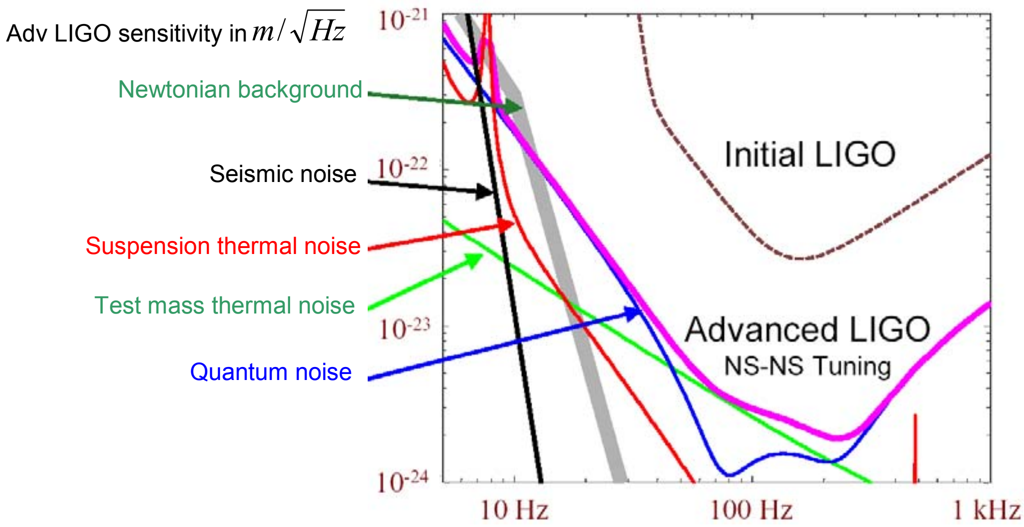

Figure 1.8: Advanced LIGO noises

a) LIGO Advanced System Test Interferometer (LASTI)

The LIGO Advanced System Test Interferometer is a user facility for members of the LIGO Laboratory and LIGO Science Collaboration. It is located at MIT and its main goal is to enable the testing and commissioning of Advanced LIGO (see below) prototypes without shutting down the running instruments at Hanford and Livingston. LASTI is used by the LIGO group to develop and test new mechanical structures, new electronics and new active control methods.

Vacuum chambers and mechanical support interfaces are identical to those found at the observatory sites. This permits testing of full-size prototypes which greatly reduces or eliminates the need for field rework or debugging at the observatory sites.

1.2.5 The seismic isolation systems for advanced ligo

To achieve the overall suspension, isolation and alignment requirements for Advanced LIGO, LIGO teams are developing three sub-systems [19] (see figure 1.9).

1. A hydraulic pre-isolator system (HEPI) for low frequency alignment and control, which will be situated outside the vacuum system. This system has already been installed in LLO and provides very good results.
2. A two-stage in-vacuum active isolation platform designed to give a factor of ~1000 attenuation at 10 Hz
3. A multiple pendulum suspension system (quadruple pendulum for the most sensitive optics and triple pendulum otherwise) that provides passive isolation above a few hertz, and minimizes suspension thermal noise by using high Q materials in the final stage.

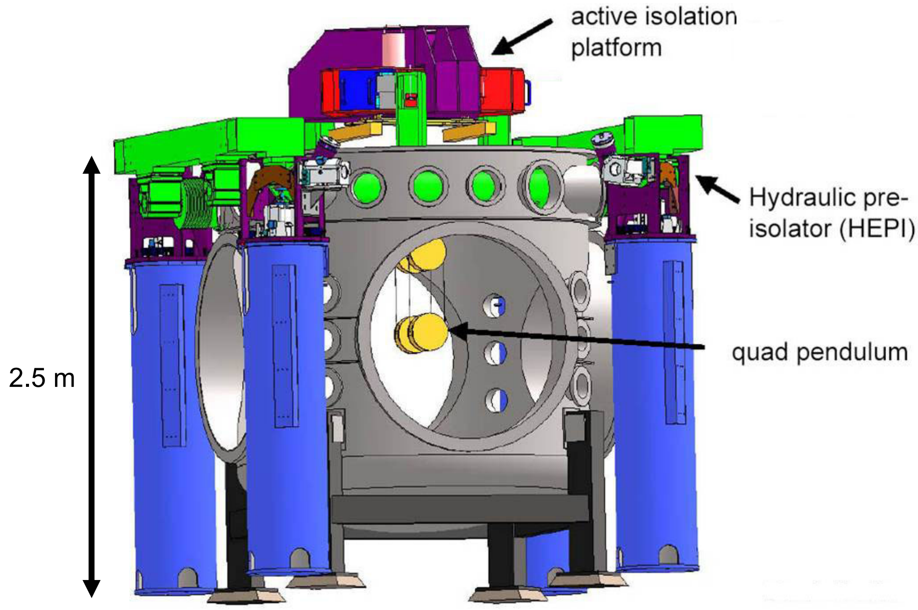

Figure 1.9: Seismic isolation systems for advanced LIGO

a) Hydraulics external pre isolator

The hydraulic external pre-isolator (HEPI) system was specifically designed to address the low frequency isolation and alignment requirements for Advanced LIGO. Actuation is required in all six degrees of freedom (DOF), and the specifications for this system are that it should be able to generate a maximum force greater than 2000 N over +/- 1 mm, have a bandwidth from 0 to ~10 Hz, and a noise level not exceeding 10^{-9} m/√ Hz at 1 Hz. A quiet hydraulic actuator can meet all of these requirements.

A schematic diagram of the basic elements of the system is shown in figure 1.10. The pump, (1), supplies a constant flow of fluid through the actuator. This fluid flows continuously through the hydraulic equivalent of a Wheatstone bridge (2), with variable resistances that are controlled in differential pairs. By controlling the resistance, one generates differential pressure across the bridge, which modifies the flow, (3), to the differential bellows, (4). These bellows act as a stiction-free piston which moves the actuator plate, (5), which is connected to the payload (not shown) with a flexure that is stiff in 1 DOF.

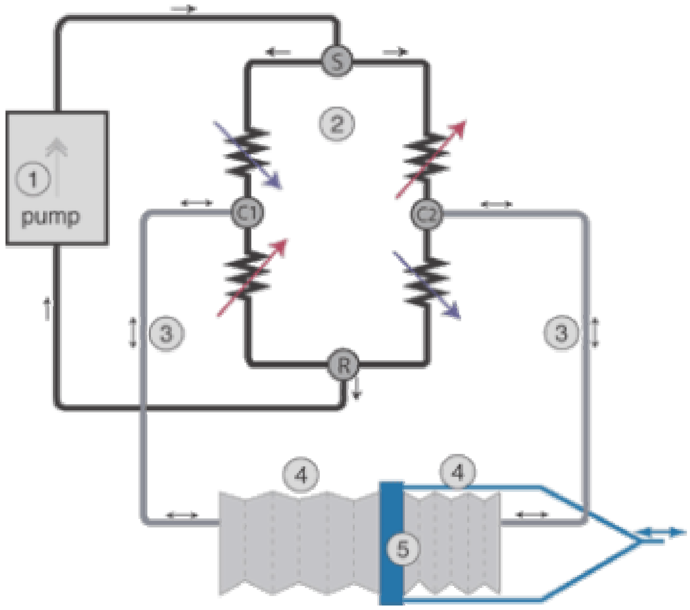

Figure 1.10: HEPI

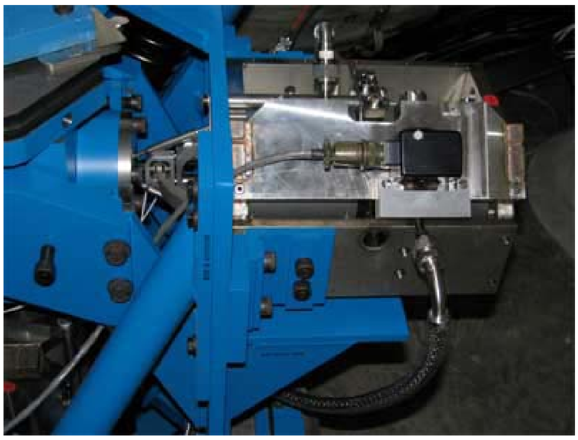

Figure 1.12: HEPI picture

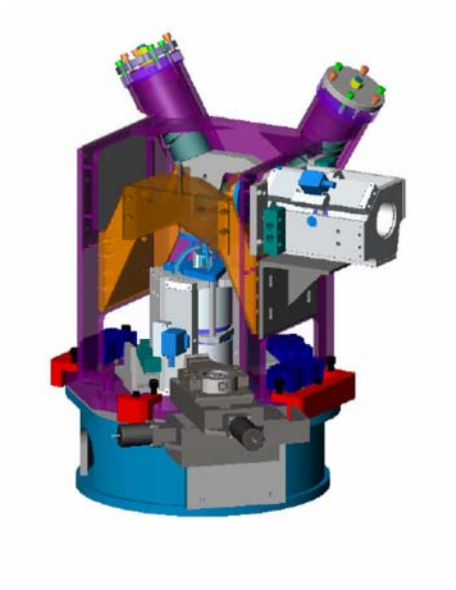

Figure 1.11: HEPI Pier

The performance requirements for LIGO include alignment and isolation. To achieve both of these requirements, two controls techniques are used, namely sensor blending and sensor correction. Each actuator is outfitted with 2 sensors:

- A displacement sensor which measures the difference between the actuator plate position and the ground
- A passive 1 Hz geophone measuring the absolute velocity of the payload.

These two signals are blended together into a “supersensor” [20]. When the supersensor is used in feedback, it is possible to control position at low frequency while still attaining isolation at higher frequencies.

The isolation can be extended to lower frequencies using sensor correction. By adding a very sensitive (at low frequencies) seismometer on the ground, one can measure the motion of the ground at lower frequencies. It is then possible to subtract this motion from the displacement measured by the displacement sensor and get an inertial value for the payload motion at low frequencies [21].

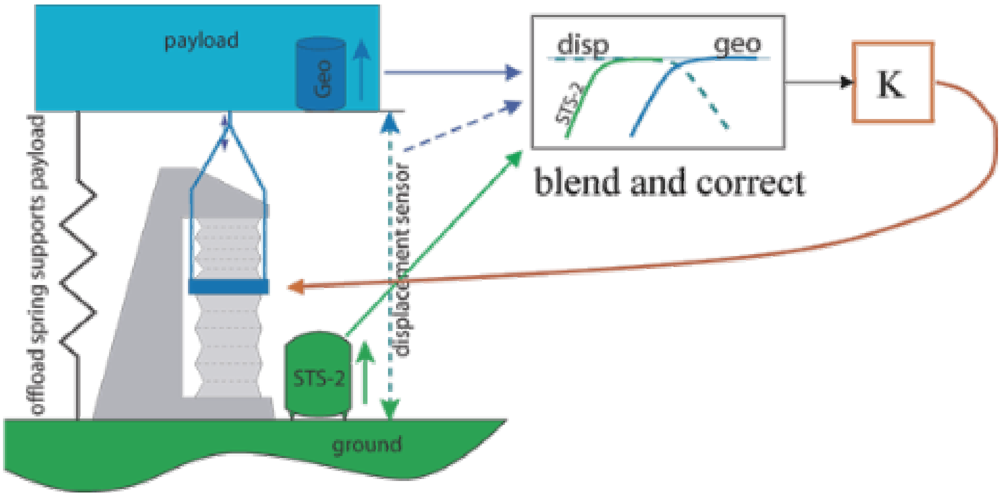

Figure 1.13: HEPI control strategy

In the LIGO application there are 8 actuators used to control the 6 DOFs, 4 horizontal and 4 vertical mounted in pairs on each of the 4 piers supporting the payload in the vacuum. Actuation can be used to track the Earth's tides, as well as to correct at each vacuum tank for large amplitude low-frequency (~0.1 Hz to several hertz) motion including the microseism which typically peaks at frequencies near 0.15 Hz.

Following extensive development and testing of the actuator design at Stanford University, prototype actuators were installed and tested on a LIGO-sized vacuum chamber at the LIGO Advanced System Test Interferometer (LASTI) facility at MIT. This system showed good performance, reducing motion between several tenths of hertz to a few hertz, achieving about an order of magnitude noise reduction between 0.5 and 2 Hz [22].

b) Internal Active Platform

We have discussed above the first stage of isolation for Advanced LIGO, which is situated outside the vacuum system. This outer stage will support the in-vacuum two-stage active isolation platform which we now describe. The basic design strategy for the isolation platform has been discussed in [23][24].

One of the most challenging problems for achieving good seismic isolation at low frequencies is tilt coupling, which is introduced because inertial sensors cannot distinguish between acceleration and gravity. Inertial sensors are made of a mass-spring system, if the sensor is tilted, the mass will react and move even though there was no "true" motion in the direction we want to measure. This problem is discussed in [25], and thus will not be covered in detail here.

The isolation platform consists of two cascaded stages, suspended through stiff blade springs and short pendulum links, giving natural frequencies in the 2-10 Hz range. The vibration of each stage is reduced by sensing its motion in 6 degrees of freedom (DOFs) and applying forces in feedback loops to reduce the sensed motion. The feedback signal for the first stage is derived by blending signals from three sensors for each DOF - a long-period broadband seismometer (Streckeisen STS-2), a short-period geophone and a relative position sensor. The second stage uses signals from a GS-13 (Geotech Instruments) low-noise geophone and a relative position sensor for each DOF. The actuators are electromagnetic non-contacting forcers, which apply forces between the support and stage one, and between stage one and stage two respectively.

The overall system will include 31 sensors and these will be merged into 12 supersensors to control each degree of freedom of this seismic isolation system. The digital control loops will use both sensor blending and sensor correction techniques.

In parallel with the research effort underway to investigate the performance and optimize the control design of the technology demonstrator at Stanford, a new prototype is currently being assembled at LASTI, which will essentially be the design for Advanced LIGO.

Figure 1.14: Internal Seismic Isolation

c) Suspensions

The last stage of the isolation system is the multiple mass suspension as shown in figure 1.15; the role of this stage is to filter the seismic noise above 10Hz and to minimize the thermal noise effects on the mirror. The suspension provides an excellent passive isolation of the high frequencies seismic noise.

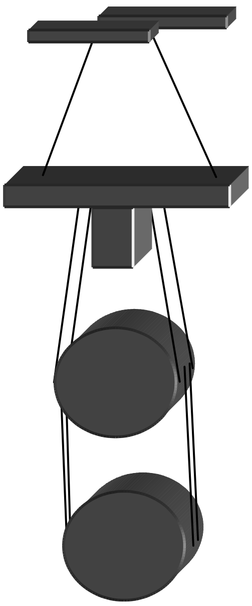

Figure 1.15: Triple pendulum suspension

The low frequency resonances of the pendulum are damped using active feedback; this is called local control because it concerns the pendulum only. Another control is used to control the arm's length of the interferometer, by actuating on the mirror, one can control the length of the interferometer's arms, and this is called global control.

The existing design used by LIGO has test masses (mirrors) hung as single pendulums on wire slings, with actuation being applied directly to the test masses via coil and magnet systems for damping (local control) of the pendulum modes and global control.

The second-generation performances requirements are more aggressive than that currently used in LIGO. In particular in terms of the reduction of thermal noise associated with the suspension of the mirrors. The Advanced LIGO suspension design aims to reach residual displacement noise of 10^{-19} m/√Hz at 10 Hz (for the most sensitive pendulums). Other noise sources such as those due to the local and global control systems are required to lie below this.

To reach these requirements, multiple pendulums are used for Advanced LIGO suspensions, the most sensitive suspensions will be quadruple pendulums, while the one requiring less filtering will be triple pendulums. In this thesis, we will discuss and study the triple pendulum only. A detailed description of this pendulum is given in section 2.

One can summarize the major improvements for the new Advanced LIGO suspensions in few points:

- Multiple mass suspension to improve isolation performances.
- Two or three stages of cantilever blade springs made of maraging steel to increase the vertical seismic isolation.
- Fused silica or sapphire mirrors (40 kg for the quadruple pendulum, 3Kg for the triple pendulum) will form the lowest stage. For the quadruple pendulum, the mirrors will be suspended on 4 vertical fused silica ribbons to reduce suspension thermal noise.
- The damping (local control) of all of the low frequency modes of the pendulums will be carried out by using 6 co-located sensors and actuators at the highest mass of the multiple pendulum, thus noise associated with the local control is isolated by the stages below.

d) Conclusion

The overall seismic isolation is the product of the isolation of the three sub-systems. The target residual noise level for the pendulum's test mass is 10^{-19} m/√Hz at 10 Hz for the longitudinal direction of the most sensitive platform (using quadruple pendulum). In this document, we will mainly focus on the suspension and especially the triple pendulums. If the methods we develop are approved, they will be transferred to the quadruple pendulums as well.

In the next section, we will discuss the state of the art concerning the active damping of the suspension, and introduce the main goals of the thesis.

1.3 THESIS MOTIVATION

1.3.1 Suspensions and GW detection

The last stage of LIGO seismic isolation system uses a pendulum to filter the high frequencies noise. Single pendulums are currently used for Initial-LIGO. Those pendulums will be replaced by multiple pendulums [26] to meet the Advanced LIGO requirements. The key improvements for advanced LIGO pendulums are

1. The overall isolation provided by the multiple stages
2. The thermal noise improvement provided by choices of new materials
3. The isolation of electronics noise associated with the damping control

Depending on their position in the interferometer and the noise requirements, both triple and quadruple pendulums will be used.

Multiple pendulums are commonly used for the seismic isolation of the GW interferometers around the world. The Italian-French project VIRGO uses a pendulum-like very massive suspended structure called a superattenuator [27], In the German-UK project GEO, the last stage of seismic isolation uses triple pendulums [28] that are very similar to the one advanced LIGO will use.

In order to provide low thermal noise and good isolation, it is required that the resonant modes of the pendulums possess a very high quality factor (Q). This leads to a very large coupling and transmission of the seismic motion at the resonances and very large motion of the suspended mirrors. Large motion makes the interferometer locking difficult to acquire because of the limited dynamics range on the global actuators (global actuators are keeping the arm's length of the interferometer constant). Therefore, it is necessary to damp those resonances.

1.3.2 Active damping, the measurement noise problem

The damping for advanced LIGO pendulums is provided by an active feedback loop. The position of the top mass of the pendulum is measured, filtered and feedback into actuators to damp the resonances. The same system is used in GEO and very well described in [28]. The control is applied using collocated optical sensors and electromagnetic actuators. The combination of one sensor and one actuator is called an OSEM (Optical Sensor and Electro Magnetic actuator). A detailed description of this device is given in [29].

This last reference also shows the performances of the sensors, we know that the measurement noise reach a value of $5e^{-11}m/\sqrt{Hz}$ above about 10Hz. If we compare this value with the expected motion of the pendulum considering the advanced LIGO seismic isolation system, we realize that the sensor noise will dominate the seismic noise above 1Hz for the triple pendulum, and be about 500 times bigger than the seismic noise at 10Hz.

This sensor noise will combine with the real measurement, and be re-injected by the active damping loop into the actuators; this dramatically decreases the performances of our suspension. The effect of sensor noise on the damping has been well studied by several LIGO laboratories [30], and different techniques and experiments are being tested to solve this problem.

Current filtering techniques don't provide adequate performances. Creating filters that maintain a good damping for the low frequencies but decrease the amplitude of the feedback quickly after the last resonance is a difficult and very long process. The filtering is limited by the need to have phase margin and gain on the last resonance mode, which increases the loop gain on the high frequencies and increases the sensor noise transmission into the loop.

Several alternate methods have been studied to solve this problem; all try to provide acceptable damping while reducing the sensor noise transmission.

One solution could be to improve the performances of the sensor by decreasing the noise generated by the sensors; we could reduce the amount of sensor noise re-injected in the actuators. Studies have been carried out to design a better sensor such as the interferometric

OSEM [31]. This sensor provides better performances and a lower noise floor, at the cost of a very complex and expensive sensor.

A second solution is to use eddy current damping [32] [33]. In this case, the damping of the pendulum would be provided by a hybrid system, the lowest modes would be damped using active feedback, while the highest modes would be damped using eddy current dampers. This solution has proven to be efficient. However, this technique also has several drawbacks: by adding strong magnets on the pendulum itself, we increase the coupling between the pendulum and the magnetic field the chamber. This coupling increases with frequency and can't be filtered.

VIRGO also faces the same issue with sensor noise injection. A very interesting technique has been studied by Losurdo and Passuelo [34]. The idea is to create an active feedback using a double loop. Two loops run in parallel, one is actually driving the pendulum to damp the low frequencies, while the other one is driving a digital model of the pendulum for the high frequencies. Those two loops, while individually both unstable, combine and form a stable loop. Most of the sensor noise is injected into the virtual model, which reduces the noise injected in the real pendulum. This technique only achieves small noise filtering and many aspects remain to be studied, among them how to guaranty the stability of the loop and how accurate the digital model needs to be.

Currently, in initial LIGO, the way to avoid this problem when running LIGO at high sensitivity is to turn the local control (damping) off and to use only the global loop (the interferometer signal is a much higher signal to noise motion detector) to control the resonances. This provides good results with the single suspensions of initial LIGO but will not be a viable solution for Advanced LIGO because of the use of multiple pendulums.

The aim of this thesis is to design an efficient damping loop that also minimizes the sensor noise transmission. Instead of patching the current technique with additional filters or systems, we will re-design the loop using a different approach and study the duality damping – sensor noise transmission.

1.3.3 *An alternate solution to reduce the sensor noise transmission: modal control and estimation*

As we have seen above, one of the main issues with the classic filtering approach is the limitation due the last mode, in order to get a safe phase margin for the control of this mode, the gain needs to be increased and this leads to high sensor noise transmission. The idea is to design a new controller that gives us additional degrees of freedom to avoid this kind of problem.

Modal control enables us to transform a MIMO system into a combination of independent SISO systems that can be easily controlled one by one. This first method that used modal control was called Independent Modal Space Control (IMSC) and has been studied by Meirovitch [35] [36] and Gawronski [37], in this method, only one mode is controlled at a given time step. Later, the technique has been modified [38] to independently control each modal state simultaneously, it is now called Independent Modal Control. The IMC possesses the advantage of giving more freedom to the designer. By controlling modes one by one, it is possible to choose which mode needs more damping or which modes transmit more sensor noise.

In designing modal feedback control, one must know the modal states, which are extracted from the real states. In our case, the real states represent the measured motion of each mass of the pendulum in all direction, while the modal states represent the modal motion of the pendulum for each mode. Unfortunately, it is not always possible to have a full real state because some part of the structures can't be measured. In this case, we need to extract the modal states from the measurement states, and reconstruct the missing data.

This can be achieved using a Luenberger Observer [39][40]. Luenberger observers use a full model of the structure that can generate as many outputs as needed, and all the modes we want to control. By comparing the outputs of this model to the measured data, we are able to make the model converge and reconstruct the missing data. It is still important for every mode to be observable; fortunately, the pendulums in LIGO have been designed to be fully observable from the top mass.

Many different kind of observers based on Luenberger technique exist. A very simple design is called disturbance observer, where the correction of the observer is made on its input, as if the observer was trying to "guess" the disturbance applied to the real system.

Several other observer designs imply direct correction on the states. The feedback is directly re-injected on every state to update the model. The optimization of such an observer is made using well-known LQ techniques [41], we will see later that those optimization techniques can also play a very important role in sensor noise transmission. This kind of observers can also directly use a modal model of the structure as described by Meirovitch [42], in this case, we can take full advantage of the orthogonality property of the modes, and get additional degrees of freedom for the design of the observer.

An interesting property of observers is that they can also be used to reduce the measurement noise. Kalman showed that observers could be extended to the estimation of noisy data [43]. Kalman estimators give an optimal estimation of data in a noisy measurement environment knowing the covariance of the input noises (called process noise and measurement noise).

Our goal is slightly different than Kalman's, we are not looking for the optimal recovery of data in the noisy measurement, instead we want to reduce the noise in this data to a minimum, even if we have to lose accuracy on the data itself. This is why we will not work with a pure Kalman estimator and chose a slightly different method using LQ optimization, while still using the properties shown by Kalman, this will enable us to have an additional degree of freedom to reduce the sensor noise transmission.

1.3.4 Summary

This thesis is organized in the following sections:

In the second section, a description of the triple pendulum is given. We describe the mechanical system and the numerical models, and check the validity of our models by comparing them with the measurements. We also study the noise sources in detail and see how the sensor noise becomes an important performance limit for the pendulum damping. Several "classic" methods are shown and their results analyzed.

In the third section, we describe the different techniques and theory used for the new damping loops. Independent Modal Control is discussed, and the reconstruction of the missing data is explained using a disturbance observer or a LQ observer.

In section 4, The combination of the Independent Modal Control and the estimator is then described and analyzed taking into account the damping and the sensor noise transmission. Several tools to optimize the choice of the parameters are designed.

These tools are then used to apply the modal control to the triple pendulum in the fifth section, several examples are given and simulated results are shown using numerical models. These results are compared with classic approach.

Finally, in the last section, we test our damping loops on a working pendulum and measure the sensor noise transmission using optical techniques that are rarely used in the field of mechanical vibration measurement.

2 THE TRIPLE PENDULUM

2.1 INTRODUCTION

The triple pendulum is the last stage of the seismic isolation. Its role is to filter the high (>10Hz) frequencies noise using 3 stages of passive isolation in the horizontal directions and 2 stages of isolation in the vertical one. It has been modeled and designed by Calum Torrie in Glasgow and Caltech [44].

2.1.1 Mechanical structure

The triple pendulum we are going to study is used for the optical mode cleaner in the interferometers. It is made of 3 masses of 3Kg each and the height from top to the center of the bottom mass is 76cm. The 3 masses are called M1, M2 and M3 as seen on figure 2.1. M0 is used to name the ground motion.

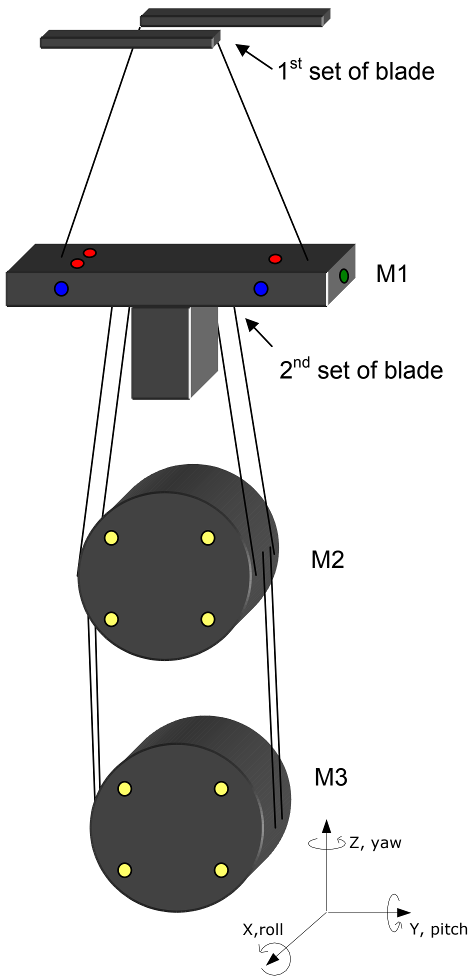

Figure 2.1: Triple pendulum

The passive isolation in the horizontal direction is provided by the 3 hanging masses. Each stage adds a $1/f^2$ filtering above its resonance frequency (between 0 and 6 Hz). The total filtering in the horizontal direction is $1/f^6$ above 6Hz.

The isolation in the vertical direction is provided by 2 stages of cantilever blades (top and first mass) which behave like very soft springs and give us very low resonances frequencies (between 0 and 5Hz) and good filtering. The total filtering in the vertical direction is $1/f^6$ after the last resonance (note that the last vertical isolation stage is provided by the wires between the 2 bottom masses, the resonance frequency of this mode is higher than for the blades (about 40Hz).

The pendulum is an excellent vibration isolation system at high frequencies. However, at low frequencies, it is necessary to damp the high Qs resonances of the pendulum. This is why the pendulum is also equipped with an active damping system.

The triple pendulum has 14 collocated sensors and actuators (see figure 2.2). The 8 bottom sensors/actuators (yellow dots on figure 2.1) are not used in the damping control but we will see later that they are required for LIGO interferometers. The 6 sensors/actuators on the first mass (red, blue and green) are used to sense and damp the pendulum in the 6 degrees of freedom.

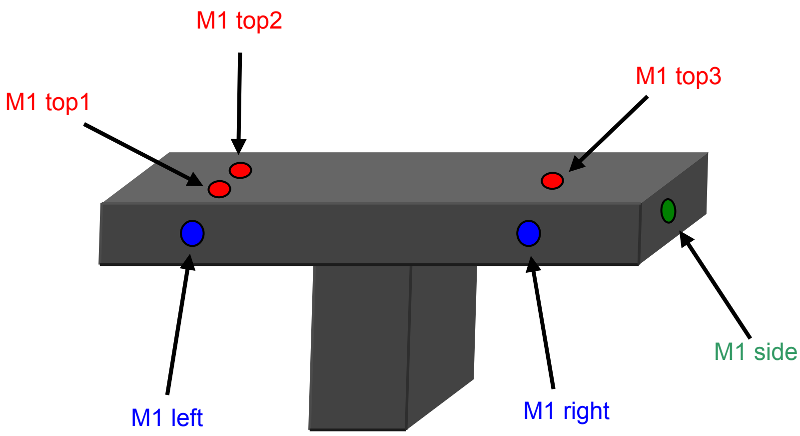

Figure 2.2: Actuators and sensors around the top mass

The first triple pendulum was assembled in May 2004 at Caltech, it was assembled in clean condition to be fully compatible with the vacuum cleanness requirements of LASTI (see figure 2.3). This was the first Advanced LIGO clean triple pendulum assembled. We'll see later that a second pendulum was needed for our experiment; this second pendulum was assembled in October 2005.

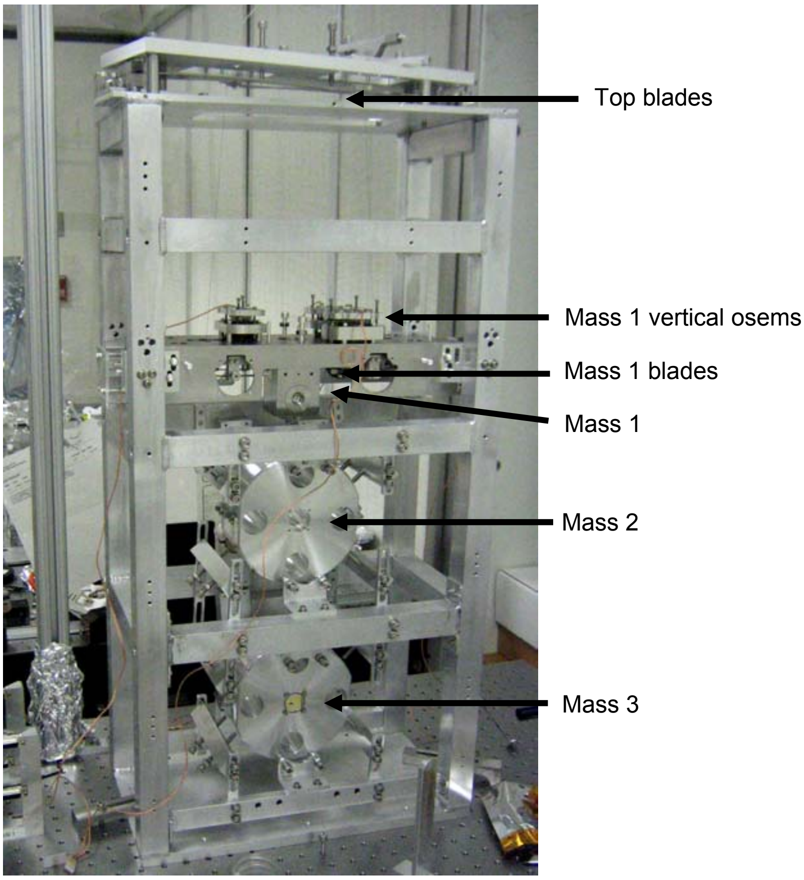

Figure 2.3: Triple pendulum picture

2.1.2 Sensors and actuators

The sensors and actuators are mounted in the same body and are called OSEM (Optical Sensor and Electro-Magnetic actuator).

The sensor is a shadow sensor (see figure 2.4 and figure 2.5). Light is generated by an infrared diode and measured by a photo-detector on the other side. In between, a flag mounted on the pendulum moves following the motion of the mass. A part of the light is blocked by this flag and by measuring how much light reaches the sensor; we can measure the position of the flag and the position of the pendulum. This is a relative sensor; it measures the position of the pendulum's mass relatively to the frame of the pendulum the OSEM is attached to.

The actuator is a simple coil/magnet system (see figure 2.4).

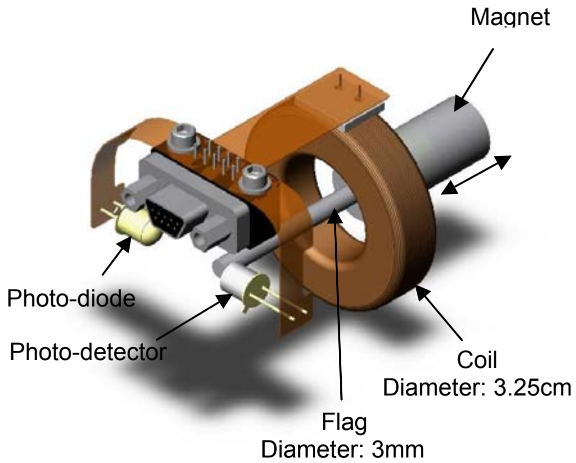

Figure 2.4: OSEM

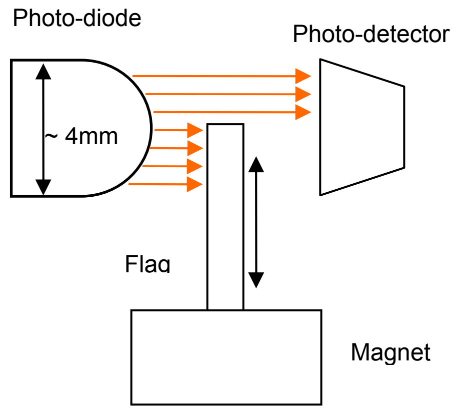

Figure 2.5: Shadow sensor

The figure 2.6 shows the coil and the photo-diode on a working OSEM.

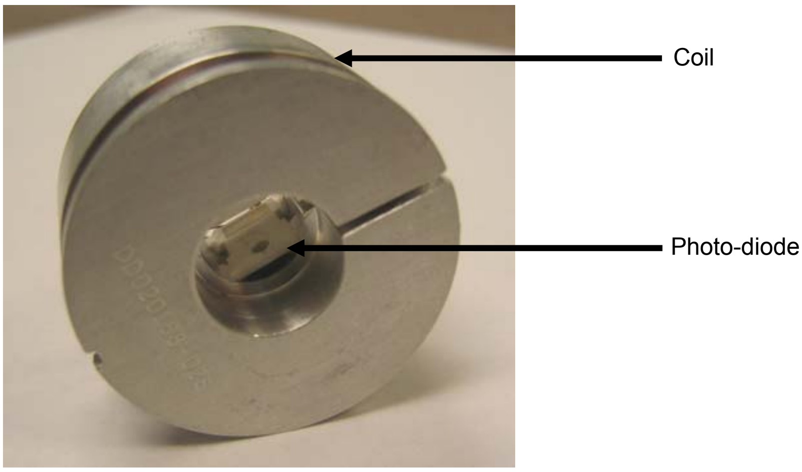

Figure 2.6: OSEM picture

2.2 NUMERICAL MODELS AND SIMULATION RESULTS

In order to understand the dynamics of the pendulum, several numerical models of the triple pendulum have been made, using different software like Mathematica, Matlab or Adams. The Matlab model has been developed by the California Institute of Technology (Caltech) and the University of Glasgow during the design of the triple pendulum. The Adams model has been realized here at MIT for this thesis. It has been created to double check the results of the Matlab model. It actually enabled us to correct few little mistakes in the Matlab code, improved our understanding of the numerical simulation, and gave us more confidence in our modeling.

The models we will study are the Matlab model, and the Adams model.
Both these models have 24 inputs and 18 outputs.

- The inputs are the 6 forces or torques (X, Y, Z, roll, pitch, yaw) for:

1. The ground motion
2. The forces and torques on mass 1
3. The forces and torques on mass 2
4. The forces and torques on mass 3

- The outputs are the 6 degrees of freedom motion for the 3 masses.

The Matlab model is divided into 4 sub-models that are uncoupled from each other. Although there might be a little coupling in the real case due to asymmetry or misalignment, we consider these kinds of couplings to be less than 0.1% and we can neglect them in our models. Those 4 models are

- Z (3 degrees of freedom)
- Yaw (3 degrees of freedom)
- X and pitch (6 degrees of freedom)
- Y and roll (6 degrees of freedom)

X and pitch (as well as Y and roll) are inherently coupled to each other due to the geometry of the pendulum, these is why we keep them in a same model.

In both models, the blades and the wire stiffness are merged and modeled by springs linking the masses to each other like you can see on the Adams model rendering (see figure 2.7)

The Matlab and Adams models have been compared with the measurement and we will see later that both agree well with each other and the measurement.

Our models also enable us to draw the eigenvectors of each mode, which can be interesting to understand how the pendulum moves and how to optimize the damping. Below is an example on the X and pitch modes. We won't show the 12 other modes but they can be drawn the same way.

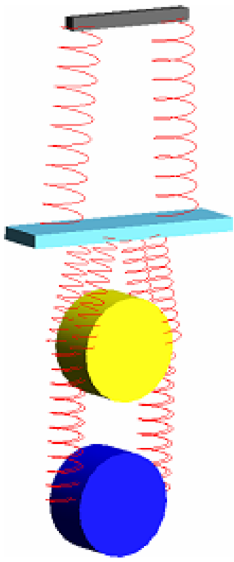

Figure 2.7: Adams model

Mode1 (X) at 0.65Hz 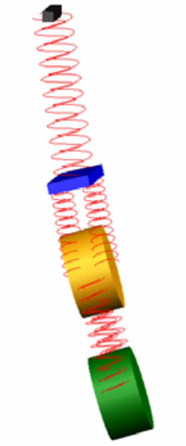	Mode2 (pitch) at 1.15Hz 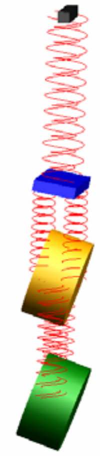	Mode3 (X) at 1.5Hz 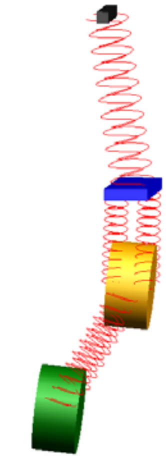
Mode4 (X) at 2.8Hz 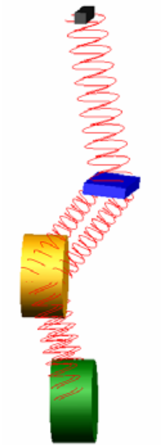	Mode5 (pitch) at 4.1Hz 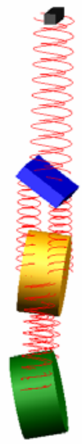	Mode6 (pitch) at 5.7Hz 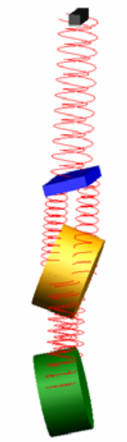

Table 2-1: Mode shapes in X-Pitch direction

2.3 CHARACTERIZATION EXPERIMENT

The first step of the project is to characterize the triple pendulum, and verify the models. It is a necessary step to be able to simulate the behavior of the damping loops we want to design. We want to measure the transfer function between the forces applied to Mass 1 in each direction and the pendulum motion, as well as the transfer function from the ground motion to the pendulum.

In order to achieve those measurements, the pendulum is placed on an optical table inside the HAM vacuum chamber in LASTI. The table can be actuated and moved in the 6 degrees of freedom using 8 actuators placed outside the chamber called HEPI (Hydraulics External Pre-

Isolator) (see section 1.2.5). 6 Geophones placed on the table measure the absolute velocity of the table in each direction. Finally, the sensors and actuators (OSEMs) on the pendulum measure the motion of the pendulum and drive the first mass.

The layout of the table is shown in figure 2.8 and a picture of the table with the pendulum and the geophones is shown in figure 2.9:

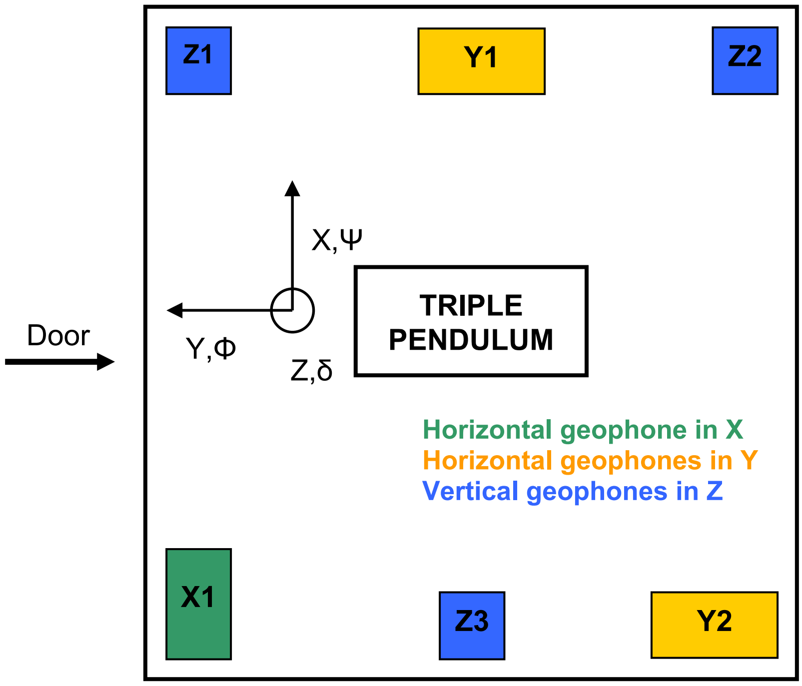

Figure 2.8: Layout of the optical table

Figure 2.9: Optical table picture

2.3.1 Acquisition methods and transfer function calculation

The actuators (osems and HEPI) are used to drive the pendulum while the sensors measure its motion to create the transfer functions. We choose to drive the pendulum modally, as opposed to a single actuator drive. Driving modally will only move the direction we want to measure and the measurement will be cleaner than with a single actuator drive.

However, we measure each sensor individually and only calculate the modal motion along the main direction later on. This enables us to keep the raw data and be able to focus on specific sensors if needed. Different methods are used for the drive, each method being the best adapted for the frequencies we want to measure (see figure 2.10).

- For low frequencies, we are using a white noise drive. It has the advantage of being relatively quick (1 hour for one drive). We filter the white noise with a band pass filter to keep only the frequencies we want to study and increase the drive's power (for example a band pass between 0 Hz to 3Hz for very low frequencies and 2Hz to 12Hz for medium ones). The 7-12Hz range of frequencies happened to be very noisy and hard to measure due to excessive seismic noise, in Appendix B you can see the technique that has been chosen to reduce this noise.

- For high frequencies (>~8Hz) however, we can use stepped sine, it is interesting to use this method because the pendulum filtering is very important at those frequencies, and being able to drive one frequency at a time gives us the opportunity to drive harder and get a better sensitivity.

We then merge all those data using the better coherence when the data overlap.

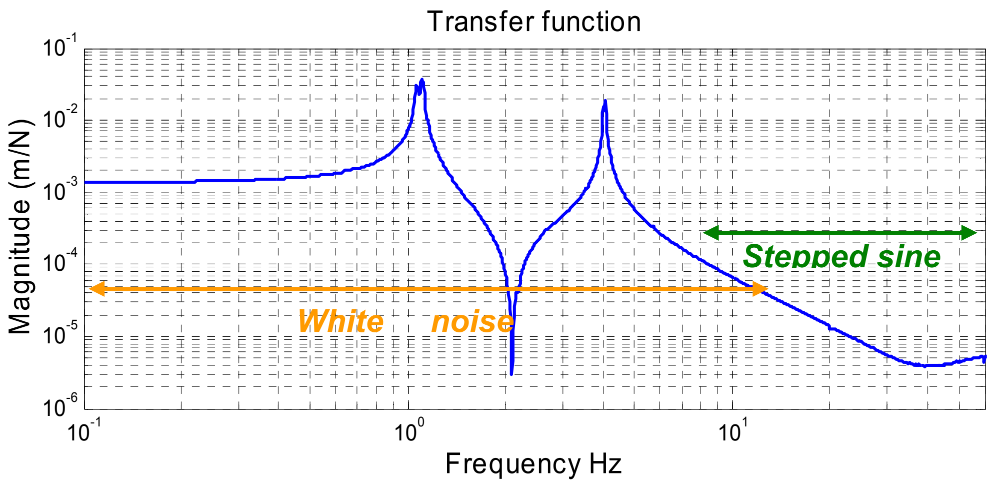

Figure 2.10: Acquisition method and frequency range

2.3.2 Results

The transfer function obtained from the measurements can now be compared to the model. There are a lot of transfer functions we have to compare to check that the dynamics is understood in the model. We will show only few of those comparisons here, the quality and agreement between the model and the plant of all degrees of freedom is similar to these plots. The models have not been modified to improve the match between the measurement and the modeling, we are directly plotting the original model transfer functions using the original parameters.

Figure 2.11 shows the transfer function from the top mass actuation to the top mass motion in the X direction, the blue curve shows the Matlab model and the red one shows the measurement. We see that both agree very well.

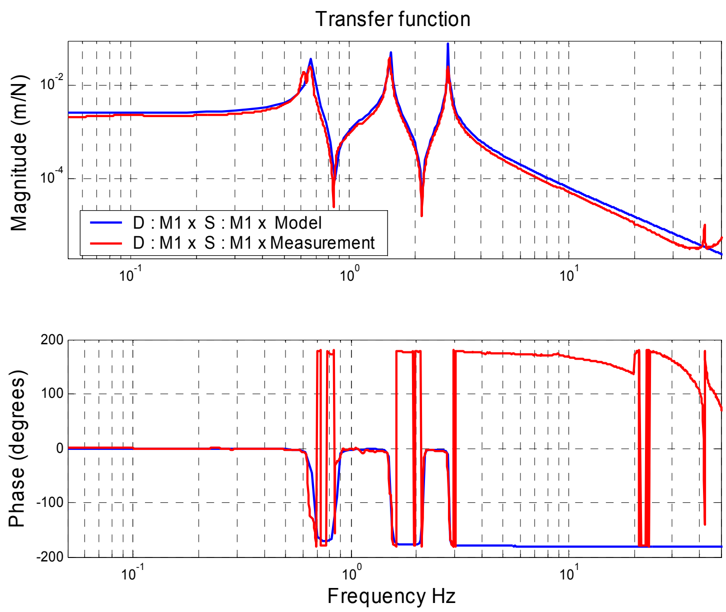

Figure 2.11: Transfer function from mass1 to mass1 in the X direction

Figure 2.12 shows the transfer function from the top mass actuation to the top mass motion in the pitch direction, once again, both agree very well.

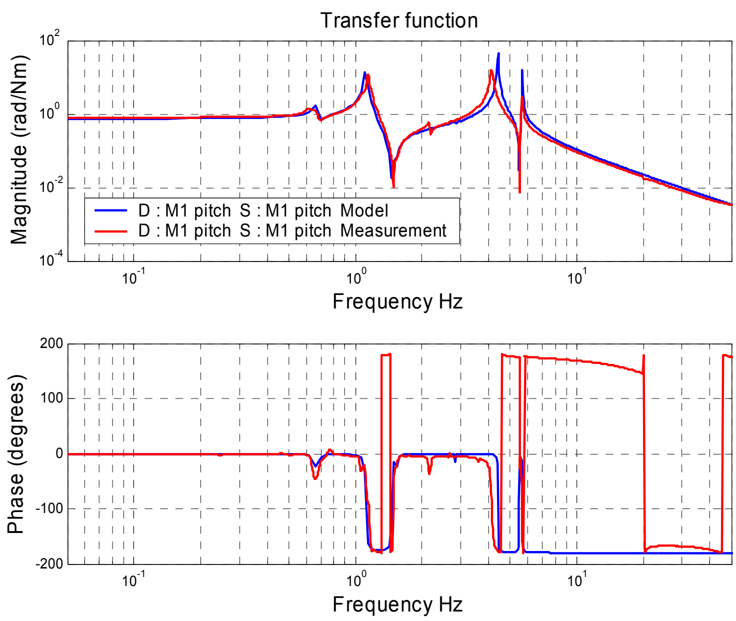

Figure 2.12: Transfer function from mass1 to mass1 in the Pitch direction

Another way to compare the models and the measurements is to collect all the resonance frequencies in one table. You can see the results in table 2-2 and check the percentage of error between each model and the measurement.

Mode	Measurement Resonance frequency (hz)	Adams (hz)	Matlab (hz)	Adams error %	Matlab error %
1 (x&pitch)	0.65	0.67	0.67	-2.57	-2.69
2 (y&roll)	0.66	0.67	0.68	-2.21	-2.33
3 (yaw)	1.09	1.09	1.09	0.40	0.23
4 (z)	1.10	1.19	1.19	-7.75	-7.86
5 (x&pitch)	1.15	1.11	1.11	3.42	3.37
6 (x&pitch)	1.51	1.53	1.53	-1.04	-1.26
7 (y&roll)	1.52	1.53	1.53	-0.43	-0.64
8 (yaw)	1.97	1.96	1.96	0.70	0.56
9 (y&roll)	2.16	2.14	2.14	1.00	0.84
10 (y&roll)	2.67	2.85	2.84	-6.71	-6.45
11 (x&pitch)	2.82	2.83	2.82	-0.26	-0.01
12 (yaw)	3.55	3.52	3.51	0.95	1.16
13 (y&roll)	3.61	3.77	3.77	-4.48	-4.56
14 (z)	4.06	4.25	4.26	-4.74	-4.87
15 (x&pitch)	4.10	4.40	4.40	-7.37	-7.43
16 (x&pitch)	5.65	5.70	5.70	-0.83	-0.88
17 (z)		46.04	46.05		
18 (y&roll)		65.47	65.49		

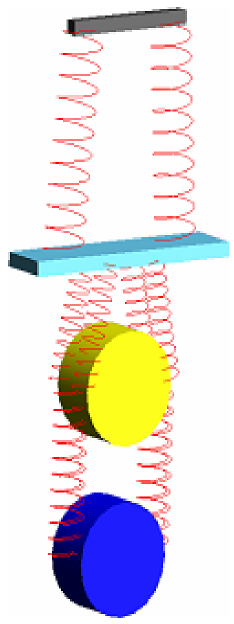

Table 2-2: Resonance frequencies, measurement and model

Once again, we see that our 2 models agree with each other and the measurement. The maximum error on the resonance frequencies reaches about 7%, which is likely due to the stiffness of the blades that can vary slightly from one blade to another.

2.4 RESONANCE DAMPING AND NOISES

We have seen before that one of the main purposes of the triple pendulum (and the suspensions in LIGO) is to filter the high frequencies seismic noise. In order to have a low thermal noise, it is important to have very low mechanical loss for the higher modes. This is why the pendulum is made of low loss materials (fused silica wires), the use of such materials also increase the Q of the low frequency rigid-body resonances. Unfortunately, this leads to a very large amplification of the seismic noise at the resonances and a large motion of the suspended mirrors.

Although these low frequencies aren't in the detection bandwidth of the LIGO interferometers, the resonances still need to be damped for several reasons. One of the main reasons is to keep the pendulum quiet enough so that the interferometers can be locked. We will see later what locking an interferometer means, but the important thing to bare in mind is that the distance between the pendulums needs to stay very stable. We can't afford large motion of the mirrors due to the high Q resonances. Therefore, the resonances must be damped.

Because there is a small coupling due to asymmetry or misalignment (about 0.1%) between the 6 degrees of freedom, all directions need to be damped.

To conclude, we need to damp the resonances at low frequencies in the 6 degrees of freedom, and let the passive isolation of the pendulum filter the high frequencies noise.

2.4.1 Noise inputs

The 2 seismic isolation stages between the ground and the pendulum (see section 1.2.4a)) filter the seismic noise to a very low level. Because those 2 stages use active isolation, the maximum isolation they can provide is determined by the noise level and the loop gain of these systems. By knowing this sensitivity, we can predict the future performances of the Advanced LIGO seismic isolation systems and know what is going to be the seismic noise level for the pendulum (see orange plot below).

At that level, the noise generated by the sensors used on the pendulum isn't negligible. This noise comes from 2 sources and has already been measured in laboratory. Above 10Hz, the noise comes from shot noise. Shot noise is a type of noise that occurs when the finite number of particles that carry energy, such as the photons in the case of our optical sensor, is small enough to give rise to detectable statistical fluctuations in a measurement. Below 10Hz, the noise goes up and this phenomenon hasn't been understood yet (see purple plot).

As we can see on figure 2.13, the sensor noise becomes the dominant noise above 0.8Hz and becomes about 500 times more important than the seismic noise coming from the ground at 10Hz. This level of measurement noise is something unusual in the active control field because it requires reaching extremely low level of displacement. The sensor noise is very often neglected. For LIGO's suspensions, the sensor noise is the main source of noise.

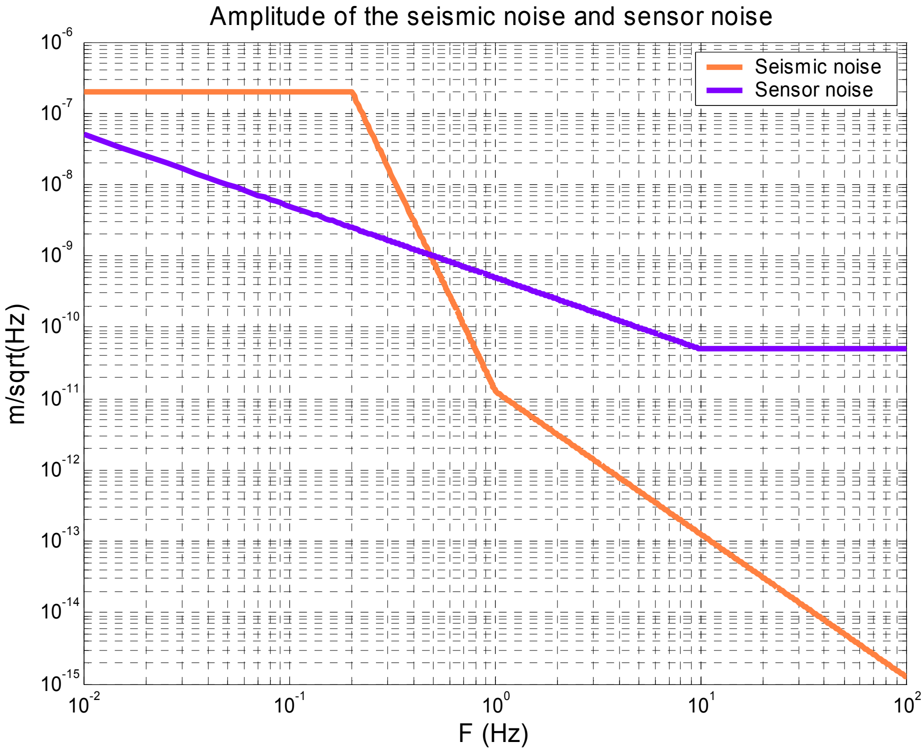

Figure 2.13: Noise sources for the triple pendulum

This is a new and very important parameter to the problem. To damp the pendulum, we need to use those sensors; however, the noise they generate is bigger than the seismic noise above 0.8Hz. This means that we are actually going to inject more noise at high frequencies, and deteriorate the passive isolation of the pendulum. The goal will be to design a control loop that damps the resonances but keeps the sensor noise transmission as small as possible.

2.4.2 Control requirements

Although the damping requirements haven't been decided in LIGO yet, we will use a simple settling time goal in order to compare different kind of control loops. Later, once the damping goals have been decided, this study will be easily adaptable to the new requirements.

We choose the settling time to an impulse excitation to be 10sec +/- 10%. We define the settling time as the time the bottom mass takes to come back below +/-10% of the maximum amplitude. We use the same damping goal for the 6 degrees of freedom, for every kind of loop we design.

The noise performances requirements for a mode cleaner triple pendulum are given in table 2-3 (see T010007-02) :

Direction	At 10 Hz $m/\sqrt{Hz}$ or $rad/\sqrt{Hz}$	At 100 Hz $m/\sqrt{Hz}$ or $rad/\sqrt{Hz}$
X	3e-17	3e-19
Pitch	3e-14	3e-16
Yaw	3e-14	3e-16
Y	3e-14	3e-15
Roll	3e-14	3e-15
Z	3e-14	3e-15

Table 2-3: Noise requirements for the triple pendulum

2.5 USUAL FEEDBACK CONTROL STRATEGY

In order to understand how the damping loop re-injects more noise in the pendulum, we will study some simple cases. We will see how the sensor noise is increasing the motion of the pendulum at high frequencies and how challenging designing a damping loop to solve this problem will be. The sensor noise will be modeled using white noise injection in the sensor path; the amplitude of this noise will match the OSEM noise.

2.5.1 Velocity damper

The usual strategy of control is to measure the first mass motion, filter this signal and re-inject it into the actuators of the first mass.

In this first example, we choose some very simple filters to damp the velocity of the pendulum for the X direction. The bode diagram of the plant, filter and open loop are shown in figure 2.14. The gain of the feedback is set so that the impulse settling time is 10sec (see figure 2.15). The equation of the filter is given below.

- $$F(s) = \frac{1.10^5 s}{(s+43.98)(s+188.5)} \qquad 2.1$$

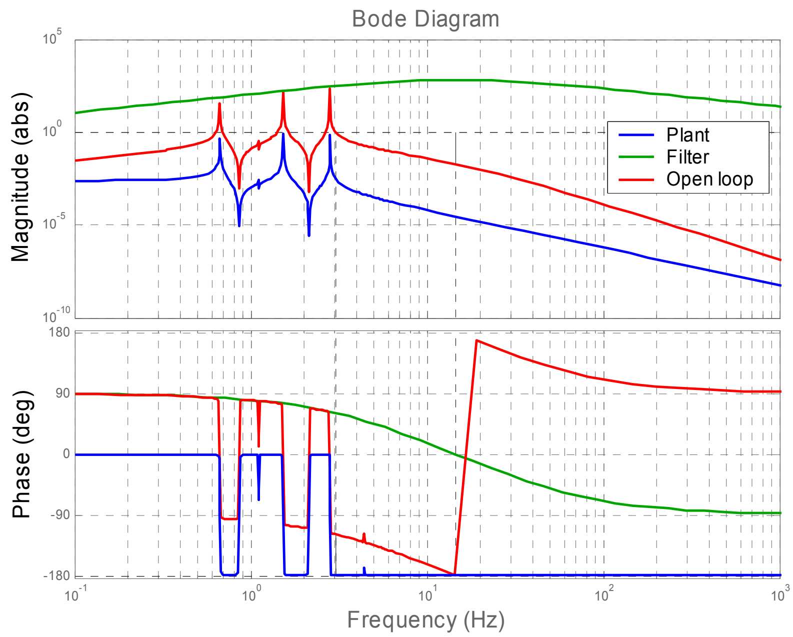

Figure 2.14: Velocity damper, loop filters

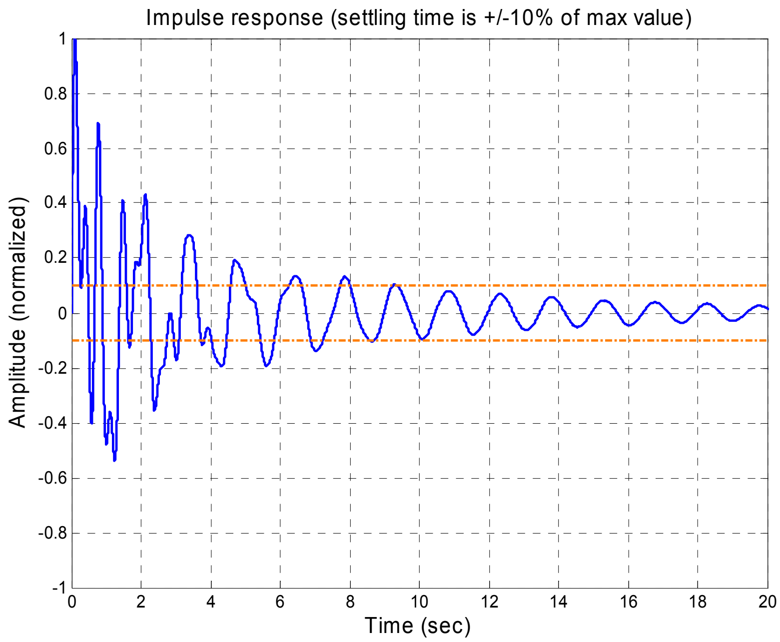

Figure 2.15: Velocity damper, impulse response

We can now look at the sensor noise transmission for this filter. A nice way to study the sensor noise transmission is to plot the amplitude of the pendulum's bottom mass motion. We use the sensor noise and seismic noise input given by the advanced LIGO estimation we have seen previously. We can study the amplitude with or without damping loop, and we can also see how much each noise (seismic and sensor) participate in the final amplitude.

Note that the final value of the Quality factor of each resonance is not accurately known yet since it will depend on many little parameters such as the quality of the assembly or the quality of the wire clamps. Moreover, it is very hard to have a frequency resolution that is good enough to get exactly the maximum amplitude of the peaks. To show this uncertainty, the amplitude of the un-damped pendulum at the resonances is plotted with dots.

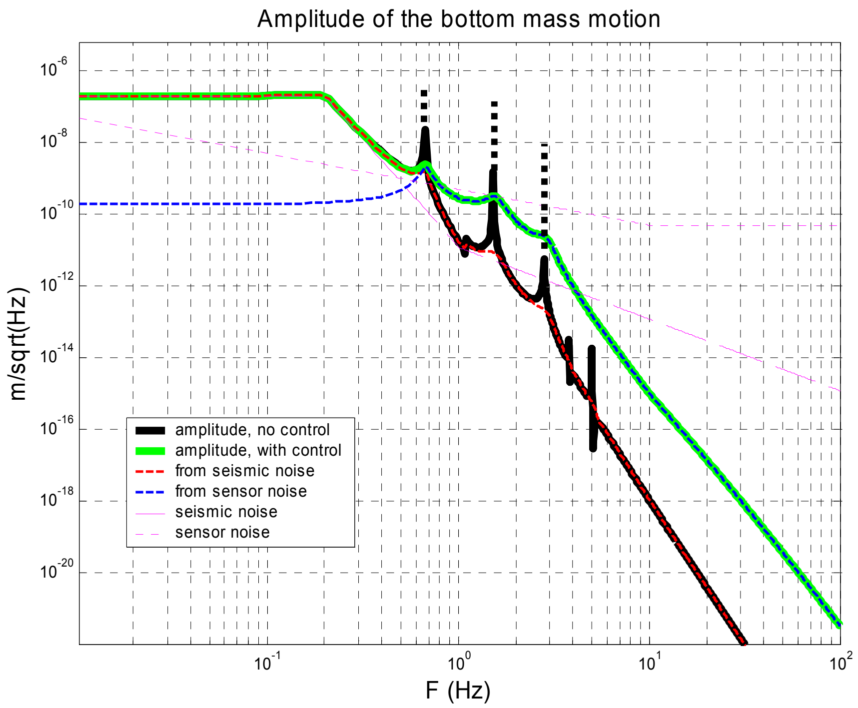

Figure 2.16: Velocity damper, amplitude of motion at the bottom mass

We see on figure 2.16 that the filter we use is very inefficient to filter the sensor noise at high frequencies. The green plot (amplitude of the bottom mass with damping on) is dominated by the sensor noise participation (blue) at high frequencies. Ideally, we would like to have the green plot as close as possible to the free swing plot (no active damping, in black) above 10 Hz. This result shows that more work needs to be done on the filtering and the damping loops.

2.5.2 Improving the filter

As we have seen before, using very simple damping filters doesn't give good performances in term of sensor noise transmission.

A first solution can be to work on more complicated filters to reduce the high frequencies gain as much as possible. The goal is to create a filter that drops down just after the last resonance. In the following example, you will see that such filters can be designed. However, it is a long and complicated process of iterations.

The filters we will use here have been designed in Glasgow, and then modified to be as efficient as possible for the triple pendulum we have in MIT.

Below is the example for the filter in the X direction (figure 2.17 and figure 2.18), you will notice the filter has been designed to minimize the noise above 10Hz while keeping a good phase margin and gain on the lowest modes to optimize the damping. This filter is a lot more complicated than the simple velocity damper shown above, the equation of the filter is written below:

- $$F(s)=\frac{6004s\,(s+13.4)(s+2.5)(s+1.9)(s+1.3)(s^2+1.6s+4027)(s^2+3.6s+5221)}{(s+37.7)(s+31.4)^2(s+1.2)(s^2+2.1s+17.6)(s^2+4.6s+2527)(s^2+28.3s+3198)} \qquad 2.2$$

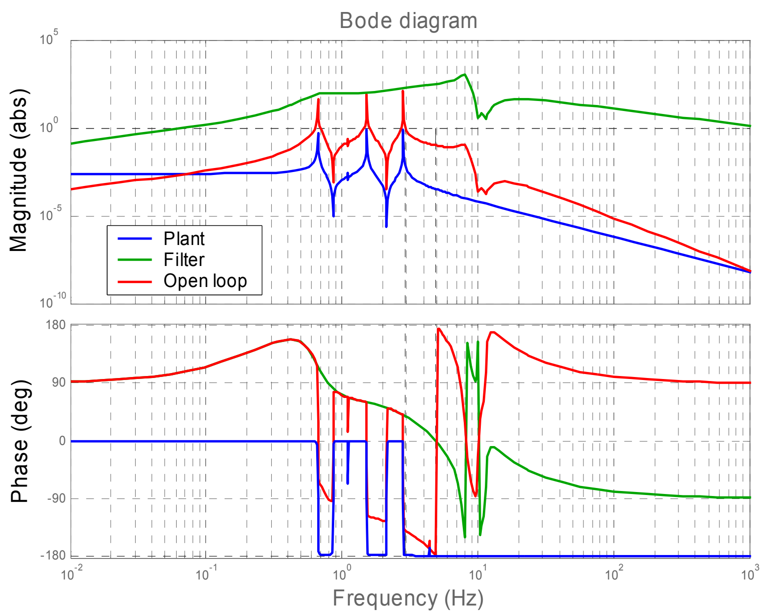

Figure 2.17: Improved damping, loop filters

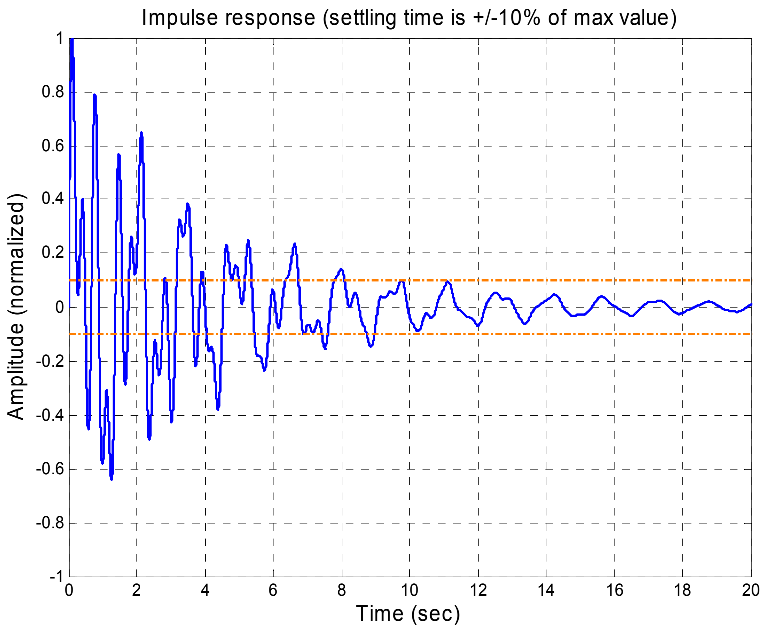

Figure 2.18: improved damping, impulse response

The amplitudes with Advanced LIGO noise inputs are now plotted in figure 2.19

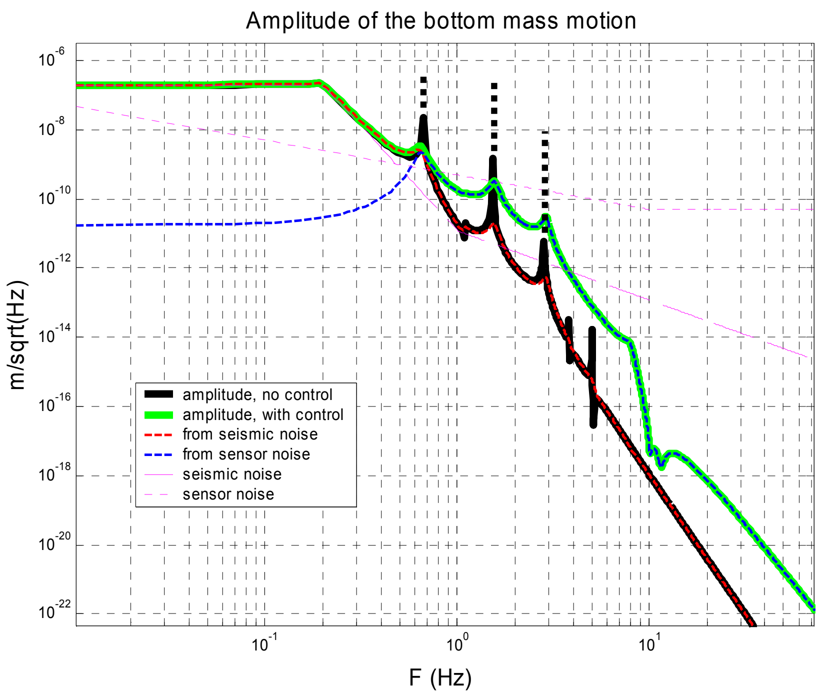

Figure 2.19: Improved damping, amplitude at the bottom mass

The sensor noise transmission has been slightly reduced compared to our previous example. But we are still adding a lot of noise in the high frequencies. This filter is giving the best results we can expect from this method, which means that improving the performances will only be possible by changing the damping method. We will see in the next sections that using a new and different approach can provide very good results.

3 CONTROL THEORY

3.1 INTRODUCTION

We have seen in the previous section that the design of the damping loops is not trivial. The sensor noise dominates the measurement above 1Hz and we need to minimize the re-injection of this noise into the pendulum.

Instead of patching the current damping loops, the idea followed in this document is to re-design the control using different techniques and study both the sensor noise transmission and the damping for every choice we make.

Several control strategy have been considered. A first solution would be to use more complicated IIR or FIR filters with notches and bumps at the resonances. This is unfortunately not very flexible, the filters would have to be re-designed for each suspension and each degree of freedom and it would be very time-consuming. The damping loop would also be difficult to tune. If a decision is taken that one mode requires more damping at some point, the whole filter would have to be re-worked. As shown previously, even complicated filters don't provide very good results.

Other more flexible methods have been considered, for example robust control method like H_∞ or H_2 could be used for the controller or the estimator [45]. These methods are easier to adapt to new suspensions since you can modify the weighting functions in the norm to modify the damping performances. However, robust controls are optimized for the worst-case scenario; they are very efficient when the model of the plant is not well known, but the performances they provide are usually poor.

In the LIGO case, the robustness is not necessary but high performances need to be achieved. The model of the suspension is very well known and this information can be used with optimal control methods. It is also necessary to design a control loop that is both simple and flexible so the loop can be adapted to other suspensions and can be modified easily if the requirements or the environment change. Modal control [35][37][38] provides this flexibility and makes the sensor noise filtering easier; the LQ method [41] is often used with modal control because the linear system can be written in its modal basis for the optimization. Last but not least, the LQ optimization ensures the stability that is necessary for such a costly system.

The method we choose is called Independent Modal Control (IMC), which involves working in a different basis where the equations of the dynamics are more simple and decoupled. In the case of the triple pendulum, the dynamics can be decoupled into 18 separate systems that we can easily control independently from each other. The technique provides excellent results and simplifies the design of complex control laws.

Because the control in modal state is simpler and equations become decoupled, we will see that it is also easier to study the sensor noise transmission.

In order to use IMC, one must know the full state of a system. This is not always possible because we can't always measure every degree of freedom of a given structure. For our triple pendulum, we can only measure the motion of the top mass. It is possible to reconstruct the full state of a system by using an observer. The observer consists of a second loop that uses the model of the structure to reconstruct missing data and minimize the error between those data and the one we can measure. Several kinds of observers can be designed and different techniques exist to optimize them. In this section, we will introduce the theory of modal control as well as the different kinds of observers, disturbance observers and LQ theory.

3.2 MODAL CONTROL

Instead of controlling the system in the "real" basis where (x1,x2,x3…) are the motion of each mass of the pendulum, we apply a mathematic change to work in a new, more simple basis called the modal state (q1,q2,q3…). In this new basis, the equations are decoupled, which provides 2 advantages:

1. The control design is easier because each mode can have it's own simple controller
2. The control of each mode can be optimized so that the sensor noise injection is reduced

The idea is simple; we want to find the basis change that will decouple the equation of motion.

3.2.1 Mathematics

Let's start with the equation of free motion in the real (x) basis (M is the mass matrix, K is the stiffness matrix and x is the vector containing the real states like the motion of the 1st, 2nd and

3rd mass). Because the quality factor of LIGO pendulum is very high (the natural damping is negligible) , the damping term is not included in the following explanations.

- $M\ddot{x} + Kx = 0$ 3.1

We apply the transformation $x = Xe^{i\omega t}$

- $\omega^2 MX = KX$ 3.2
- $M^{-1}KX = X\omega^2$ 3.3

This is an eigenvalues problem where ω^2 are the eigenvalue of $M^{-1}K$ and X are the eigenvectors of $M^{-1}K$. We call ϕ the matrix formed by the eigenvectors X .

Let's now write two solutions of equation 3.3

- $\begin{cases} \omega_i^2 M\phi_i = K\phi_i \\ \omega_j^2 M\phi_j = K\phi_j \end{cases}$ 3.4

By pre-multiplying by $\phi_j^{\,t}$ and $\phi_i^{\,t}$

- $\begin{cases} \omega_i^2 \phi_j^{\,t} M\phi_i = \phi_j^{\,t} K\phi_i \\ \omega_j^2 \phi_i^{\,t} M\phi_j = \phi_i^{\,t} K\phi_j \end{cases}$ 3.5

We then transpose of the second equation, because M and K are symmetrical matrices, we have $M = M^t$ and $K = K^t$

- $\begin{cases} \omega_i^2 \phi_j^{\,t} M\phi_i = \phi_j^{\,t} K\phi_i \\ \omega_j^2 \phi_j^{\,t} M\phi_i = \phi_j^{\,t} K\phi_i \end{cases}$ 3.6

- $\left(\omega_j^2 - \omega_i^2\right)\phi_j^{\,t} M\phi_i = 0$ 3.7

If $\omega_j^2 \neq \omega_i^2$ which is the case most of the times, it follows that

- $\phi_j{}^t M \phi_i = 0$ *3.8*

Similarly, one can show that

- $\phi_j{}^t K \phi_i = 0$ *3.9*

By applying the transformation $x = \phi\, q$ to the equation of motion and by pre-multiplying by ϕ^t, we obtain the modal equation of motion

- $\phi^t M \phi + \phi^t K \phi = \phi^t F$ *3.10*

These equations are now uncoupled and working with the new variable q enables a better and easier design of the control loop.

3.2.2 Application to control

Having the computer applying the variable change inside a control loop is simple, as you can see on the diagram in figure 3.1:

- We change the basis by multiplying the real output by ϕ^{-1}
- The new variables (q1,q2,q3,…) can be controlled one by one without having to worry about coupling.
- We go back to the real basis by multiplying the real data by $(\phi^t)^{-1}$ to apply the force

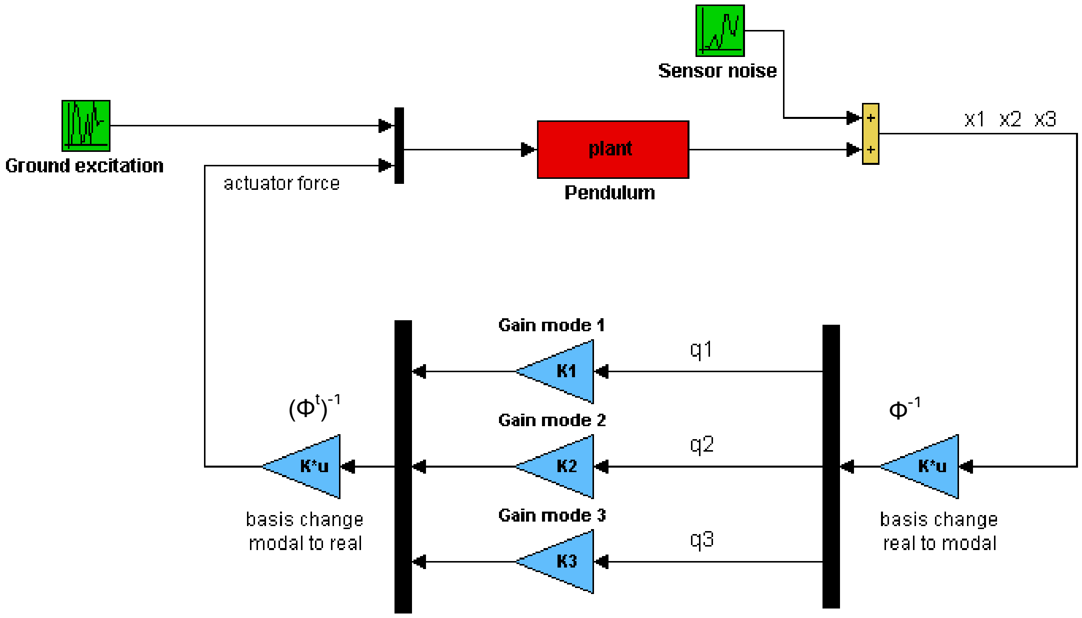

Figure 3.1: Modal control loop diagram

In the following example, we will study the case of the vertical (x becomes z) motion of the mode cleaner triple pendulum; this is a 3 dof system with 3 resonances at 1.2 Hz, 4.8Hz and 46.3 Hz.

We use this plant in our diagram shown above and check the results of the basis change :

- We plot the Bode magnitude of the transfer function from ground to z1 (motion of the first mass in the vertical direction), q1, q2 and q3 (modal displacements)
- We plot the step response from ground to z1, q1, q2 and q3

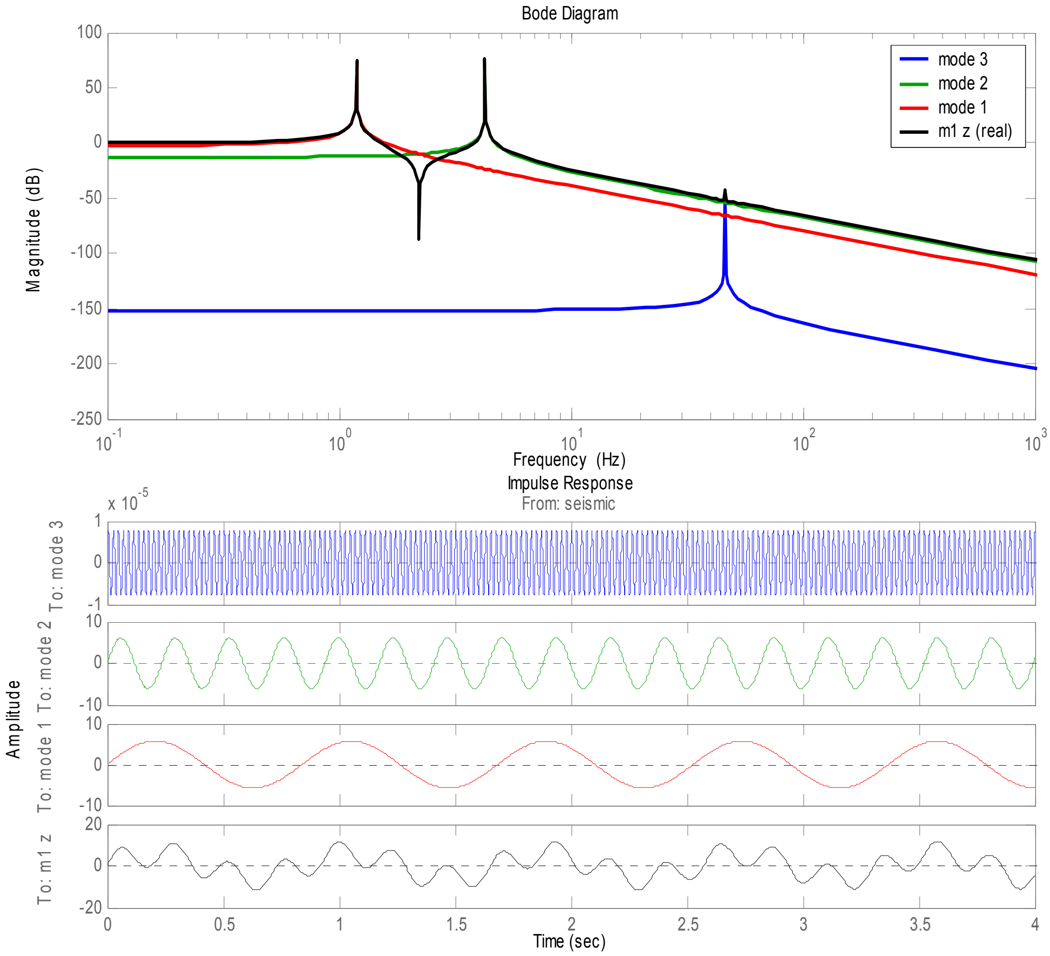

Figure 3.2: Modal decomposition

As we can see in figure 3.2, Instead of having one complex 3dof system (black), we have 3 simple single dof systems that we can control separately. We are now able to design a control more easily.

3.2.3 Modal control and sensor noise

We have seen how modal control makes the control easier to design. In term of damping/sensor noise, the main advantage of this technique is that each mode can be studied and controlled one by one:

- The lowest modes are the dominant mode in term of energy and motion, thus the biggest gain are required on the lowest modes

- Because the lowest modes are at the lowest frequencies, they are very easy to filter. By looking at the plots above, one can notice the lowest modes already naturally filter the high frequencies and thus the sensor noise.
- The highest modes have a very weak participation in term of energy and motion, the gain required to damp them can be much smaller
- The highest modes carry most of the sensor noise in the loop, by using small gain on those modes; we can reduce the sensor noise transmission in the control loop.

To conclude, the modal control enables us to use high gain on the lowest mode, while using lower gain for the highest modes (and thus decrease sensor noise transmission). Each mode can also have its own filter optimized to reduce the sensor noise re-injection.

3.2.4 Conclusion

We have seen the modal control method has 2 main advantages

1. It makes control design easy
2. It helps to reduce sensor noise injection

However, it is important to remember it also have drawbacks:

1. It needs a good model to generate the eigenvector matrix
2. We need to measure as many degrees of freedom as the number of modes we want to control (i.e. we need to know the "full state"). This is not always possible.

In our case, we don't have as many sensors as degrees of freedom, which make a direct modal decomposition impossible to achieve. To surmount this problem, we will use an observer that will reconstruct the missing states. There are several types of observers, in the following sections; we will look at the theory for the disturbance observers and the state observers.

3.3 OBSERVING THE STATES OF A SYSTEM

We have seen previously that we can only use modal control if we can measure the full state; which is unfortunately not the case in the Advanced LIGO suspensions. We need to have a way to generate this missing data.

The method we will use is called an observer and has been developed by Luenberger [38], It consist of running a model of our structure in parallel with the real plant. The model can generate as many outputs as needed to reconstruct the data we can't measure; however, the model doesn't have all the inputs of the plants (the seismic noise is unknown and not measurable for example), the model can also be slightly inaccurate. In order to compensate for those two unknowns, the outputs of the model are compared to the outputs of the plant we can measure, and the difference is used as an error to minimize by applying a feedback loop to the model.

There are different ways to apply this feedback into the model. We will see in the following sections different methods to optimize this system.
First, we will study a very simple observer with a feedback applied to the input force of the model, this is called disturbance observer because we minimize the observation error by trying to re-construct the disturbance applied to the plant.

Then, we will study a more advanced observer using LQ optimal control techniques to apply the feedback directly on the states. We will see that this kind of observer can also directly provide the modal states of the system.

3.4 SIMO DISTURBANCE OBSERVER

This observer consists of a model of the plant running in parallel with the real plant. This model generates the outputs that we can measure as well as all the outputs that are impossible to measure. However, this model doesn't "see" the inputs to the real plant.

In order to have the model follow the plant without having the seismic input, we will use the output of the observer and compare it with the signal we can measure on the real plant. This comparison gives us an error between the model output and the plant output. We can then feedback this error to the model to minimize it.

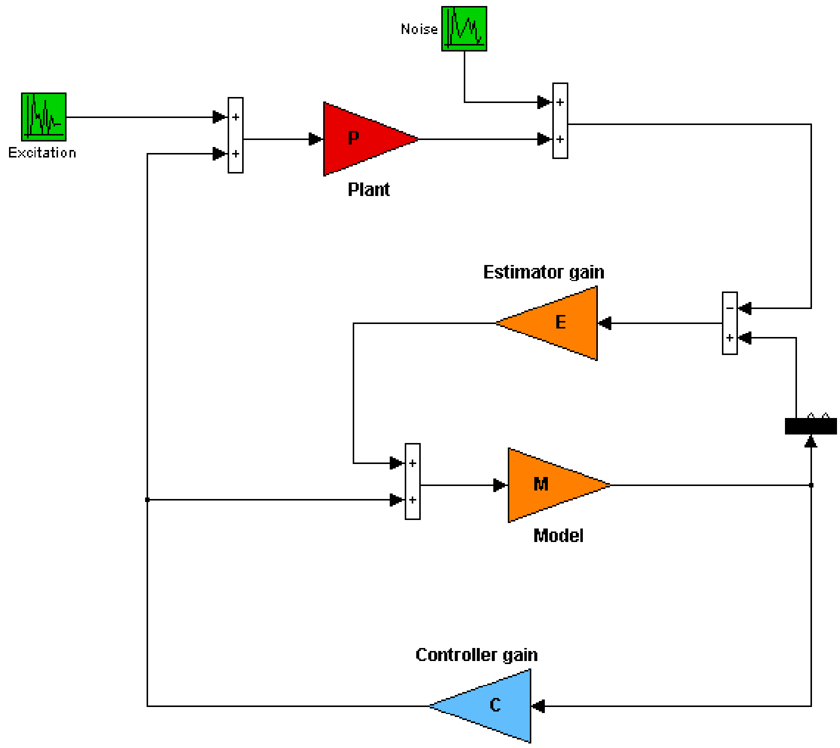

Figure 3.3: Loop diagram with controller and observer

Let’s now focus on the observer only and forget the controller for a few moments:

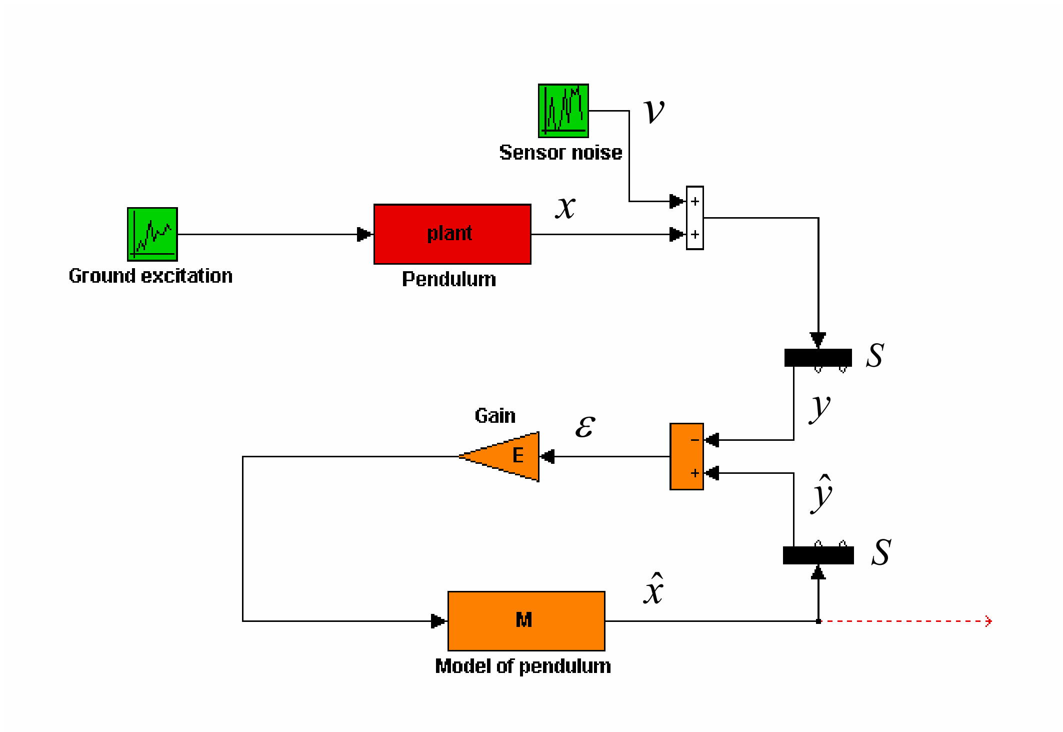

Figure 3.4: Disturbance observer loop diagram

1. The ^ sign is used for estimated states and measurements
2. x is the complete state (for ex $m1_x$ $m2_x$ $m3_x$)
3. y is the part of the state we can measure ($m1_x$)
4. The gain E is the feedback gain and filter
5. S is a simple matrix represented by the 2 black demux boxes. S is the matrix to go from the full state to the measured state. For example, for a 3dof system, S=[1 0 0] if we can only measure the first DoF

- $\varepsilon = \hat{y} - y = S.\hat{x} - S.x - S.v$ 3.11
- $\hat{x} = M.E.\varepsilon$ 3.12
- $\hat{x} = M.E.S.\hat{x} - M.E.S.x - M.E.S.v$ 3.13
- $\hat{x} = M.E.S.[M.E.S - 1]^{-1}.x + M.E.S.[M.E.S - 1]^{-1}.v$ 3.14

The observer enables us to retrieve the entire state because each mode is coupled to the first mass (the suspensions have been designed for that), M is not diagonal and we can generate missing data with the model and signal we can measure.

The observer feedback (called observer filter or observer gain) can be any kind of control; it can be SISO, SIMO or MIMO.

We will see later that we only use this kind of observer as a SIMO system (we measure one state and observe and reconstruct several states), because the control laws are easy to determine and it is possible to analyze the sensor noise transmission in this case. This observer is very well adapted to the degrees of freedom Z and yaw, because we only have one measurement (the motion of the top mass) and try to reconstruct the 3 modes.

However, it is more complicated to use for the coupled degrees of freedom X and Pitch, or Y and roll. In that case we have 2 inputs (angle and displacement) and 2 outputs (torque and force) and all are coupled to each other.

In the following section, we will use another approach, the state space formulation, as a tool to design and optimize a MIMO observer. We will use what is called optimal control technique and see how they can be applied to our system. The word “optimal” doesn’t mean that we will find the one solution that is the best; rather, the idea is to give the designer a tool, a cost function, to optimize the control laws to suit their wishes.

3.5 OPTIMAL CONTROL, LINEAR QUADRATIC REGULATOR

Before looking at the observer, let’s look at the LQR method and how to optimize a MIMO control using the state space approach. This method will be directly translated to the design of a MIMO observer.

We have the following discrete state-space system:

- $x_{k+1} = Ax_k + Bu_k$ *3.15*

And the following control loop

- $u_k = -Kx_k$ *3.16*

The following method describes how to find the optimal K (K is a matrix for a MIMO system) to minimize a cost function chosen by the designer. The diagram of the loop is shown below.

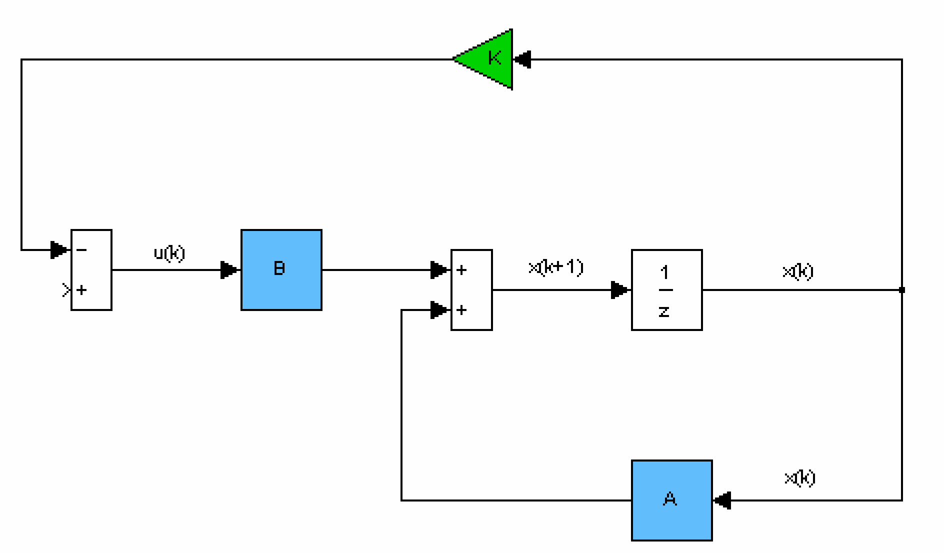

Figure 3.5: LQR control diagram

Our goal is to choose u to minimize the following cost function:

- $$J = \frac{1}{2}\sum_{k=0}^{N} x_k^T Q_1 x_k + u_k^T Q_2 u_k \qquad 3.17$$

While constraining

- $$-x_{k+1} + Ax_k + Bu_k = 0 \qquad 3.18$$

Note that this cost function contains 2 terms, one is related to the motion of the system, and weighted by the matrix Q_1, the other one is related to the quantity of force injected, and is weighted by the matrix Q_2. Those 2 matrices need to be positive and symmetrical (this is easily accomplished by picking those matrices to be diagonal with all diagonal elements positive or zero). By tweaking Q_1 and Q_2, the designer can decide the relative importance of the various states and controls.

This is a standard constrained-minima problem which can be solved using the method of Lagrange Multipliers which consist in turning a constraint problem in n variables to an unconstrained problem with n+1 variables.

We introduce one Lagrange multiplier vector, called $\lambda(k+1)$ for each value of k.

- $$J^{'} = \frac{1}{2}\sum_{k=0}^{N} x_k^T Q_1 x_k + u_k^T Q_2 u_k + \lambda_{k+1}^T\left[-x_{k+1} + Ax_k + Bu_k\right]$$ 3.19

We are looking for the minimum of $J^{'}$ with respect to $x(k)$, $u(k)$ and $\lambda(k+1)$

- $$\frac{\partial J^{'}}{\partial u_k} = u_k^T Q_2 + \lambda_{k+1}^T B = 0 \qquad u_k = -Q_2^{-1} B^T \lambda_{k+1}$$ 3.20
- $$\frac{\partial J^{'}}{\partial \lambda_{k+1}} = -x_{k+1} + Ax_k + Bu_k = 0 \qquad x_{k+1} = Ax_k + Bu_k$$ 3.21
- $$\frac{\partial J^{'}}{\partial x_k} = x_x^T Q_1 - \lambda_k^T + \lambda_{k+1}^T A = 0 \qquad \lambda_k = A^T \lambda_{k+1} + Q_1 x_k$$ 3.22

Equation 3.20 is called the control equation, 3.21 is called the state equation and 3.22 is the adjoint equation.

One method to solve this system of equations is to use the sweep method and assume

- $$\lambda_k = S_k x_k$$ 3.23

This definition allows the transformation of the two-point boundary-value problem in x and λ to one in S with a single-point boundary condition.

The control equation (3.20) becomes

- $$u_k = -Q_2^{-1} B^T S_{k+1} x_{k+1}$$ 3.24
- $$Q_2 u_k = -B^T S_{k+1}\left[Ax_k + Bu_k\right]$$ 3.25
- $$\left[Q_2 + B^T S_{k+1} B\right] u_k = -B^T S_{k+1} A x_k$$ 3.26
- $$u_k = -\left[Q_2 + B^T S_{k+1} B\right]^{-1} B^T S_{k+1} A x_k$$ 3.27

The adjoint equation (3.22) becomes

- $S_k x_k = A^T S_{k+1} x_{k+1} + Q_1 x_k$ 3.28
- $S_k x_k = A^T S_{k+1} A x_k + A^T S_{k+1} B u_k + Q_1 x_k$ 3.29
- $S_k x_k = A^T S_{k+1} A x_k + A^T S_{k+1} B\left[Q_2 - B^T S_{k+1} B\right]^{-1} B^T S_{k+1} A x_k + Q_1 x_k$ 3.30
- $S_k - A^T S_{k+1} A + A^T S_{k+1} B\left[Q_2 + B^T S_{k+1} B\right]^{-1} B^T S_{k+1} A - Q_1 = 0$ 3.31

This last equation is known as the Ricatti equation.

The steady state is assumed when there is no variation of S anymore, we can then assume that

- $S_{k+1} = S_k$ 3.32

The Ricatti equation becomes the algebric Ricatti equation :

- $\boxed{S - A^T SA + A^T SB\left[Q_2 + B^T SB\right]^{-1} B^T SA - Q_1 = 0}$ 3.33
- $\boxed{u = -\left[Q_2 + B^T SB\right]^{-1} B^T SAx}$ 3.34

K is the control gain given by

- $\boxed{K = \left[Q_2 + B^T SB\right]^{-1} B^T SA}$ 3.35

The resolution of this equation is purely mathematics and won't be explained here. A good description of the solution using the eigenvector decomposition is explained in reference [41].

3.6 USING OPTIMAL CONTROL TECHNIQUE TO DESIGN A MIMO OBSERVER

We have seen how to design a MIMO control to minimize a cost function. We will now see that it is fairly easy to adapt this method to the design of a MIMO state observer.

The state observer is similar to what we have seen with the SIMO disturbance observer. The main difference is that the feedback is not made on the force input, but directly on the states. The feedback matrix is now called L instead of K. The diagram of this observer is shown in figure 3.6

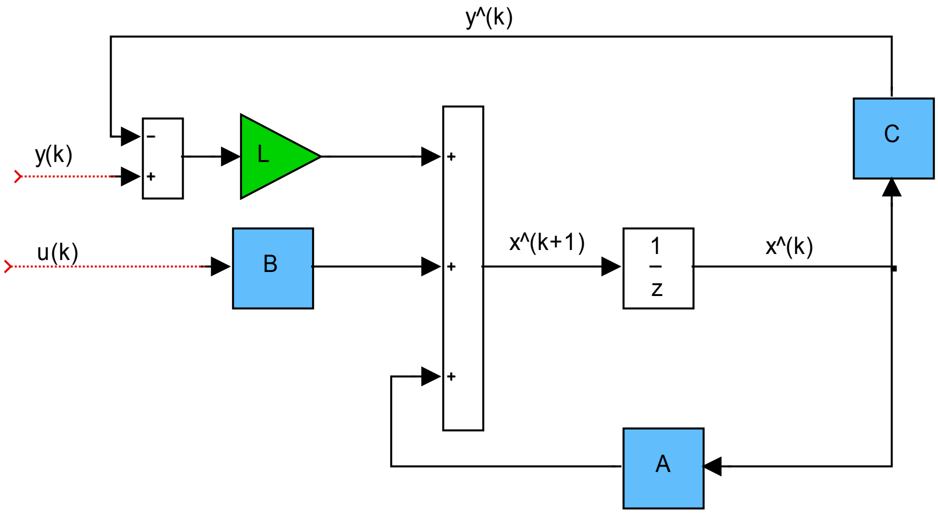

Figure 3.6: Luenberger observer diagram

The new discrete state-space loop becomes

- $\hat{x}_{k+1} = A\hat{x}_k + Bu_k + L(y_k - \hat{y}_k)$ 3.36

Where y_k is the measured state and $\hat{y}_k$ is the estimated measured state.

We call the estimation error ε_k

- $\varepsilon_k = x_k - \hat{x}_k$ 3.37
- $\varepsilon_{k+1} = Ax_k + Bu_k - A\hat{x}_k - Bu_k - L(y_k - \hat{y}_k)$ 3.38
- $\varepsilon_{k+1} = A(x_k - \hat{x}_k) - LC(x_k - \hat{x}_k)$ 3.39
- $\varepsilon_{k+1} = A\varepsilon_k - LC\varepsilon_k$ 3.40

Because the dynamics (eigenvalues) of $A - LC$ and $A^T - C^T L^T$ are the same, we can write:

- $\varepsilon_{k+1} = A^T \varepsilon_k - C^T L^T \varepsilon_k$ 3.41

We retrieve a structure similar to the one seen for the LQR design:

- $\varepsilon_{k+1} = A^T \varepsilon_k + C^T z_k$ 3.42
- *with* $z_k = -L^T \varepsilon_k$ 3.43

We can solve this problem the same way we did before by replacing:

- $A \longrightarrow A^T$ 3.44
- $B \longrightarrow C^T$ 3.45
- $K \longrightarrow L^T$ 3.46

The new cost function is

- $J = \frac{1}{2}\sum_{k=0}^{N} \varepsilon_k^T Q_1 \varepsilon_k + z_k^T Q_2 z_k$ 3.47

Q_1 now weights the estimation error for each state (how well do we want to estimate each state).
Q_2 weights the feedback we want to use to compensate for the estimation error (How much do we want to use the measurement to estimate the next state), the smaller this weight is, the less sensor noise we will transmit but the slower will our control loop be.

By tweaking Q_1 and Q_2, we can now design an optimal state observer and minimize the sensor noise transmission of our observer.

However, we also see that Q_1 is not very easy to choose: how can we decide which state is more important than another, since we are going to use the modes, and not the state, in our controller.

3.7 MIMO MODAL OBSERVER

A simple solution is to build a modal observer, where the observer doesn't generate the states, but directly the modal states of our system. At the output of the observer, the modes can be combined to form the real states, and we can compare these states to the measurement in order to feedback the observer. The new diagram becomes:

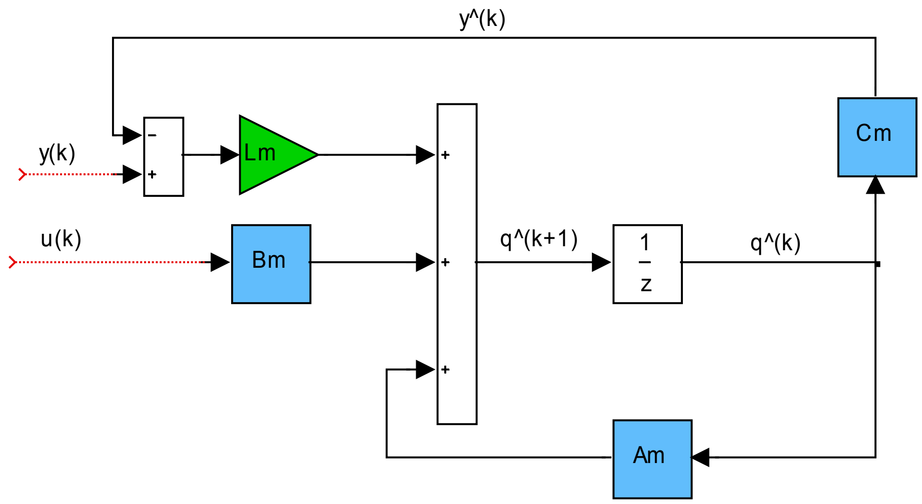

Figure 3.7: Modal observer diagram

Where (see section 3.2)

- $A_m = \phi^{-1} A \phi$ 3.48
- $B_m = \phi^{-1} B$ 3.49
- $C_m = C\phi$ 3.50

The new observation error is applied on the modes:

- $\delta_k = q_k - \hat{q}_k$ 3.51

And the new observer is described by the following equation

- $\delta_{k+1} = A_m{}^T \delta_k - C_m{}^T L_m{}^T \delta_k$ 3.52
- $\delta_{k+1} = A_m{}^T \delta_k + C_m{}^T z_k$ 3.53
- *With* $z_k = -L_m{}^T \delta_k$ 3.54

The modal states are now estimated instead of the real state. The problem can be solved the same way we did before with those new matrices and using the new cost function:

- $J = \frac{1}{2} \sum_{k=0}^{N} \delta_k^T Q_1 \delta_k + z_k^T Q_2 z_k$ 3.55

The difference is that Q_1 now weights each modal state instead of each real state, and is easier to choose, we could for example decide to estimate the lower modes more accurately than the highest modes.

4 MODAL DAMPING AND ESTIMATION, A NEW APPROACH TO REDUCE SENSOR NOISE TRANSMISSION

We have seen in the previous section how to build an Independent Modal Controller as well as an observer. We have described the mathematics and theory for two kinds of observers, the disturbance observer, and the state-space observer.

In this section, we will see that the observer can also become a great tool to reduce the sensor noise transmission. When used to reconstruct the original states of a system using noisy measurement, the observer can be called an estimator.

4.1 SIMO DISTURBANCE ESTIMATOR AND MODAL CONTROL

4.1.1 From observer to estimator, behavior with sensor noise

In section 3.4 we have seen that the observer output could be written as a function of the real output and the sensor noise. In order to study the behavior of the estimator with sensor noise, we will study a one degree of freedom system, the conclusions can then be adapted to a n-dof system and we would use matrices of transfer functions instead of simple transfer functions. We can write equation 3.10 as:

- $$\hat{x} = \frac{M.E.S}{M.E.S-1}.x + \frac{M.E.S}{M.E.S-1}.v \qquad 4.1$$

Where

- $\hat{x}$ is the estimated state (at the output of the estimator)
- x is the real state (at the output of the plant)
- v is the measurement noise
- M is of the model of the plant (transfer function)
- E is the observer/estimator filter (transfer function)
- S is the matrix to go from the full state to the measured state

At first sight, it seems that the measurement noise and the real states are treated the same way by the estimator. However, it is important to remember that M is the model representing the plant, and its dynamics plays an important role.

We will study the transmission of the estimator close to the resonance (where the estimation needs to be accurate) and at high frequencies (where the measurement noise needs to be filtered).

At resonance, when the model transfer function is big:

- $\hat{x} \xrightarrow{M \to \infty} x + v$ 4.2

The estimated output is equal to the real output plus the sensor noise, the accuracy of the estimation will be good, although no sensor noise will be filtered (which is not important at those frequencies).

At high frequencies, where the model transfer function is very small due to the passive filtering of the pendulum:

- $\hat{x} \xrightarrow{M \to 0} M.E.S.x + M.E.S.v$ 4.3

The noise and the real data are filtered, the accuracy of the estimation decreases. This is useful above the resonances to filter out the sensor noise.

We see that the estimator loop has an interesting behavior for noise filtering. At the resonance, it will keep the transmission high which enables us to add a control and damp those resonances. At higher frequencies, the transmission will go down and it will filter the measurement noise. Overall, the estimator will act like a tuned filter that keeps the dynamics untouched at the resonance frequencies but filters the high frequencies out.

One can plot the transfer function from $x \; to \; \hat{x}$ for a single dof system (simple pendulum with a resonance at 1Hz) for different gains of E (we will use a very simple estimator filter for this example):

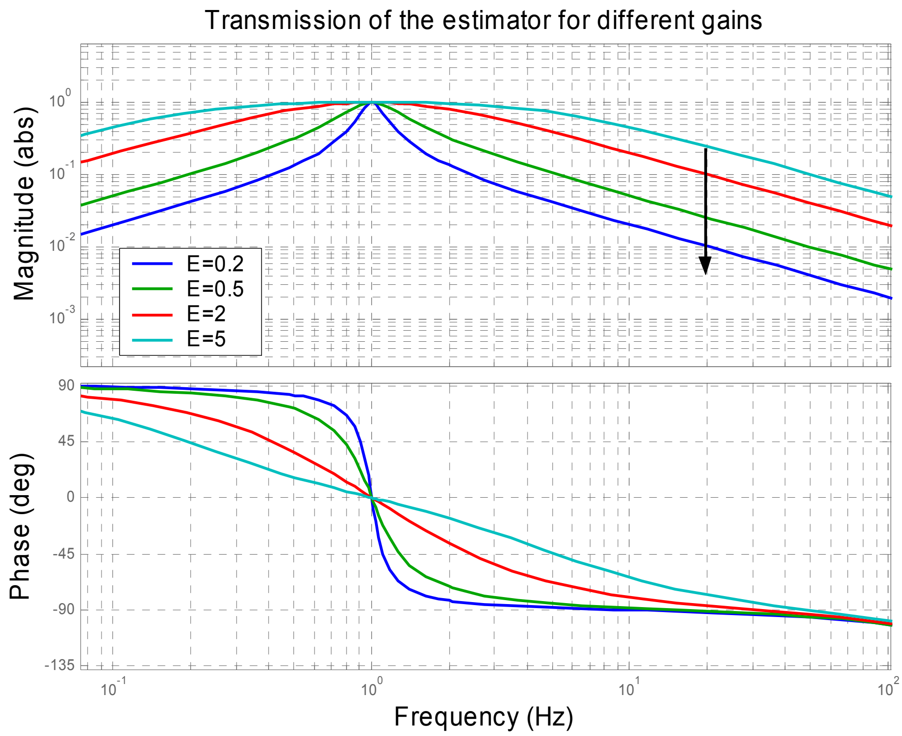

Figure 4.1: transmission of the estimator for several values of the estimator feedback gain

Figure 4.1 confirms what we saw above. The transmission at the resonance (1Hz) stays high even with lower estimator gains. Meanwhile, reducing the gain enables us to reduce the transmission at high frequencies (see arrow). Reducing the estimator gain is a good way to reduce the high frequencies measurement noise transmission. However, the drawback of reducing the gain is that the phase around the resonance frequency drops faster, which could cause problems with the damping performances or even stability. We will see below how to choose this gain to optimize the estimator and keep the control loop stable and efficient at the same time.

4.1.2 Control and SISO disturbance estimator, loop model

Let's now focus on the combination of the controller and the estimator, and see how it behaves with noisy measurements.

The diagram of the loop is shown in figure 3.3.

The plant is driven by the seismic noise w and the output of the plant is added to the measurement noise v. This signal is then injected into the estimator and the output of the estimator $\hat{x}$ (reconstructed state) is injected in the controller C to generate the feedback force.

The mathematical model of the loop is:

- $x = P.(w+u)$ 4.4
- $x = P.(w + C.\hat{x})$ 4.5

Let's now calculate the estimated state

- $\hat{x} = M.(u + E.\varepsilon)$ 4.6
- $\hat{x} = M.(C.\hat{x} + E.(\hat{x} - x - v))$ 4.7
- $\hat{x} = \dfrac{M.E.(x+v)}{M.C + M.E - 1}$ 4.8

If we introduce $\hat{x}$ into the first equation

- $x = P.w + \dfrac{P.C.M.E.(x+v)}{M.C+M.E-1}$ 4.9
- $\boxed{x = \left[\dfrac{P.M.C + P.M.E - P}{M.C + M.E - 1 - P.C.M.E}\right].w + \left[\dfrac{P.M.C.E}{M.C + M.E - 1 - P.C.M.E}\right].v}$ 4.10

4.1.3 Behavior with sensor noise

The model gives us x as a function of the seismic noise and of the sensor noise. Let's now study its behavior at limits.

When E is big:

$E \to \infty$

- $x = \left[\dfrac{P}{1-P.C}\right].w + \left[\dfrac{P.C}{1-P.C}\right].v$ 4.11
- This is the behavior of a loop with no estimator. The measurement noise is re-injected in the loop as shown in the second term.

When E is small:

$E \to 0$

- $x \to \left[\dfrac{P.(M.C-1)}{M.C-1}\right].w + \left[\dfrac{0}{M.C-1}\right].v$ *4.12*
- $x \to [P].w + [0].v$ *4.13*
- When the estimator gain goes to 0, the loop behaves as if there was no control. The measurement noise isn't injected anymore and the pendulum is free-swinging.

The goal will be to choose the best shape and gain for the estimator E. A compromise between sensor noise transmission and damping efficiency needs to be made.

The shape of the filter is easy to design; it needs a high gain on the resonance bandwidth and a lower gain at high frequencies. It is also important to keep the estimator loop stable. The following shape meets all these requirements:

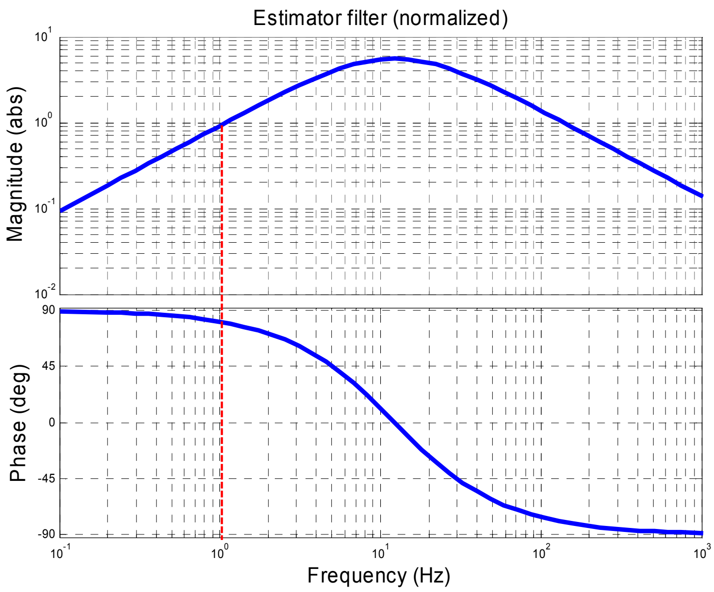

Figure 4.2: Estimator filter shape, normalized at 1Hz

To begin with, the filter's magnitude is normalized using the first resonance frequency. Then we will tweak the gain of this filter to optimize the loop. How this gain is optimized is explained below.

The gain of the estimator filter still needs to be determined, in order to choose the best value of the estimator gain E, one can use the loop's model to study both the sensor noise transmission and the damping efficiency for a given value of E.

For each gain of the estimator E, we compute the settling time. It is indicated by the red arrow on figure 4.3.

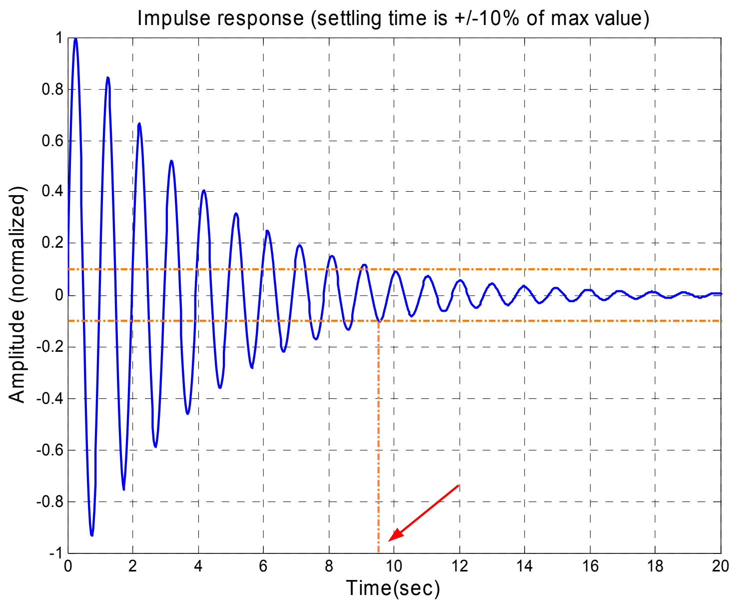

Figure 4.3: Impulse response for E=-1

And the sensor noise transmission (red arrow) at a given frequency (we choose 20Hz) is shown on figure 4.4:

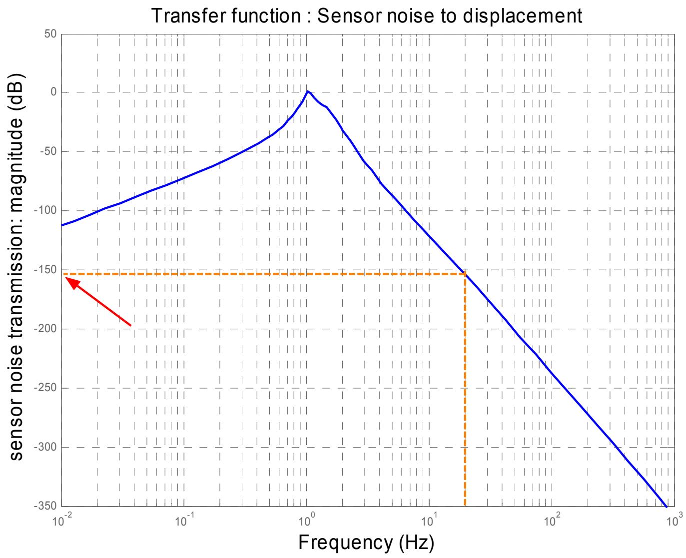

Figure 4.4: Sensor noise transmission for E=-1

Both the settling time and the sensor noise transmission at 20Hz are then combined in figure 4.5 (As an example, the values indicated by red arrows in the figures above is shown). The color shows the estimator gain, the X value is the sensor noise transmission (the lower the better), and the Y value is the settling time representing the damping performances (the lower the better). The best area for damping and sensor noise in this plot is the lower left one.

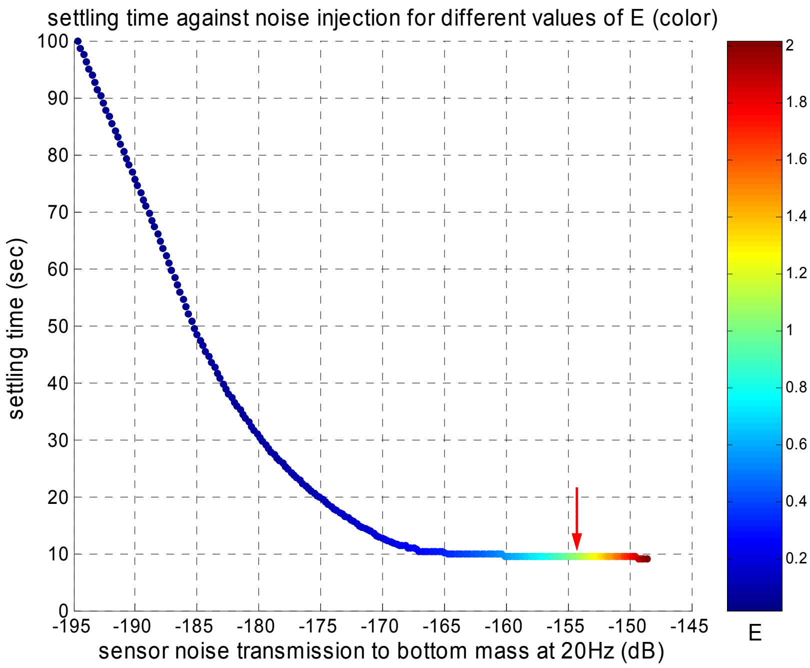

Figure 4.5: Settling time against sensor noise transmission at 20Hz, for different values of E

We can easily notice that the lower the estimator gain, the lower the sensor noise transmission is. However, if the gain becomes too low, the damping performances start to decrease significantly. This plot will enable us to choose the best value for the estimator gain by optimizing both sensor noise and damping at the same time.

Let's now discuss the stability of the loop.

4.1.4 Stability

The first important thing to keep in mind about stability is that it is not affected by sensor noise, even if it is large, it can't turn a stable control to an unstable one in the linear regime.

From the equation above, we can get the open loop transfer function:

- $$\frac{P}{1+L} = \left[\frac{P.M.C + P.M.E - P}{M.C + M.E - 1 - P.C.M.E} \right] \qquad 4.14$$

Where L is the open loop transfer function (TF from w to u)

- $$L = \frac{-P.C.M.E}{C.M + E.M - 1}$$ 4.15

The system is unstable if L=-1

The entire loop is stable as long as $M.C + M.E - 1 - P.C.M.E \neq 0$

This is unfortunately difficult to solve, unless we consider the case where M=P (Model = Plant)

- $$M.C + M.E - 1 - M.C.M.E = (1 - M.C).(1 - M.E)$$ 4.16

This is easier to solve, it means that the 2 inner loops have to be stable (loop with no estimator and internal estimator loop). We can write the 2 stability criteria:

- $1 - M.E \neq 0$ (the inner estimator loop must be stable)
- $1 - M.C \neq 0$ (the loop with no estimator must be stable)

These rules are the only one if the plant and the model are the same. However, it is not guaranteed that the model will match the plant perfectly, in most cases, there will be some mismatch and we need to be able to study the stability in that case.

A more global approach is to study the location of the poles of the closed loop in a real/imaginary map. If all of the poles have a negative real part, then the loop will be stable.

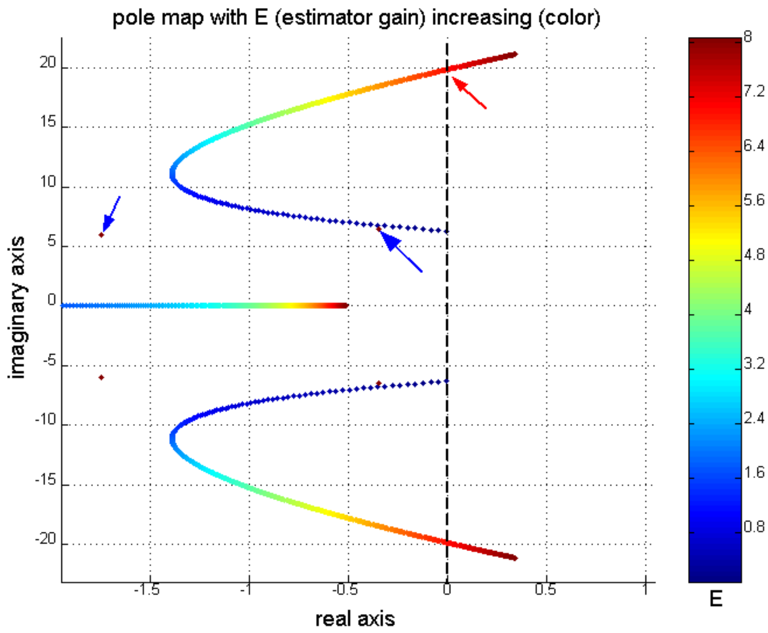

Figure 4.6: Pole map of the closed loop for different values of E

Figure 4.6 enables us to see very quickly what the maximum gain is for E (color), in this example (1 DoF) the poles start to be positive when E goes above 7, the estimator loop turns unstable above that value. For a simple system, this plot might not be necessary, but when the dynamics become more complex with several resonances and some model mismatch, it becomes a very easy way to check the stability of the loop. Note that some of the poles (blue arrows) do not depends on the estimator feedback gain E, these poles are the poles of the control filters.

4.1.5 Model mismatch

Studying the influence of mismatch between the plant and the model is not easy for a control loop using an observer. Quantitizing the model mismatch is the first difficulty that one might face when trying to address this issue In order to simplify this problem and understand the influence of model mismatch, we will start with a simple 1DoF system and a resonance frequency mismatch. The model we use has a resonance frequency at 1Hz, and we will study the stability and loop efficiency when the plant resonance frequency is higher or lower than 1Hz

1. Plant resonance is 20% higher (1.2Hz) than the model's one (1Hz):
    - Stability :

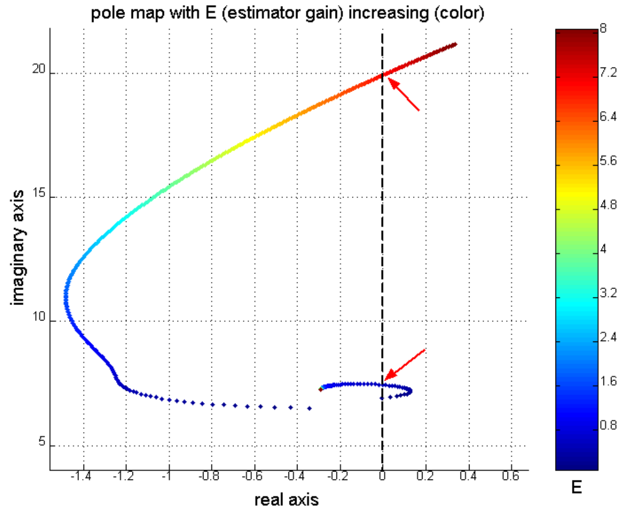

Figure 4.7: Pole map when the plant resonance frequency is 20% higher than the model

The mismatch affects the stability for low values of the estimator gain, for the lower gains, the loop is unstable.

- performances :

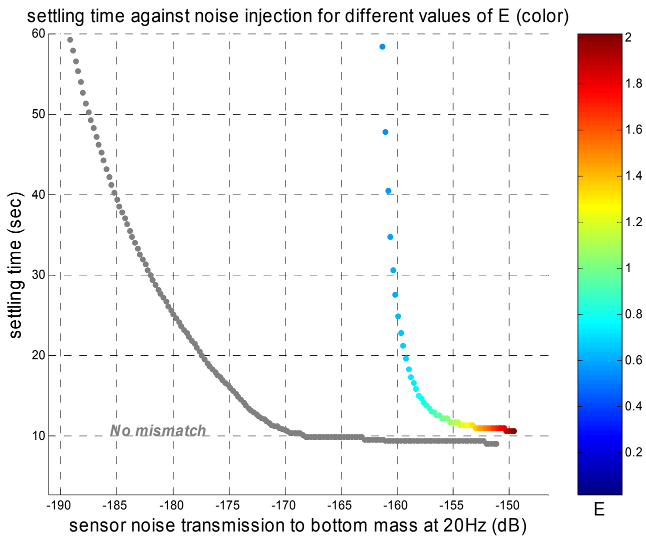

Figure 4.8: Damping against sensor noise plot when the plant resonance frequency is 20% higher than the model

Like the stability, the performances of the loop significantly decrease for lower values of E. Very low values of E make the estimator/control loop less when the plant resonance is higher than the model resonance.

2. Plant resonance is 20% lower (0.8Hz) than the model's one (1Hz) :

    - Stability :

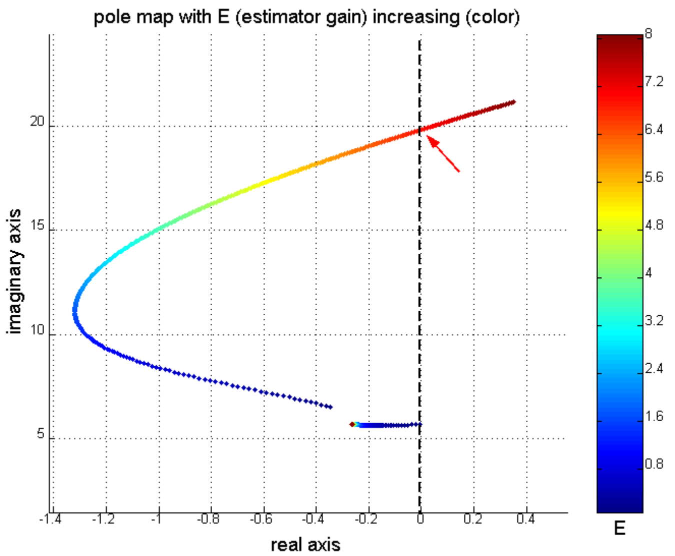

Figure 4.9: Pole map when the plant resonance frequency is 20% lower than the model

In this case, the mismatch doesn't make the loop unstable for low value of E. However, it slightly changes the maximum value E can take before the loop becomes unstable. Overall, this mismatch does not really threaten the stability of the loop.

* performances :

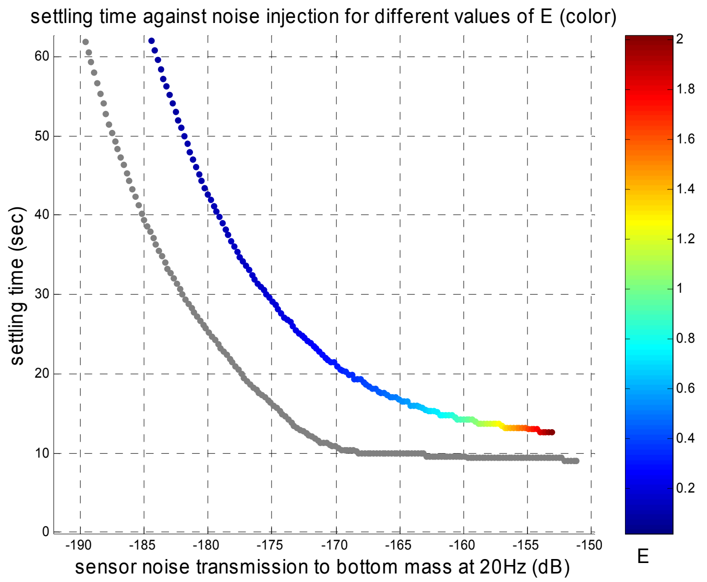

Figure 4.10: Damping against sensor noise plot when the plant resonance frequency is 20% lower than the model

The noise/damping performances are decreased by this mismatch, the settling time is increased by about 20%.

A positive and negative mismatch of 20% on the resonance frequencies has been applied in this simple example for a single degree of freedom system. It helped us to understand how the model mismatch can decrease the performances and/or threaten the stability of the loop.

For LIGO pendulums, we expect the resonance mismatch to be less than 10% (and could be made much less with some work, see Appendix A) and model mismatch shouldn't be a big issue for the design of the control loops. However, one can anticipate the effect of a model mismatch and choose safe values of E using the tools we have seen above. These are also useful plots to check a given design in case the plant doesn't match the model.

4.1.6 Mismatch in the model for multi dof systems

We have discussed the effect of a model mismatch on a single DoF system. However, it is not easy to adapt this study to a multi-DoF system. The main difficulties we are facing with multi-DoF mismatch are:

1. How to quantify a model mismatch for a multi dof system (all resonances off, only one, random error…) ?
2. Having the frequencies of the model match doesn't guaranty that the modal shapes are correct.

A mathematical solution to this problem is very hard to find, for systems with 2 or 3 DoFs, we could anticipate several kind of model mismatch and plot the poles or the performances like we have seen above. When the system becomes more complicated, this becomes impossible and we need to find other solutions.

It is important to understand where the model mismatch comes from. The dynamics of a pendulum are very well known and negligible approximations are made in the equation of motions (small angles for example). The main sources of model mismatch are the difference between the model parameters and the plant parameters. For example if the length of a wire is slightly bigger in the plant, it will produce a mismatch and shift the resonance frequencies and the mode shapes.

It is possible to simulate such parameter changes in our loop. We can use a Monte-Carlo like method in order to simulate the influence of random parameter mismatch on the stability of the loop.

By randomly changing the parameters in the plant simulation, we can anticipate the positions of the poles for the loop in case of a parameter mismatch. If we repeat those random changes for every parameter for a given number of tries, we can plot an area where the poles are likely to be and estimate the probability to have an unstable loop.

The procedure we use is the following one:

- Randomly change parameters around the initial ones while constraining a maximum mismatch (5, 10 or 20% for ex)
- Create a new plant using those random parameters
- Simulate the new loop using this modified plant
- Plot the poles of the new closed loop on a real/imaginary axes

- Repeat the same steps few hundred times with new random parameters every time

The case where the plant and model are identical (no mismatch) is the red cross, all the blues dots correspond to a randomly generated error.

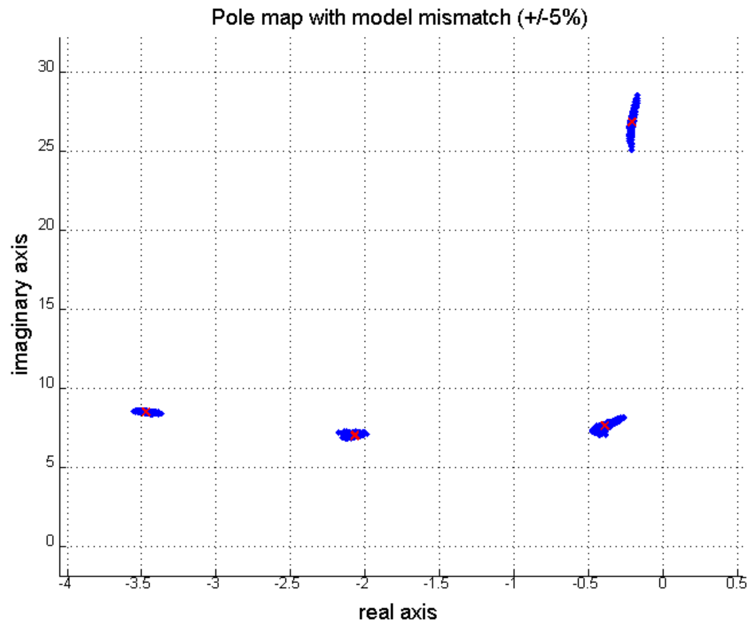

Figure 4.11: Pole map with model mismatch (5%)

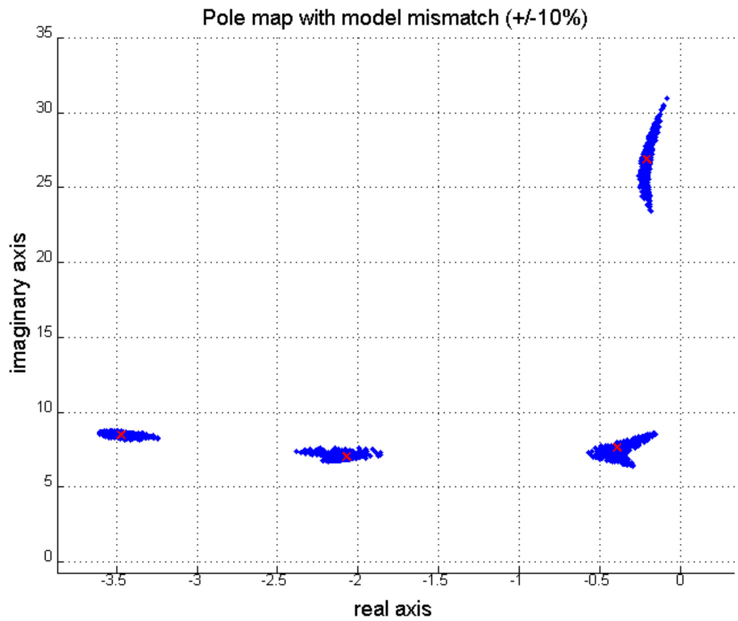

Figure 4.12: Pole map with model mismatch (10%)

In those figure 4.11 and figure 4.12, the probability to obtain an unstable loop is 0. If we keep increasing the mismatch, we will see that this probability increases:

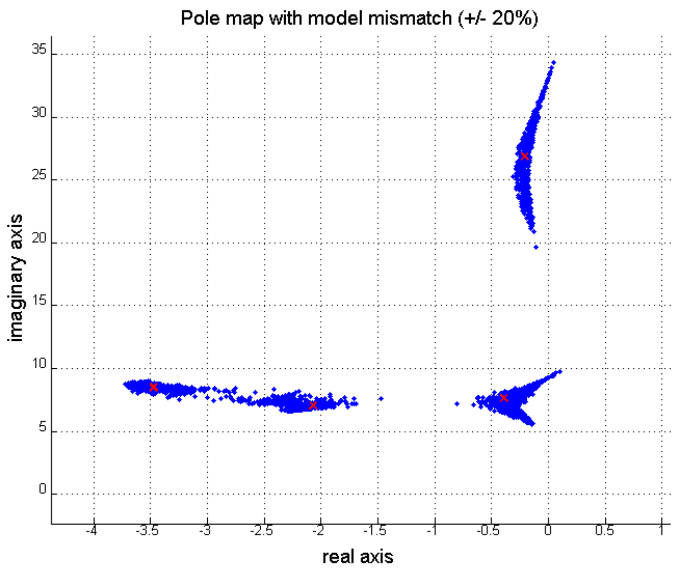

Figure 4.13: Pole map with model mismatch (20%)

In Figure 4.13, if the mismatch on parameters reaches 20%, then the probability to get an unstable loop becomes 4.8% (+/- 2%).

Although this method doesn't give the certainty that the loop will not be unstable if the plant and the model mismatch, it enables us to be more confident with the robustness of the control. We see from the figures that there has been no unstable loop generated if the mismatch is less then to 10%. However, about 5% of the loops were be unstable when the mismatch was +/- 20%.

We don't expect any parameter mismatch to be bigger than 5% for the triple pendulum.

4.1.7 Conclusion

Using the mathematical model of the loop with an estimator and modal control, one can predict the damping performances, the stability and the noise performances of the loop and optimize it.

We have studied the influence of the estimator gain on the noise/damping performances and see how to choose the optimized value of E to guarantee good damping and sensor noise filtering.

We also have worked on the stability. To obtain the best performances, we chose a control loop using filters instead of robust control techniques. Once designed, the loop must be validated in the case the model and the plant don't match perfectly. The Monte-Carlo method provides a way to check in which proportion the plant parameters could be off before the loop could become unstable.

In section 5, we will use those tools to optimize the loop for the yaw loop of the triple pendulum. We choose the yaw loop because it has 3 observable modes and we only measure one state (the top mass), this is a perfect example for the SIMO estimator. A comparison with classical approach will be shown.

4.2 MIMO MODAL LQ ESTIMATOR AND MODAL CONTROL

The method discussed above is very efficient at controlling a simple system with only one input and no couplings between several directions, for example Z and Yaw. When the system has several inputs, many outputs and when the degrees of freedom are coupled to each other,

it is more difficult to use SIMO disturbance estimators. This is the case for the longitudinal-pitch and transverse-roll systems. Both have 2 measurement inputs, the angle and the displacement of the first mass that are coupled to each other, they also have 2 outputs, the angle and displacement of the bottom mass.
In order to design the loop for those multi-inputs multi-outputs systems, we will use a different kind of estimator, the MIMO modal state estimator. This estimator directly generates the modal state and the internal feedback is a MIMO gain that is optimized by minimizing a cost function the user chooses. The choice of this cost function will impact the performances of the loop, both damping and sensor noise transmission are linked to the choice of this cost function.

4.2.1 The MIMO modal estimator

We have seen in section 3.7 how to design a MIMO modal observer, the loop diagram is shown in figure 4.14. We will see in this section that the observer can become an estimator and help us to reduce the sensor noise transmission in the loop.

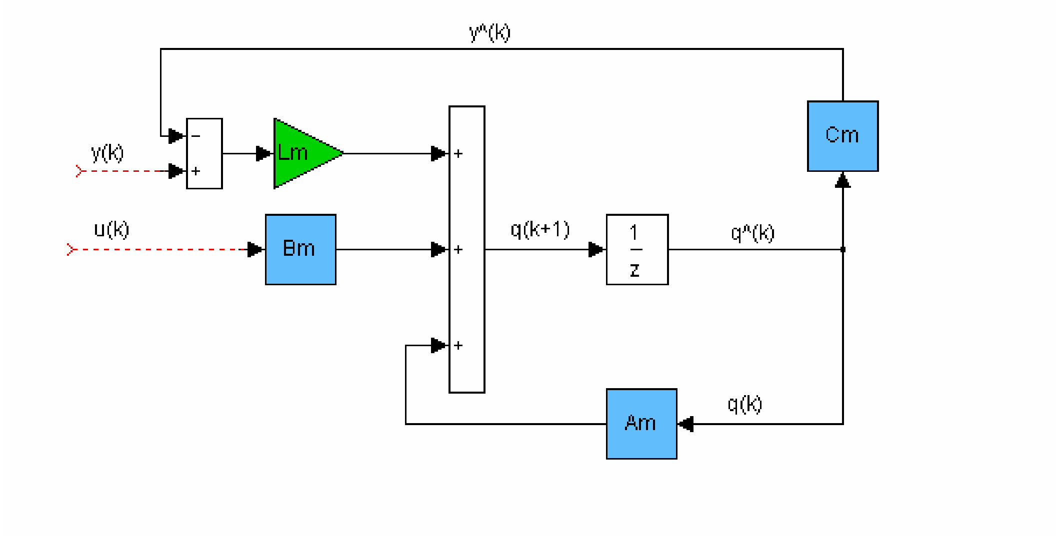

Figure 4.14: MIMO modal estimator diagram

The dynamics of the observer is given by the following equation:

- $\delta_{k+1} = A_m{}^T \delta_k + C_m{}^T z_k$ 4.17
- With $z_k = -L_m{}^T \delta_k$ 4.18

And L_m is calculated to reduce the cost function:

- $$J = \frac{1}{2}\sum_{k=0}^{N} \delta_k^T Q_1 \delta_k + z_k^T Q_2 z_k \qquad 4.19$$

The first term of this cost function is related to the accuracy of the observation. The second part is related to what is often called "measurement update", it drives the amplitude of the estimator's internal feedback.

In order to understand how this cost function works, let's extend it for a 6 DoFs system where 2 DoFs are measured.

- $$J = \frac{1}{2}\sum_{k=0}^{N} \begin{bmatrix} \delta_{k1} & \delta_{k2} & \cdots & \delta_{k6} \end{bmatrix} \begin{bmatrix} Q_{11} & & & \\ & Q_{12} & & \\ & & \ddots & \\ & 0 & & Q_{16} \end{bmatrix} \begin{bmatrix} \delta_{k1} \\ \delta_{k2} \\ \vdots \\ \delta_{k6} \end{bmatrix} + \begin{bmatrix} z_{k1} & z_{k2} \end{bmatrix} \begin{bmatrix} Q_{21} & \\ & Q_{22} \end{bmatrix} \begin{bmatrix} z_{k1} \\ z_{k2} \end{bmatrix} \qquad 4.20$$

- Q_1 enables us to weight how accurately we want to observe each mode. Its size is defined by the number of modes in the plant we are working with. It gives us the ability to tune the estimator differently for different resonance frequencies. The bigger these terms, the more accurate the estimation will be (it will force δ to be small), but the more feedback and "measurement update" will be used, which can translate into a bigger sensor noise transmission.

- Q_2 enables us to weight the participation of each measurement in the estimator dynamics. Its size is defined by the number of measurements. The bigger these terms, the less feedback will be used (it will force z to be small), this will translate to a decrease in accuracy but a better sensor noise filtering.

It is important to note that only the ratio of those different weights compared to each other matters.

In order to find a method to optimize those weights, we need to reduce the number of parameters and write the weights a different way.

As mentioned above, the Q_1 matrix weights the observation of each mode, the bigger the term in the matrix, the more accurate the estimation for this mode will be. In order to simplify the choice of this matrix, we will make the choice to design Q_1 so that each mode gets a gain inversely proportional to its resonance frequency. The lowest modes will have the biggest gains to get an accurate observation; the highest modes will get smaller gains to filter the measurement noise.

- $$Q_1 = \begin{bmatrix} \frac{1}{f_1} & & & \\ & \frac{1}{f_2} & & \\ & & \ddots & \\ & & & \frac{1}{f_6} \end{bmatrix} \qquad 4.21$$

The terms in Q_2 remain to be chosen. In the 6 DoFs case shown above, 2 terms of the matrix needs to be chosen to weight the feedback in the estimation. If this gain is big, the feedback ("measurement update") will have to be small to reduce the cost function; this will reduce the sensor noise transmission. If the gain is small, more feedback will be allowed and the measurement contribution will increase.
Instead of choosing both term of the matrix separately, we will write the Q_2 matrix the following way:

- $$Q_2 = R_1 \begin{bmatrix} R_2 & \\ & \frac{1}{R_2} \end{bmatrix} \qquad 4.22$$

Where R_1 and R_2 are:

- R_1 weights the overall weight of Q_2 compared to Q_1 (how big the contribution of the measurement is).
- R_2 weights one measurement relative to the other, it enables the designer to create an estimator that gives more importance to one measurement if necessary, and deal with cross-coupling.

In this section, we will study how the damping and sensor noise transmission behaves with R_1 and R_2.

4.2.2 The loop model

In the case of the SIMO estimator, it was possible to write the equation of the loop in transfer function formulation and calculate the noise transmission or damping performances with this equation.

For the MIMO modal estimator, it is not possible to use the transfer function formulation anymore, because the equations would be too complex. Instead, we will use the state-space formulation.

The equations of the whole loop are obtained by combining the 3 state-space systems:

1. The plant
2. The estimator
3. The controller

The inputs and outputs of each system are linked as needed by manipulating the matrices. The final result is a bigger state-space system where inputs and outputs can be chosen anywhere in the loop. The inputs we care about are the sensor noises and the seismic noises, the outputs are position or velocities of the plant for each mass.

4.2.3 Behavior of the MIMO estimator

Once the control loop has been created in state-space formulation, it is possible to study how to optimize the estimator to minimize the sensor noise transmission and provide a good damping.

First of all, we will see that there are similarities between the MIMO modal estimator and the SIMO disturbance estimator we have seen previously. By applying the MIMO estimator to a 3DoFs system with one measurement, we will see that we can tweak the cost function to reduce the sensor noise transmission while keeping good damping performances.

The cost function in that case is :

- $$J = \frac{1}{2}\sum_{k=0}^{N}\begin{bmatrix}\delta_{k1} & \delta_{k2} & \delta_{k3}\end{bmatrix}\begin{bmatrix}Q_{11} & & \\ & Q_{12} & \\ & & Q_{13}\end{bmatrix}\begin{bmatrix}\delta_{k1}\\ \delta_{k2}\\ \delta_{k3}\end{bmatrix} + [z_{k1}][Q_2][z_{k1}] \qquad 4.23$$

The Q_1 terms are determined by the inverse of the resonance frequencies. The only parameter to choose for this cost function is Q_2.

One can now plot the damping performances for different values of Q_2 using the same controller, the settling time is plotted against Q_2 in figure 4.15.

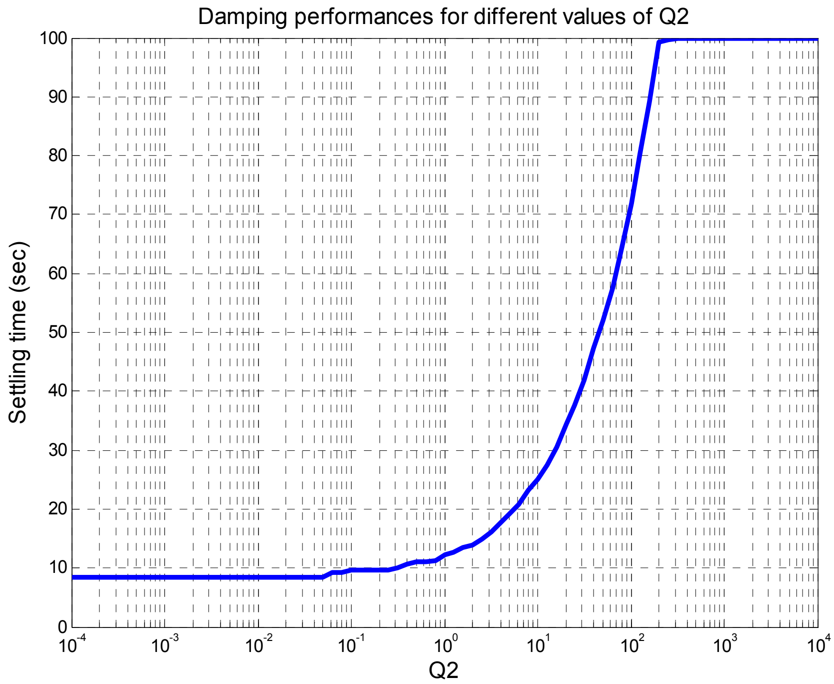

Figure 4.15: Settling time as Q2 increases

We see that the bigger Q_2 is, the more the settling time increases. This is due to the fact that we are adding a "penalty" to the estimator's internal feedback term in the cost function. When Q_2 increases, the contribution of the measurement decrease, this leads to a reduction of the damping performance.

However, if we plot the sensor noise transmission (transfer function from sensor noise to bottom mass) on figure 4.16, we notice that the transmission decreases as Q_2 increases.

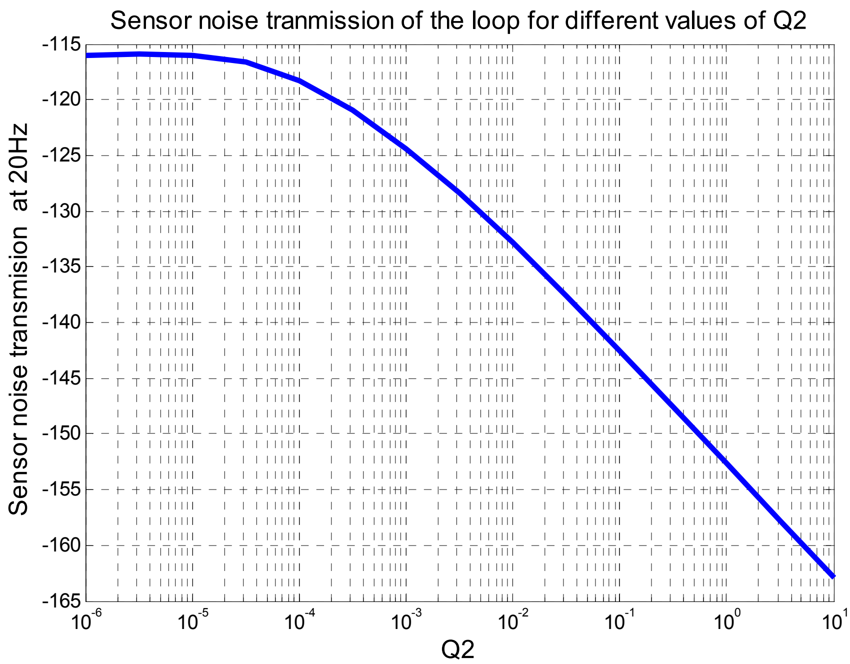

Figure 4.16: Sensor noise transmission at 20Hz as Q2 increases

By choosing the right compromise between damping and sensor noise transmission, we can choose the best value of Q_2.

This behavior is very similar to the one we have seen in the SIMO disturbance estimator. The main difference is that the estimator gain has been replaced by the cost function. This cost function leads to the estimator feedback after minimization.

This first simple example shows that we can use the MIMO estimator and the cost function to optimize the damping while reducing the sensor noise transmission into to the loop.

4.2.4 Tools for MIMO estimator optimization

We now need to develop similar tools to optimize the MIMO modal estimator for more complex systems, where several measurements are made and several outputs need to be studied.

For the triple pendulum, we will need to design a control loop for a 6 DoF system with 2 measurement inputs and 2 outputs to optimize, while taking into account every (all of the) cross couplings. For example, for the longitudinal and pitch direction, both the pitch and X outputs will be considered and cross couplings between the angle and displacements need to be taken into account.

In that case, the cost function can be written as in equation 4.20.
We have seen previously that the Q_1 terms are determined by the inverse of the resonance frequencies. We have also seen that we can change the way to write Q_2. The cost function becomes:

- $$J = \frac{1}{2}\sum_{k=0}^{N}\begin{bmatrix}\delta_{k1} & \delta_{k2} & \cdots & \delta_{k6}\end{bmatrix}\begin{bmatrix}\frac{1}{f_1} & & & \\ & \frac{1}{f_2} & & \\ & & \ddots & \\ & 0 & & \frac{1}{f_6}\end{bmatrix}\begin{bmatrix}\delta_{k1} \\ \delta_{k2} \\ \vdots \\ \delta_{k6}\end{bmatrix} + \begin{bmatrix}z_{k1} & z_{k2}\end{bmatrix}R_1\begin{bmatrix}R_2 & \\ & \frac{1}{R_2}\end{bmatrix}\begin{bmatrix}z_{k1} \\ z_{k2}\end{bmatrix}$$

4.24

We need to choose both R_1 and R_2. Those 2 parameters will have to be studied together. The damping performances can be plotted against R_1 for different values of R_2 in figure 4.17.

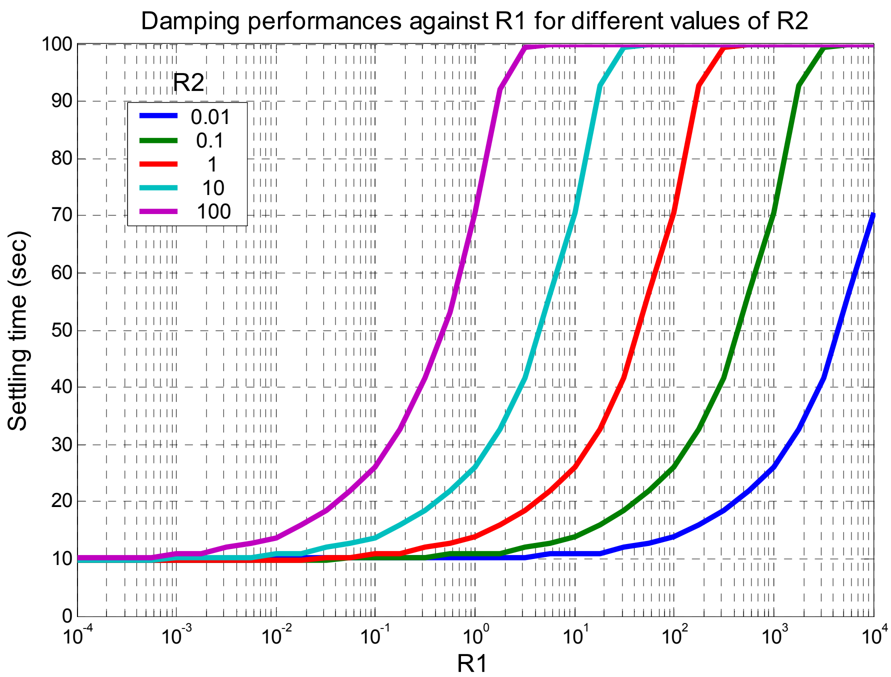

Figure 4.17: Settling time for several values of R1 and R2

To optimize the whole control loop, it would be necessary to plot this figure for every degree of freedom. Then, it is possible to choose a range of values for R_1 and R_2 where the damping performances satisfy the requirements.

The sensor noise transmission can be plotted the same way. However, since cross couplings can play an important role, it needs to be taken into account. Instead of plotting the sensor noise transmission directly, we will plot the amplitude of the bottom mass motion due to every contributing sensor noises (for example both angular and displacement sensor noise) in figure 4.18. This allows us to add all the different paths for the noise and take the cross coupling into account.

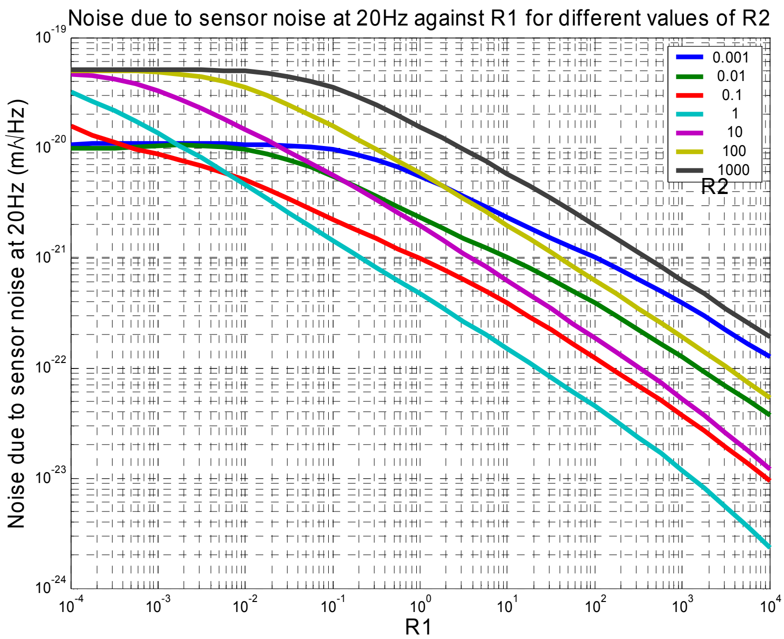

Figure 4.18: Noise due to sensor noise at 20Hz for several values of R1 and R2

We see that the trend we have seen with the simple case still exists here, the higher R_1 is, the lower the sensor noise transmission. We can also notice that R_2 plays a very important role here. When R_2 decreases, the overall sensor noise transmission decreases too (black to light blue). However, after R_2 reaches a given value (light blue here), the sensor noise transmission starts to increase (light blue to blue). This is due to cross couplings, after we have reached the optimal value of R_2, the cross coupling and the sensor noise coming from the other DoF (for example X sensor noise to pitch motion) starts to dominate.

It is very interesting to plot the same figure by swapping R_1 and R_2. In figure 4.19, the sensor noise will now be plotted against R_2 for different values of R_1 (color).

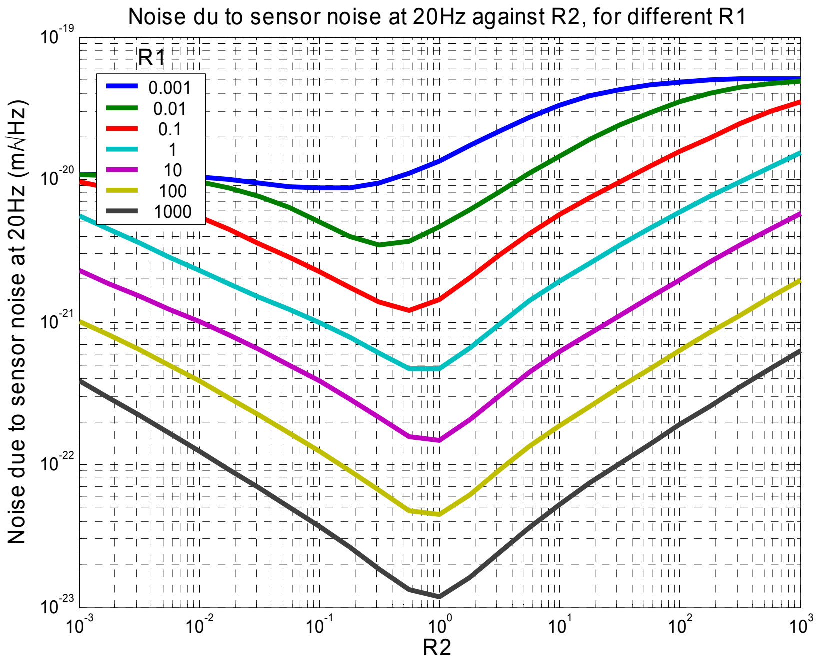

Figure 4.19: Noise due to sensor noise at 20Hz for several values of R1 and R2

As we have seen with figure 4.18, the sensor noise increases after R_2 reaches about 1, this is due to the cross coupling.

As for the damping performances, the sensor noise must be plotted for all of the outputs in order to choose the best value for R_1 and R_2. We will see that applied to the triple pendulum in the next section.

4.2.5 Stability

In order to study the stability of the loop, we need to write the equations of the controlled system and the equation of the estimator. It is important to keep in mind that these equations are correct only if the model and the plant match perfectly.

- $x_{k+1} = Ax_k - BK\hat{x}_k = Ax_k - BK(x_k - \varepsilon_k)$ *4.25*
- $\varepsilon_{k+1} = A\varepsilon_k - LC\varepsilon_k$ *4.26*

- $$\begin{Bmatrix} x_{k+1} \\ \varepsilon_{k+1} \end{Bmatrix} = \begin{bmatrix} A-BK & BK \\ 0 & A-LC \end{bmatrix} \begin{Bmatrix} x_k \\ \varepsilon_k \end{Bmatrix} \tag{4.27}$$

The characteristic equation can be written

- $$\det[\lambda I - (A-BK)].\det[\lambda I - (A-LC)] = 0 \tag{4.28}$$

In other words, the characteristic poles of the complete system consist of the combination of the estimator poles and the controller poles that are unchanged from those obtained assuming actual state feedback. This is called the separation principle and show that we can design a stable control, and a stable estimator and the combination of both will be stable.

However, this rule only applies if the model and the plant match perfectly. If not, the poles of the complete system will be different from the poles of the estimator alone and controller alone.

If the model and the plant don't match perfectly, it is possible to use the poles maps we have seen previously for the disturbance estimator, although that method doesn't give the guarantee that the loop will be stable in case of a mismatch, it does increases our confidence with the robustness of the control.

4.2.6 Conclusion

As for the SIMO estimator in transfer function formulation, we have seen that the MIMO modal estimator in state-space can be optimized to reduce the sensor noise transmission. The gain of the estimator feedback has been replaced by the cost function that will ultimately be minimized to obtain the feedback matrix gain.

By using the loop model and the cost function, one can make sure the damping performances are meeting the requirements; it is also possible to reduce the sensor noise transmission. The cross couplings are taken into account and need to be carefully studied to optimize the loop.

5 APPLICATION TO ADVANCED LIGO TRIPLE PENDULUM

We have seen how to design a control loop for the triple pendulum using a new approach. The modal state control enables us to create a more flexible loop. By adjusting the gains of each simple controller, we will be able to control the sensor noise transmission without decreasing the damping performances of the loop.

The modal control needs to be used with an estimator in order to create the data that we can't measure. This estimator is also very useful to reduce the sensor noise transmission and we have seen how to optimize two different kinds of estimators.

In this section, we will apply the modal control and the disturbance estimator to the triple pendulum. First, we will study the Yaw direction and use the tools previously designed to optimize the damping loop, we will then check our results and compare them with the classic approach using standard filtering.

Then we will apply the modal control and the MIMO modal estimator to a more complicated system: the X and pitch model. Those two degrees of freedom are coupled to each other and this coupling has to be taken into in the damping loop design. We will also compare this loop to the classic feedback approach.

5.1 DESIGNING THE CONTROL FILTER

The first step is to design the control filters, here (figure 5.1) is the diagram of the modal control loop for a 3dof system.

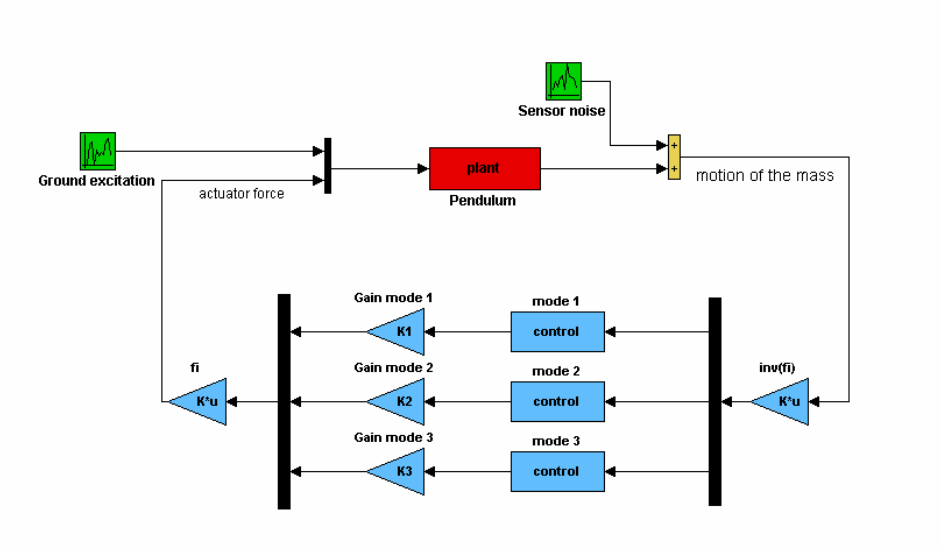

Figure 5.1: Schematic of the modal control loop

The 3 modes are controlled by different controllers, with different gains and filters. Those filters need to provide damping for a single DoF system, which is easy to design. The filter will be parameterized with the resonance frequency of the mode so that each filter is optimized for the mode it has to control.

The requirements for such a filter are :

1. Large gain and good phase margin at resonance for an efficient damping
2. Good filtering after the resonance to reduce sensor noise injection

The filter we chose uses a zero at 0Hz to gain phase and reduce DC control (it damps the velocity), and then a complex pair of poles at twice the resonance frequency to filter the higher frequencies by keeping a good phase margin. A very small bump is then added on the resonance to increase the gain without excessive decrease of the phase margin.

Below (figure 5.2) is an example of this filter on a single dof system for different gains, with a resonance at 1Hz :

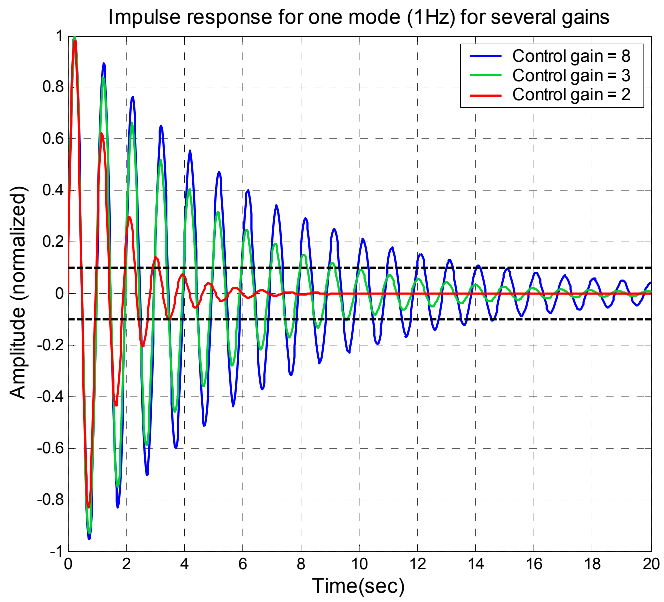

Figure 5.2: Impulse response for the modal control filter

If we choose the gain so that the settling time is 10sec, the open loop is plotted below:

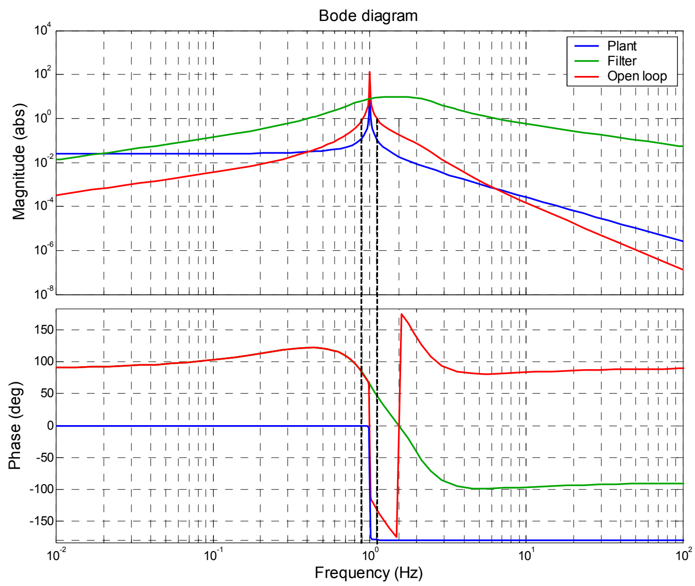

Figure 5.3: Filter, plant and open loop transfer function for the modal filter

As you can see in figure 5.3, the phase margin at the resonance is large (45 degrees), this is important for the robustness of the loop, especially in case our model doesn't match the plant perfectly.

We will use this filter for all of the modes; as we have discussed before, the filter is parameterized with the mode frequency.

5.2 MODAL CONTROL AND SIMO DISTURBANCE ESTIMATOR FOR THE YAW DIRECTION

We will now focus on the design of the Yaw DoF using modal control and the disturbance estimator. The tools we have seen in section 4.1 will be used to choose several important parameters for this loop:

- The gain of each independent modal controller
- The shape of the estimator filter
- The gain of the estimator feedback

5.2.1 Introduction

We only use the model of the yaw DoF here; this is a 3dof plant with

- 3 outputs m1_yaw, m2_ yaw and m3_ yaw (yaw of each mass of the pendulum)
- 4 inputs forces on m0-T_{yaw} (frame motion), m1-T_{yaw}, m2-T_{yaw}, m3-T_{yaw}

The resonance frequencies and mode shapes are shown below :

Mode1 at 1.1Hz	Mode2 at 2Hz	Mode3 at 3.5Hz
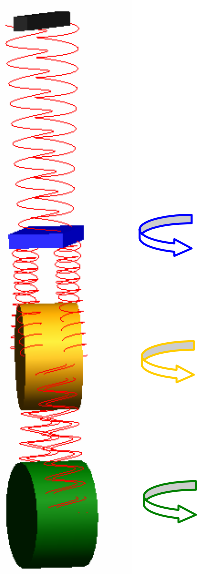	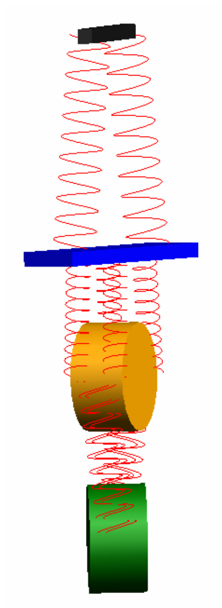	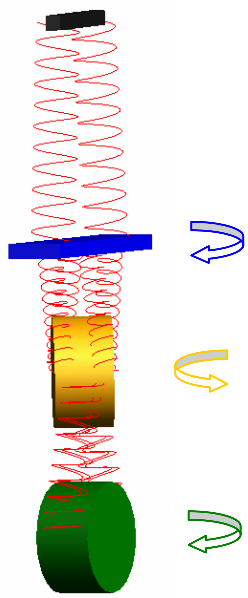

Table 5-1: Mode shape for the Yaw DoF

The noise inputs, the yaw seismic noise and the yaw sensor noise, are plotted in figure 5.4:

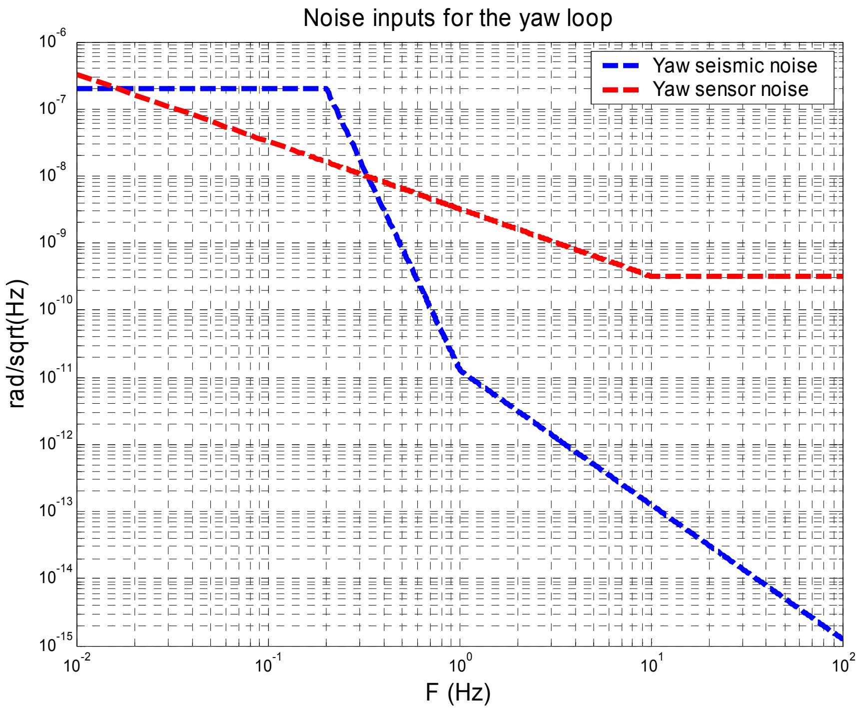

Figure 5.4: Noise inputs for the Yaw degree of freedom

5.2.2 Modal control, no estimator

We have seen above the design of the modal filter, each controller uses a parameterized version of this filter where the parameter is the resonance frequency of the mode to control. The gain of each of these controllers must now be chosen.

To begin with, we choose the 3 gains so that the settling time of each mode is 10sec. The gains are:

- Mode 1 : $K=35.10^{-2}$
- Mode 2 : $K=7.10^{-2}$
- Mode 3 : $K=24.10^{-2}$

The impulse response of each mode and the impulse response of the bottom mass are shown in figure 5.5.

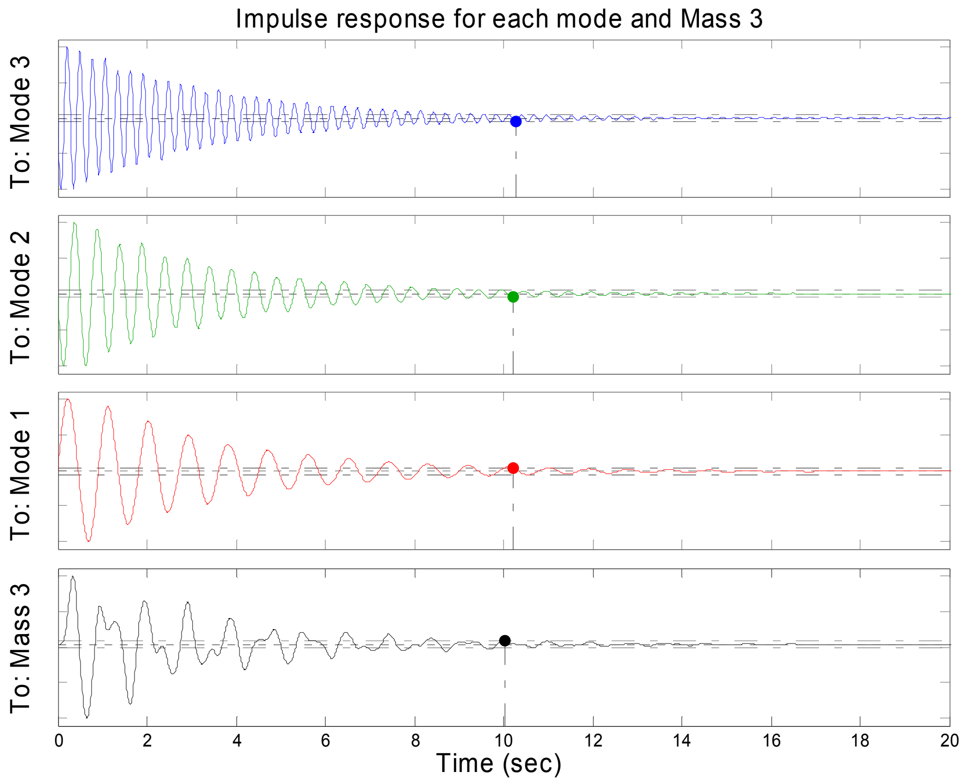

Figure 5.5: Yaw, impulse response for each mode and mass 3

We will see later that these gains can be improved to reduce the sensor noise transmission in the loop. But before we can study the sensor noise transmission and optimize the gains, the estimator needs to be designed.

5.2.3 Estimator filter and gain

Below is a schematic of the estimator + modal control loop. The first step will consist in choosing the shape of estimator filter.

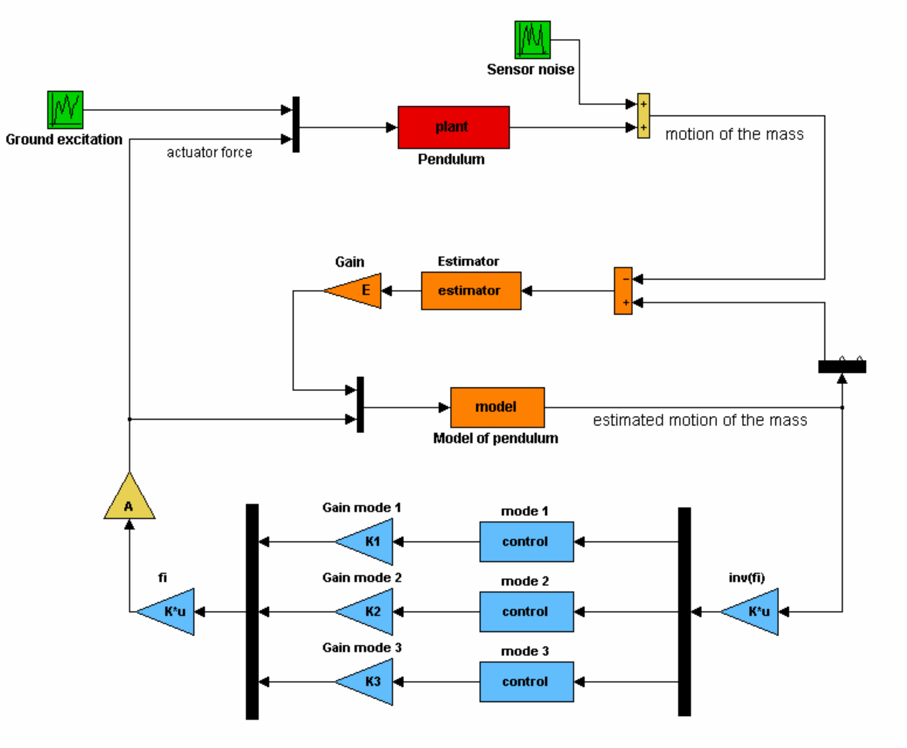

Figure 5.6: Diagram of the modal control loop with estimator

As we have seen before, the estimator filter needs to have a large gain where the resonances are located and a small gain where we want to filter the sensor noise. It must also be a stable and robust filter. The highest resonance we will have to control is 3.5 Hz, we choose a simple filter that gives phase at this frequency. The bode diagram of the filter is plotted in figure 5.7, with the 3 resonances of the yaw model indicated in red.

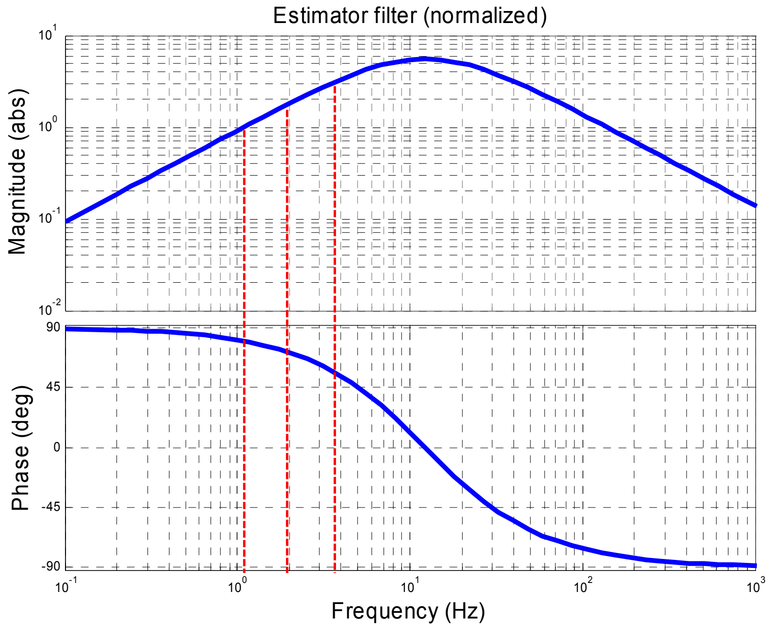

Figure 5.7: Estimator filter shape (normalized at the first resonance frequency)

We want to choose a gain to keep our system stable. In order to do that, we plot the poles of the closed loop for different values of the estimator gain E, poles with a positive real part are unstable.

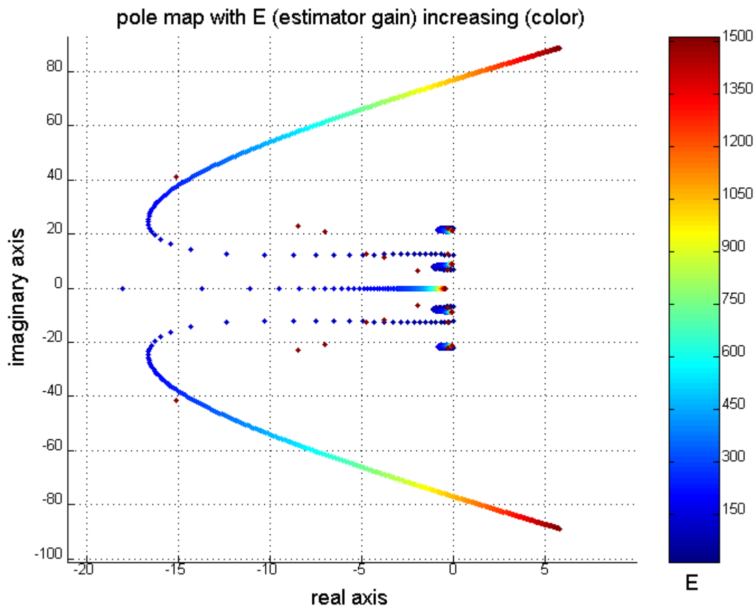

Figure 5.8: Yaw DoF, pole map for different values of the estimator gain E

In Figure 5.8, we see that we can choose E between 0 and 1000. We will optimize this value later. For now, we will choose the estimator gain to be E=500, which will enable us to have a complete loop and optimize the modal controllers.

5.2.4 Optimizing the gains

Now that we have chosen some values for the modal gains and the estimator, we can start to optimize the loop by looking at the result and see where it can be improved.

a) Optimization: damping and filtering duality

It is important to understand what optimization means in this case. We are not trying to develop the most robust or the most efficient control. We need a control that provides decent damping performances while maintaining the sensor noise transmission to a minimum. Figure 5.9 shows a simplified diagram of the loop.

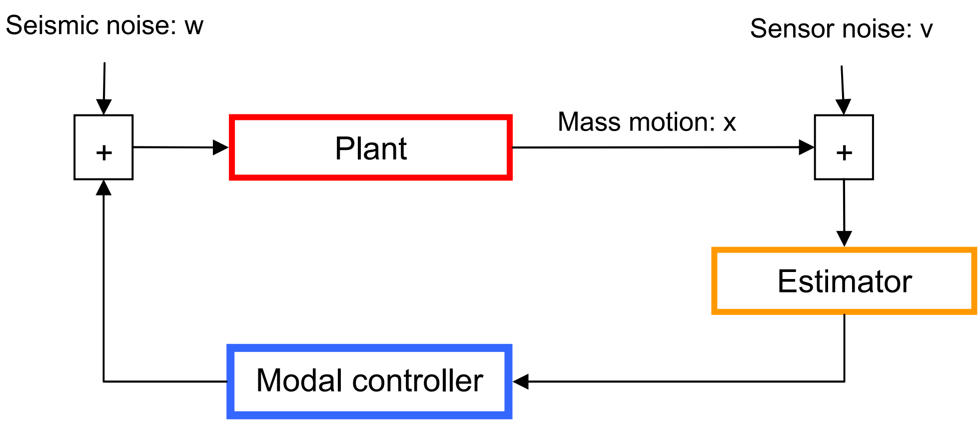

Figure 5.9: Simplified control loop diagram

The real motion of the mass can be written as a function of the 2 uncorrelated input noises: the seismic noise and the sensor noise: $x = TF_{seismic}.w \ + \ TF_{sensor}.v$.

When we optimize the loop, the goal is to minimize TF_{sensor} in high frequencies (above 10Hz). This transfer function is often referred as sensor noise transmission and only its high frequencies amplitude is important.

Meanwhile, we want to damp the rigid body resonances in $TF_{seismic}$ to reduce the Q of the pendulum.

b) Modal controller gains

To optimize the modal controller gains, it is interesting to plot the participation of each modal controller in the sensor noise transmission. We can plot the transfer function between the sensor noise and the bottom mass with only one modal controller on at a time, the final transmission is the rms of those transfer functions.

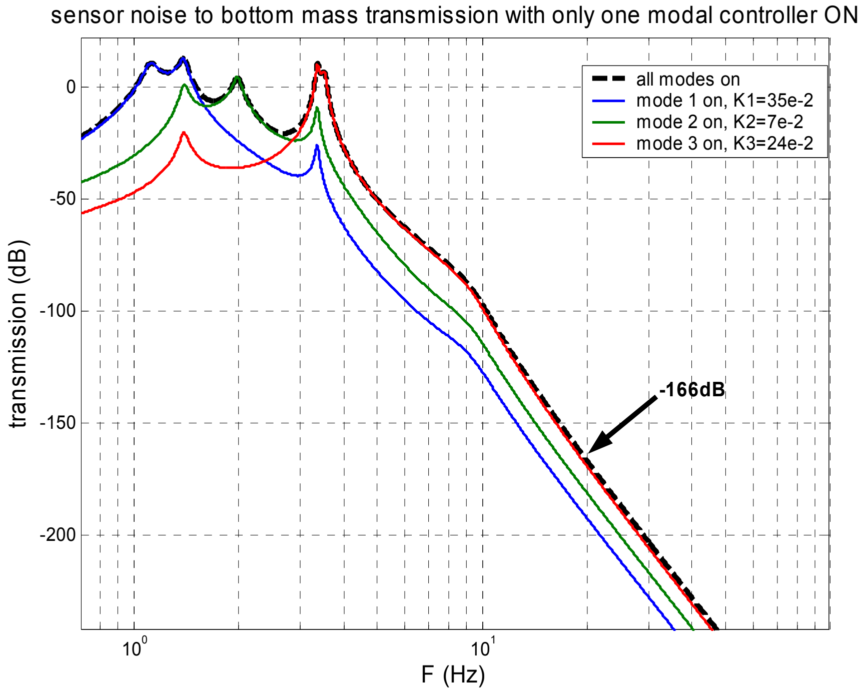

Figure 5.10: Modal participation, sensor noise transmission for each modal controller

We are looking at the high frequencies, the low frequencies are not very important on this plot. Above 10Hz, we want to reduce the sensor noise transmission. In figure 5.10, we can see that the total transmission at 20Hz when all of controller is on is -166dB.

We can improve this loop, the sensor noise is mostly carried by the modal controller of the 3rd mode, and the control gain of this mode can be reduced, while the gain of the two other controllers can be increased safely without adding sensor noise. It is also important to remember that the lower modes carry the most energy and contribute the most to the impulse response.

The new gains we chose are the following:

- Mode 1 : $K=55.10^{-2}$ *(old value : 35e-2)*
- Mode 2 : $K=7.10^{-2}$ *(old value : 7e-2)*
- Mode 3 : $K=5.10^{-2}$ *(old value : 24e-2)*

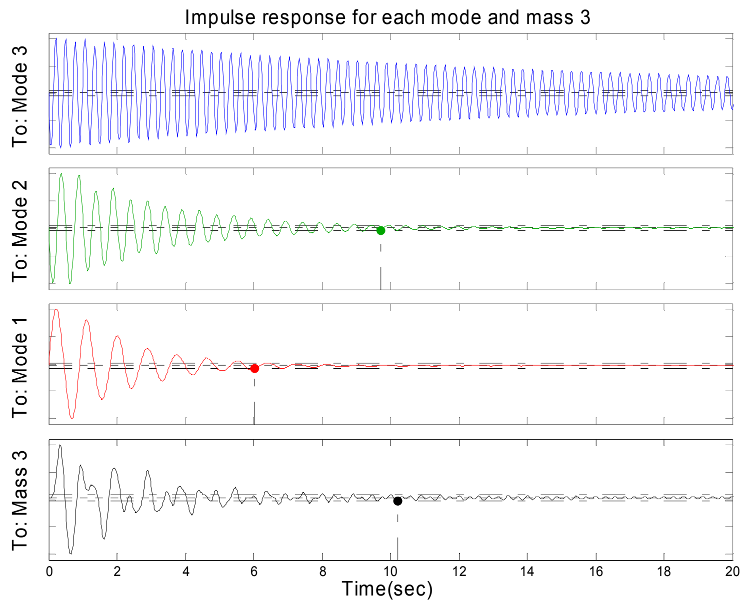

Figure 5.11: yaw, impulse response for each mode and mass3

We see that the impulse response on mass 3 hasn't been modified. We have balanced our control to have more gain on the lowest mode and less on the highest frequency mode.
We can now look on the impact for the sensor noise transmission.

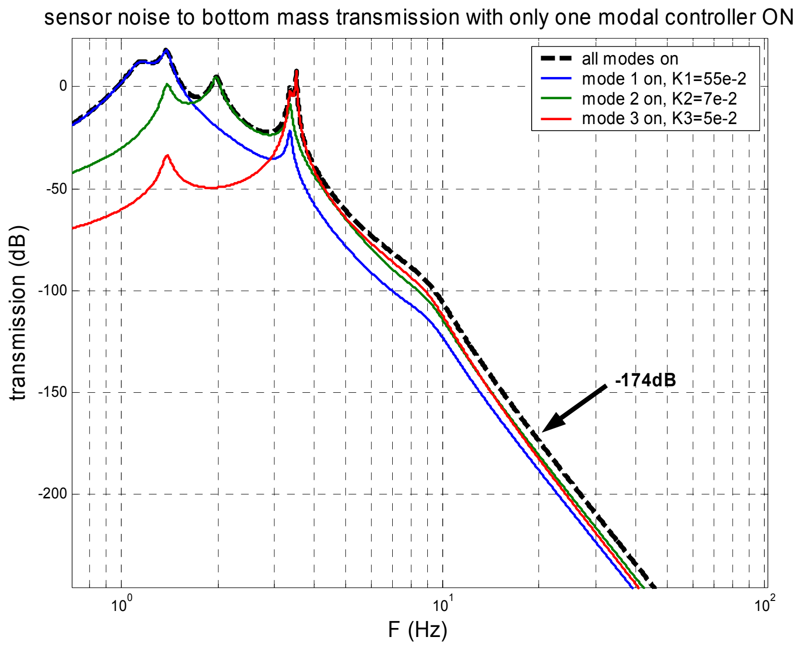

Figure 5.12: Modal participation, sensor noise transmission for each modal controller

The modal controllers are now more balanced and the sensor noise transmission at 20Hz has been reduced to -174dB. This improvement has been done at no cost for the controller; we have simply balanced our gains between the 3 modal controllers.

c) Estimator gain

The last step is to optimize the choice of the estimator gain. The plot showing both damping and sensor noise transmission we have seen in section 0 will help us to make this choice.

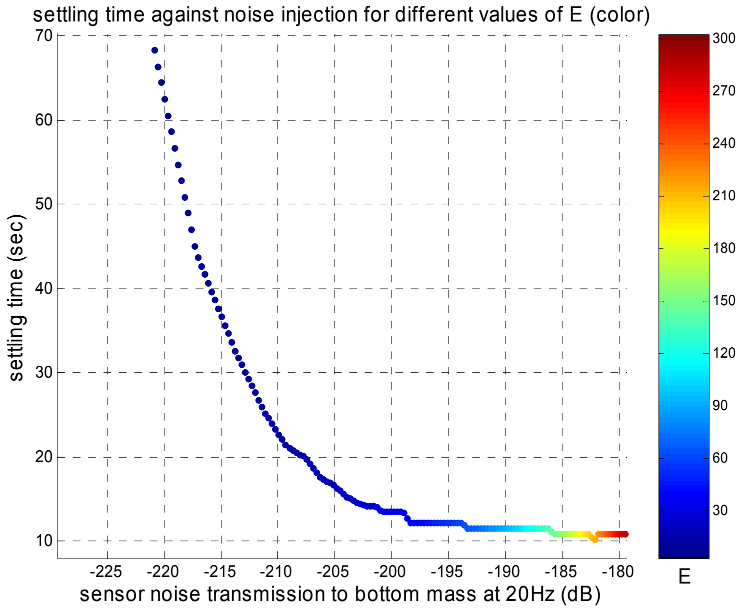

Figure 5.13: Settling time and sensor noise transmission at 20Hz for different values of E

Using figure 5.13, we see that the performances of the damping start to decrease significantly below E=75. Above that value, the settling time stays about the same. We will choose E=120, to take advantage of the estimator sensor noise reduction. With this gain the sensor noise transmission to the bottom mass at 20Hz is about -190dB.

5.2.5 Analyzing the result

A first simple test to analyze the entire loop is to plot the open loop from Mass1_yaw to Mass1_yaw and check the phase margin (Figure 5.14)

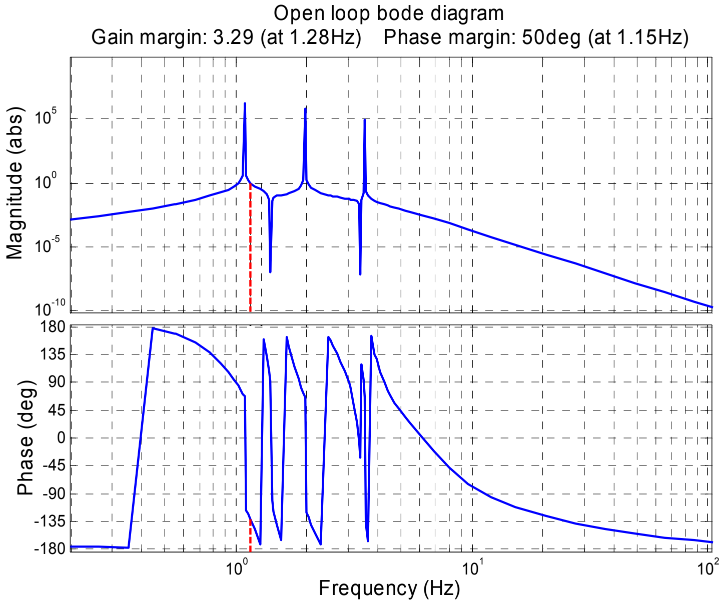

Figure 5.14: Yaw, phase margin of the open loop for the modal control + estimator

We see that the phase margin is large, another interesting thing to notice is that the first mode is the one with the smallest margin (50deg at 1.15Hz, 55.5deg at 2hz and 59.8deg at 3.15Hz), which is due to the fact that each mode are controlled one by one and the lower mode has the biggest gain.

The control performances are plotted in figure 5.15, we see that the settling time is well under 10 seconds.

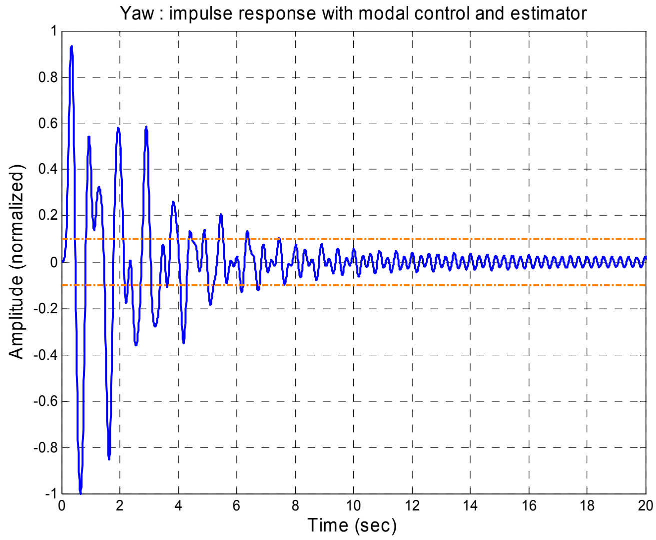

Figure 5.15: Yaw impulse response with the modal control and estimator

We can now plot the amplitude of motion at the bottom mass like we did in section 0 for the classic control.

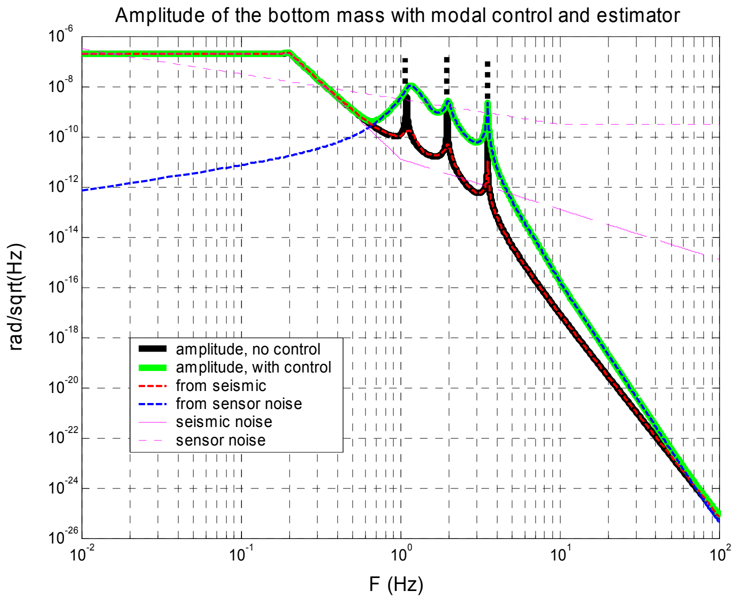

Figure 5.16: yaw, angular noise at the bottom mass with the modal control and estimator loop

Below (figure 5.17), you can find the same plot using a classic approach of filtering. We can see that the difference is very substantial.

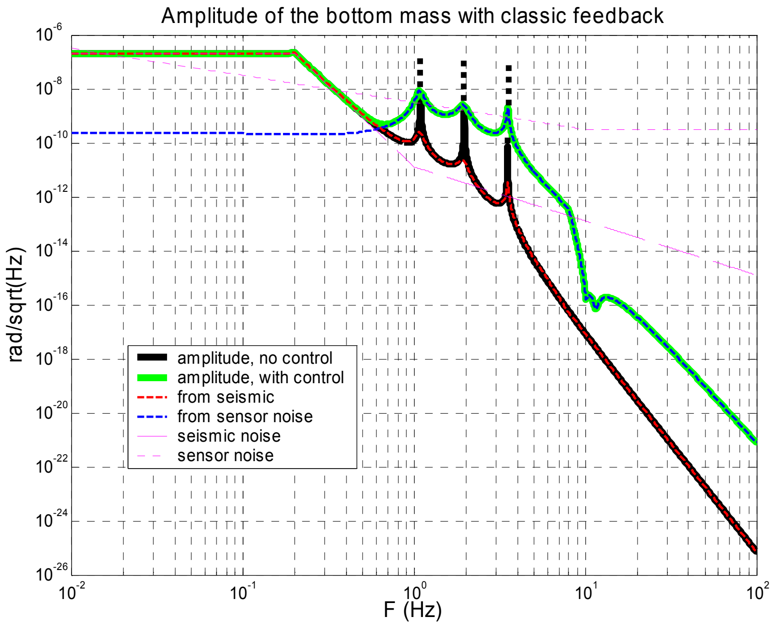

Figure 5.17: Yaw, angular noise at the bottom mass with the classic feedback loop

Finally, an interesting way to compare the classic approach with the modal control loop is to plot the transfer function between the sensor noise and the bottom mass motion for both methods (figure 5.18)

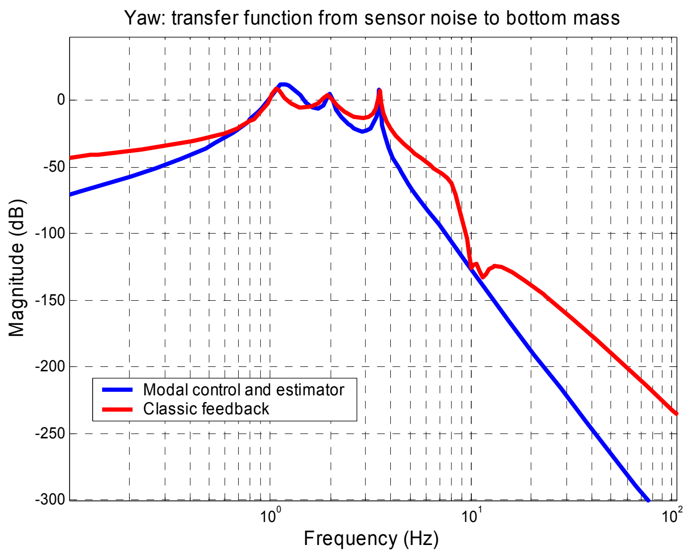

Figure 5.18: Yaw, sensor noise transmission comparison

This method showed very good results for the Yaw direction. The sensor noise transmission has been decreased by a few dozen dB above 10Hz (50dB at 20Hz), while keeping the same damping performance. Unfortunately, applying this same method for the coupled directions like the longitudinal-pitch or transverse-roll would be difficult. In this case, the cross couplings must be taken into account and several outputs must be optimized at the same time. It is necessary to use a different approach to design the control loop of these systems.

5.3 Modal control and MIMO modal estimator for the Longitudinal-Pitch model

Instead of using the simple disturbance estimator seen previously, we will use a MIMO modal estimator optimized with techniques based on optimal control. This method will also be generalized to MIMO system with coupled degrees of freedom or simpler SIMO systems.

5.3.1 The longitudinal-pitch system

We use the model of the longitudinal/pitch direction here; this is a 6dof plant with

- 6 outputs : m1_x, m2_x and m3_x, m1_pitch, m2_pitch and m3_pitch
- 8 inputs : forces on m0-x and m0-pitch (frame motion), m1-F_x, m2-F_x and m3-F_x, m1-T_{pitch}, m3-T_{pitch} and m3-T_{pitch}

Pitch and X are coupled to each other which is why we have to consider both degrees of freedom at the same time. The pendulum’s pitch is not directly coupled to the ground’s pitch because there are only two wires at the top. A pitch rotation about the suspension point won’t couple to the pendulum.

The resonance frequencies and mode shapes are shown in table 5-2.

Mode1 (X) at 0.65Hz	Mode2 (pitch) at 1.15Hz	Mode3 (X) at 1.5Hz
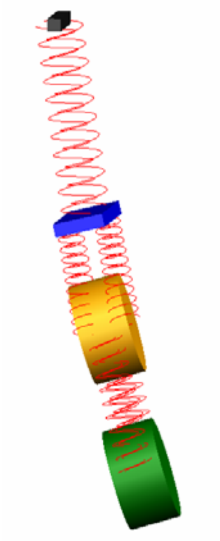	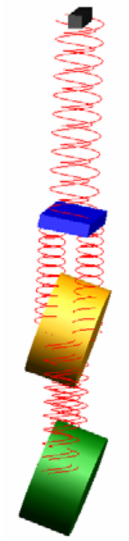	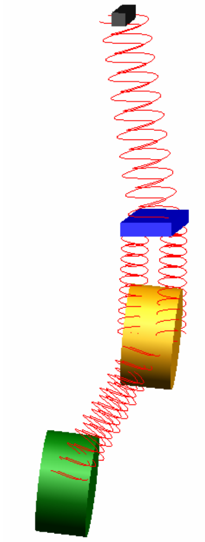
Mode4 (X) at 2.8Hz	Mode5 (pitch) at 4.1Hz	Mode6 (pitch) at 5.7Hz
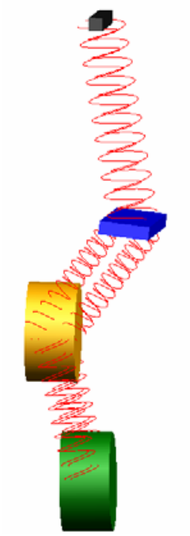	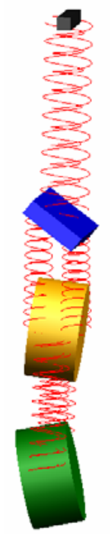	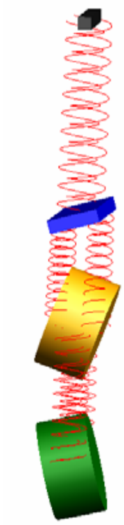

Table 5-2: Mode shapes for the Longitudinal/Pitch degrees of freedom

5.3.2 Noise inputs for the longitudinal-pitch system

Although each sensor individually generates the same sensor noise, the noise in pitch (in $rad/\sqrt{Hz}$) and the noise in the X direction (in $m/\sqrt{Hz}$) are different because the sensors measuring the pitch are very close to each other (6cm, short lever arm).

The platform on which the pendulum is sitting is designed to be sensor limited, the seismic attenuation provided by this platform will reach the noise floor of the sensors it is using (sensitive seismometers). Since the sensors on the platform are about 1m apart from each other, the seismic noise in both pitch and X is supposed to be identical. This noise is dominated by the measurement noise of the sensors placed on the internal seismic isolation system, on this system, the sensors used for the pitch are placed about 1m away from each other.

The noise levels for the seismic and sensor noises are plotted in figure 5.19:

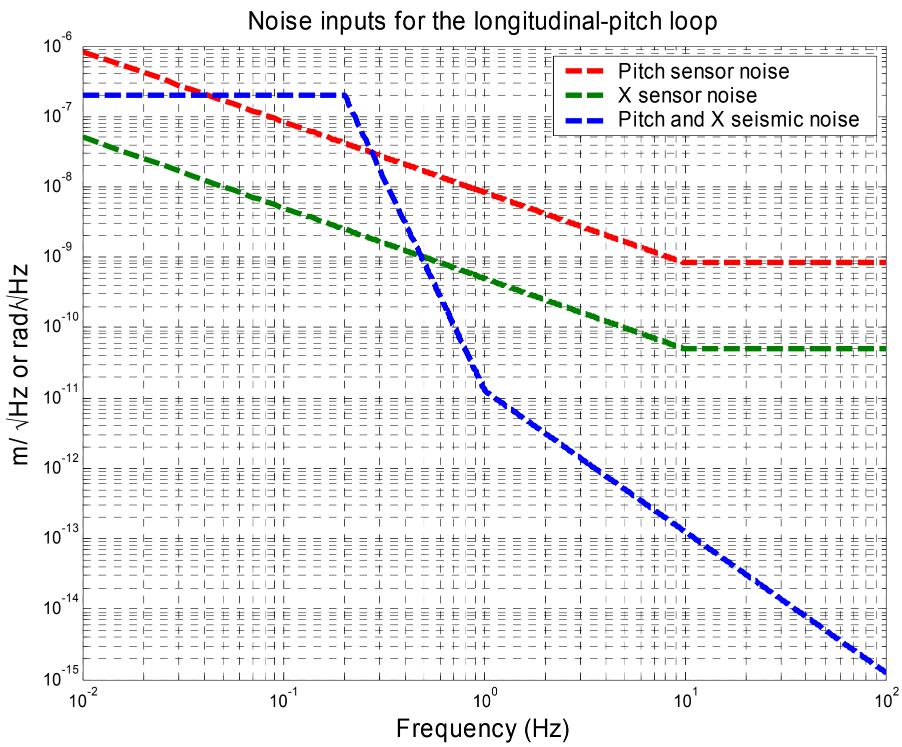

Figure 5.19: Noise inputs for the Longitudinal/Pitch degrees of freedom

5.3.3 Modal controllers

The modal controllers will remain the same as the one used for the yaw system (the filters are parameterized with the X/Pitch frequencies). The gain for each controller is optimized to get the best compromise between damping and sensor noise transmission. As for the Yaw system, the lowest modes get a bigger gain while the highest modes get smaller gains. It is also possible to plot the sensor noise transmission for each mode like we have done before. For the longitudinal-pitch model, the gains are chosen as followed:

- Mode 1 : K=120
- Mode 2 : K=8.10^{-2}
- Mode 3 : K=5
- Mode 4 : K=2
- Mode 5 : K=3.10^{-3}
- Mode 6 : K=1.10^{-3}

The impulse response for each mode and for the bottom mass is plotted below. Note that there are many way to get an impulse response depending on where the impulse excitation is applied. In this case, we apply the impulse on mass 1 in both X and Pitch at the same time.

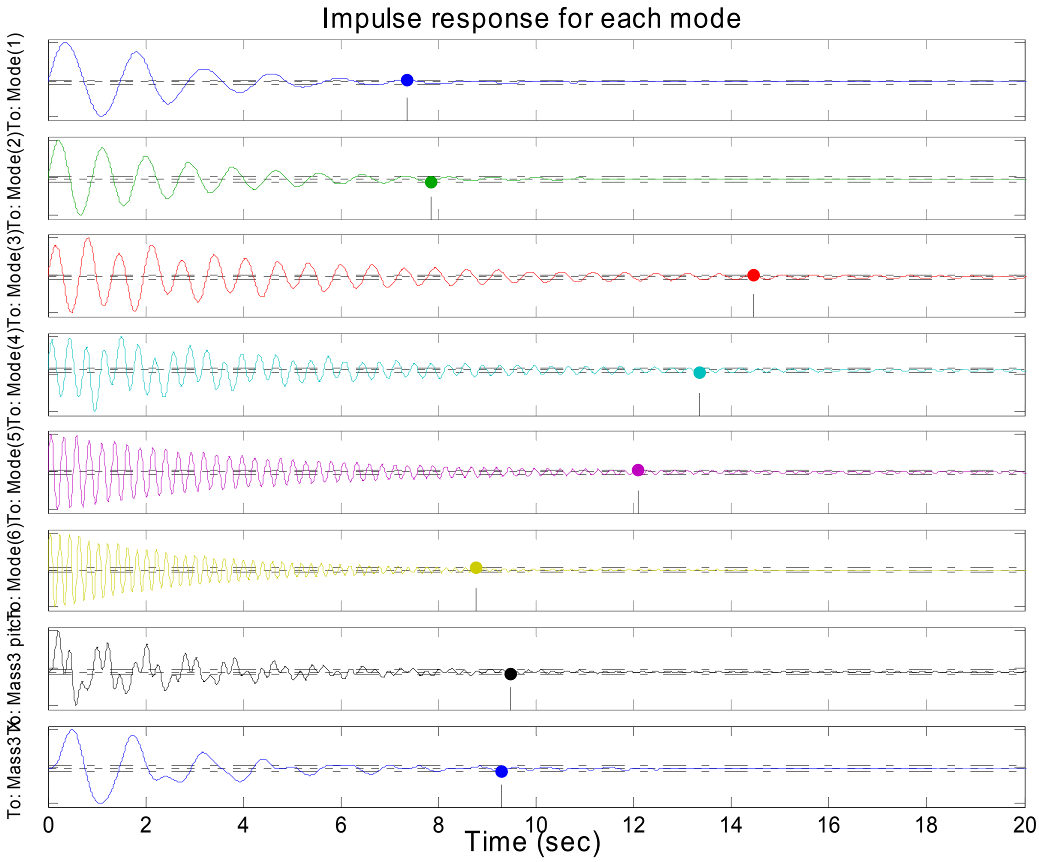

Figure 5.20: X/Pitch, impulse response for each mode and mass 3

5.3.4 Optimizing the estimator

The estimator will now be a MIMO modal estimator optimized by using the LQ technique described previously. As we have seen in section 4.2, the key to optimizing this loop is to choose the parameters of the cost function to minimize the sensor noise transmission. The cost function is given by equation 4.24.

We need to chose the parameters R_1 and R_2. These will determine the accuracy of the estimation (and thus the damping performances) as well as the sensor noise filtering in the loop.

We will first plot the displacement noise at 20Hz due to the sensor noise (figure 5.21). The cross coupling between pitch and X is taken into account. We use the sensor noises seen in figure 5.19

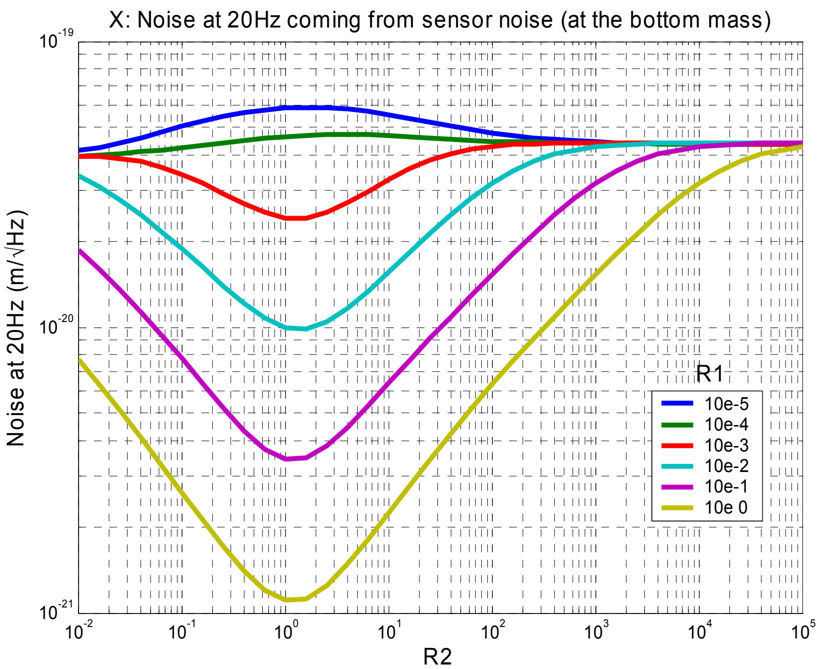

Figure 5.21: X displacement noise at the bottom mass at 20hz for different values of R1 and R2

We can also plot the angular noise at 20Hz in figure 5.22

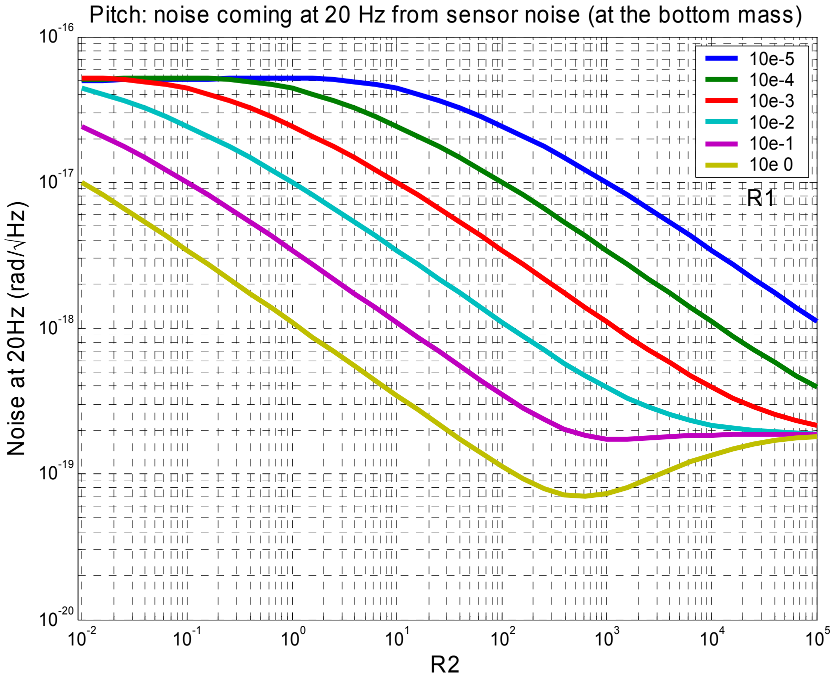

Figure 5.22: pitch angular noise at the bottom mass at 20hz for different values of R1 and R2

As we see on figure 5.21 and figure 5.22, the bigger R_1 is, the less the sensor noise transmission to the bottom mass. We also see that the plots have a dip; this is the limit where cross coupling becomes more important than the direct transmission. To the left of the dip, the noise at the bottom mass is dominated by the pitch sensor noise; right of the dip, the noise is dominated by the X sensor noise.

In order to minimize the cross couplings, it is useful to choose values of R_1 and R_2 so that the working point is located between the dips of those 2 figures. Therefore we can choose R_2 to be above 1 and below 300. It is also important to remember that the R_2 parameter balance the estimation of both degrees of freedom. If R_2 is too big or too small, one DoF will be very well estimated while the other will not, which can create problems. Choosing a value of R_2 close to 1 can alleviate this problem.

We can now study the damping performances, the settling time to a X impulse is plotted in figure 5.23 for several values of R_2.

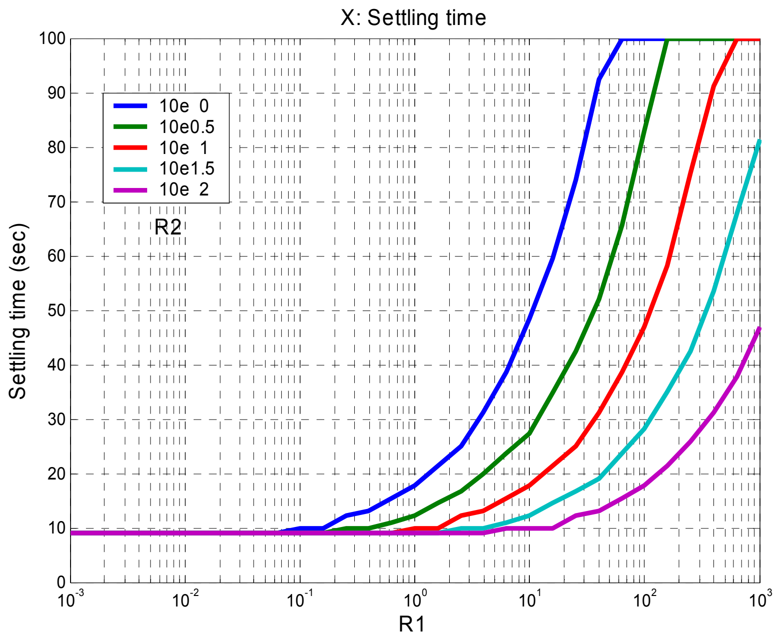

Figure 5.23: X settling time for different values of R1 and R2

The settling time is now plotted for the pitch direction in figure 5.24:

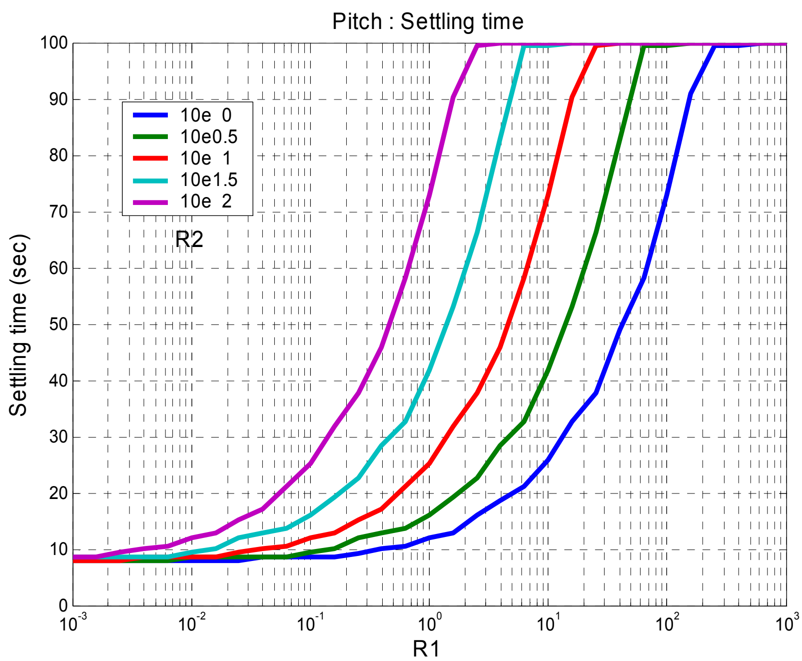

Figure 5.24: pitch settling time for different values of R1 and R2

This plot shows what we were discussing previously, the R_2 parameter balances the estimation of both degrees of freedom, and if this value is too high or too small, one DoF will have very good damping performances while the other won't. Using those plots, we can see that the best values for R_2 are the green and dark blue curves.

By studying the noise plots and the damping plots together, we see that a good compromise to get good damping on both degrees of freedom and a good sensor noise filtering is :

- $R_1 = 0.1$
- $R_2 = 10^{0.5} \approx 3$

These are the parameters we will choose for our loop. Now that all the parameters have been chosen, we can plot the performances of our damping loop. The impulse responses in both directions are plotted in figure 5.25 and figure 5.26.

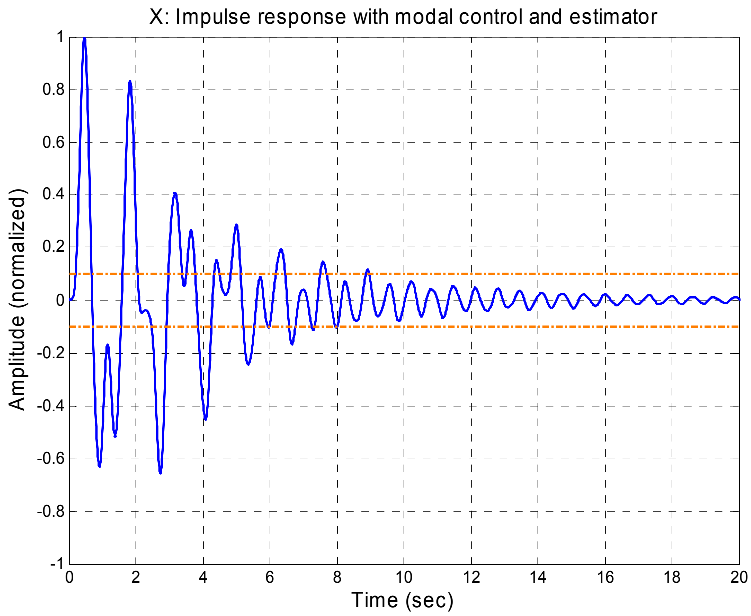

Figure 5.25: X impulse response with the modal control and estimator loop

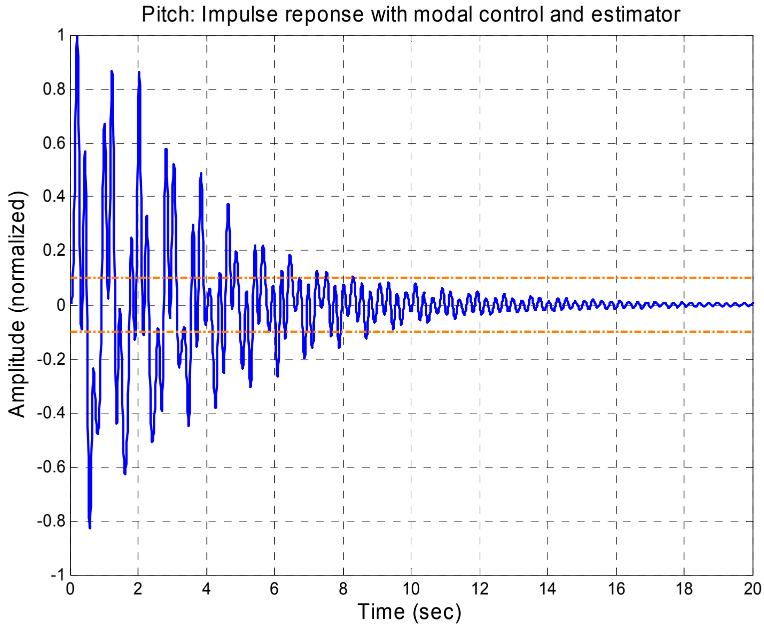

Figure 5.26: Pitch impulse response for the modal control and estimator loop

We see that both meet the damping requirements, the estimator didn't reduce the damping performances.

In figure 5.27, we plot the displacement noise at the bottom mass using the noise inputs of advanced LIGO.

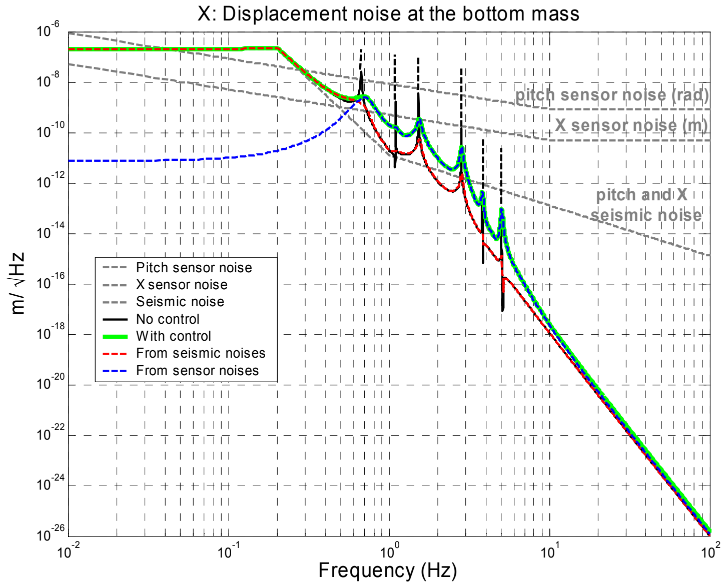

Figure 5.27: X displacement noise at the bottom mass using the modal control and estimator loop

This plot can be compared to the one we would get using a classic damping loop:

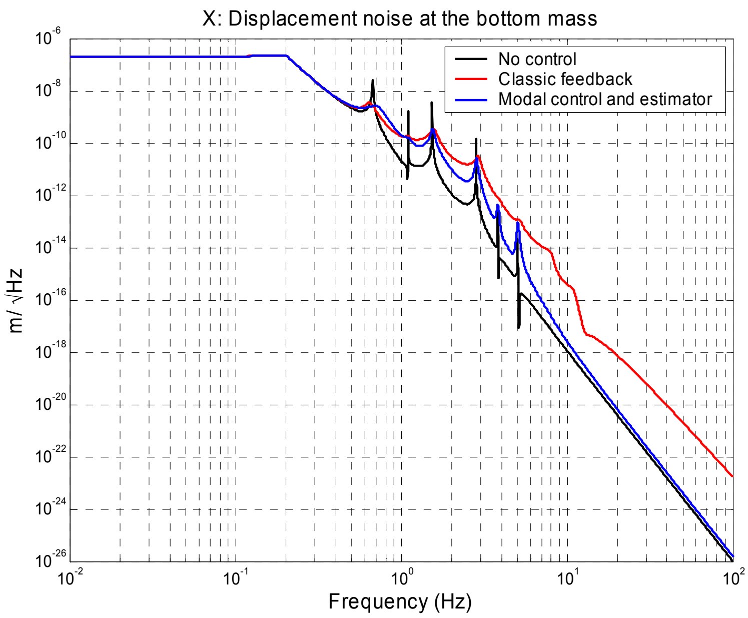

Figure 5.28: X displacement noise at the bottom mass, comparison

We see that the sensor noise filtering is much better; there is a factor of 100 between the classic loop noise and the modal loop noise at 20Hz.

The same results can be obtained for the angular noise in pitch at the bottom mass (figure 5.29). AS discussed previously, there is no direct coupling between the ground pitch and the pendulum pitch, the seismic noise only comes from the ground motion in X here, which explains the very low level of the seismic contribution.

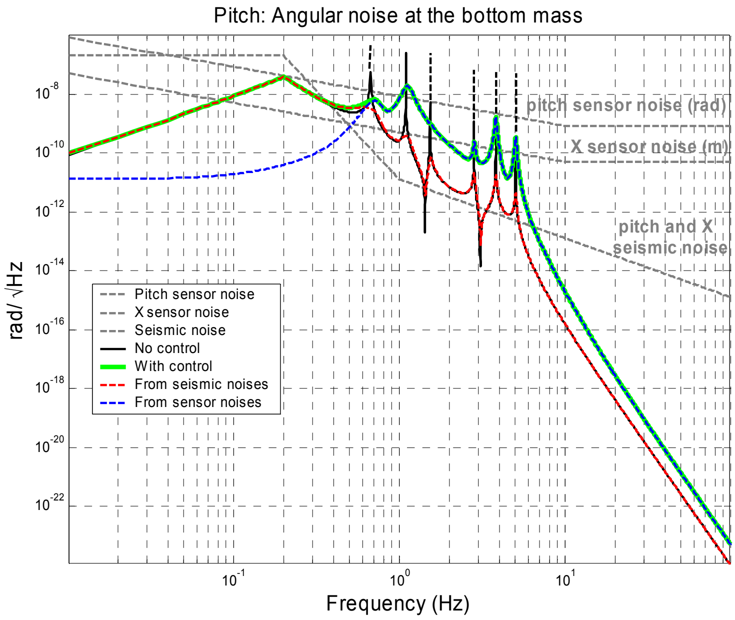

Figure 5.29: Pitch angular noise at the bottom mass using the modal control and the estimator

Let’s now compare this plot to the classic feedback.

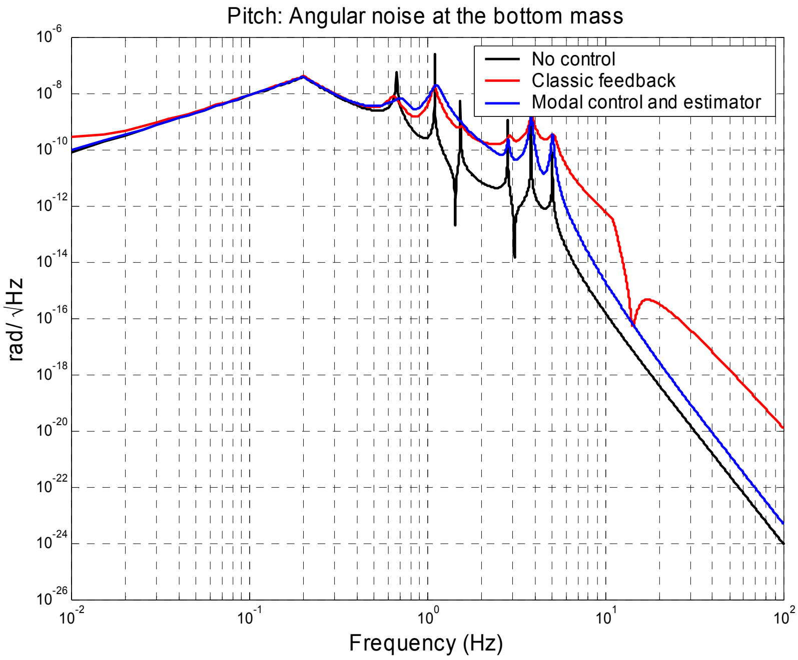

Figure 5.30: Pitch angular noise at the bottom mass, comparison

Once again, the performances of the modal loop are significantly better than the classic feedback approach.

5.4 CONCLUSION

We have seen in this section how to apply the modal state control and the estimator techniques to two different systems. The choice of the parameters for the modal controllers and the estimator feedback are easy to make. The idea is to keep good damping performances while pushing the estimator feedback gain to low values to filter the sensor noise at high frequencies.

We have plotted the noise amplitude at the bottom mass by using those loops for the Yaw and Longitudinal-Pitch systems. The noise inputs of advanced LIGO were used and the results were compared to classic filtering feedback. Overall, the modal control loop provides much better performances.

So far, all these results were produced using simulations and a model of the triple pendulum. The next section will describe the experiment used to check the loop model, and compare the experimental results with simulation results.

6 EXPERIMENT, VALIDATION OF THE CONTROL LOOP

6.1 INTRODUCTION

We have seen above how to design and optimize a MIMO estimator and a modal control for the triple pendulum. We have developed a model to calculate the transmission between seismic or sensor noise and the pendulum motion. The next step is to verify our model experimentally, and check that both the damping and the seismic/sensor noise transmission agree with our model.

Unfortunately, Advanced LIGO isolation systems are not all available yet, and we are unable to reach the seismic noise level we expect for advanced LIGO (see section 2.4.1). The solution is to increase the sensor noise. We will artificially inject more sensor noise in the sensor inputs so that the ratio of sensor noise to seismic noise signal approximates that which will be found in Advanced LIGO. We will then study the transfer functions between this noise and the pendulum motion.

We will first check the damping performances for the 3 directions discussed in the previous section (X, Pitch, Yaw). Then, we will use advanced measurement techniques rarely used in vibration measurement to validate our noise transmission model.

6.2 CHECKING THE DAMPING PERFORMANCES

The damping loops designed in the previous section are applied to the working pendulum. In order to check the damping performances, we apply an impulse to the top mass of the pendulum and measure the displacement of this mass. The settling time is then compared to the loop model. It is important to note that we are measuring the top mass motion, the settling time of this mass can be slightly different than the one at the bottom mass that is used in the loop optimization.

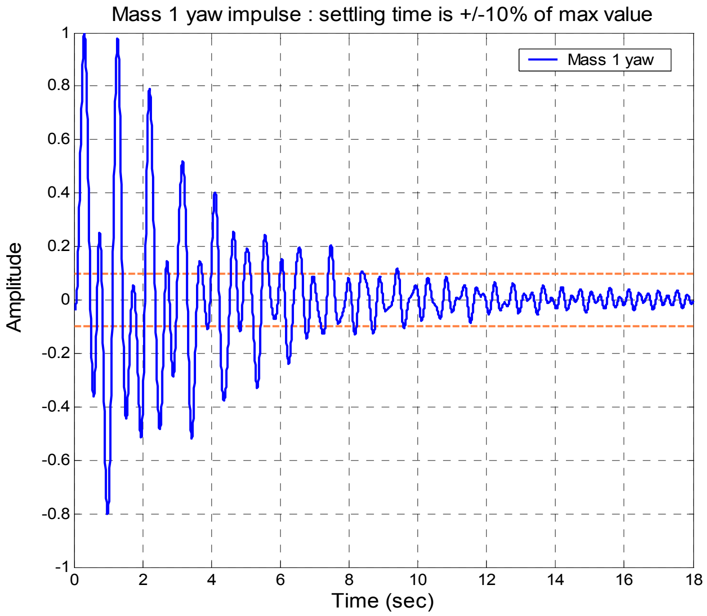

Figure 6.1: Impulse response for the top mass, Yaw measurement

The loop model predicts a 9 sec settling time for the top mass. As we can see on this plot, the experiment gives us a settling time of 9.2 sec. The model and the experiment agree very well.

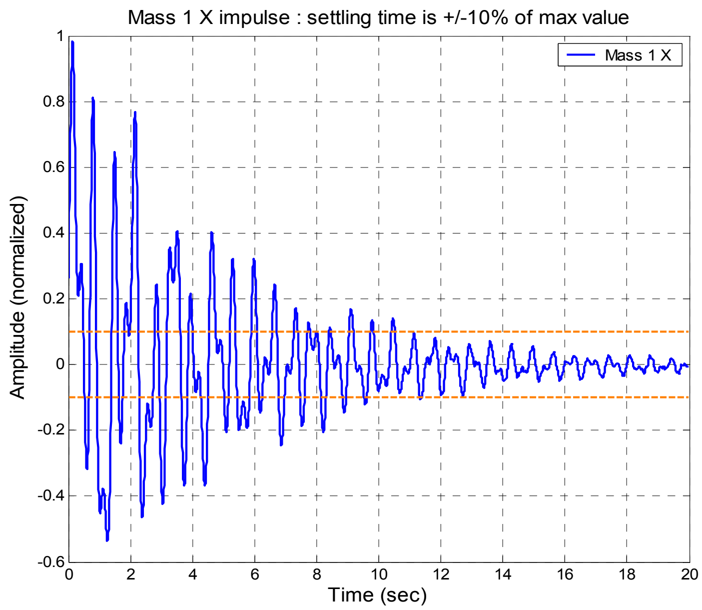

Figure 6.2: Impulse response for the top mass, X measurement

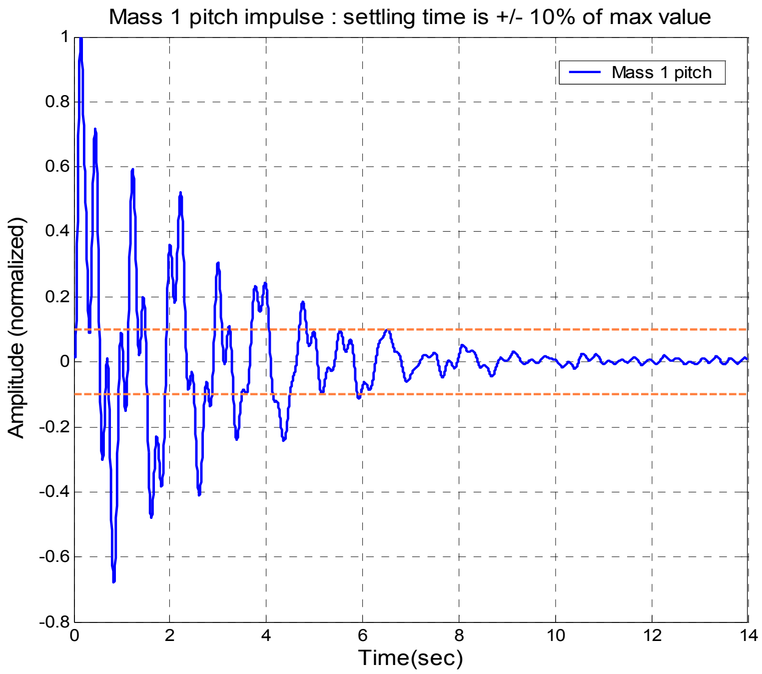

Figure 6.3: Impulse response for the top mass, Pitch measurement

For the X/Pitch loop, the model gives us a settling time of 12.4 seconds for the X direction and 8.1 seconds for the pitch direction. As we see on figure 6.2 and figure 6.3, the experiment validates these damping performances.

This simple experiment validates our loop model for the damping performances, we now need to validate the sensor noise transmission.

6.3 THE OPTICAL CAVITY EXPERIMENT, MEASURING THE SENSOR NOISE TRANSMISSION TO THE BOTTOM MASS MOTION

Using the top mass works perfectly when you want to check resonance frequencies, impulse response, or damping loops. However, we now want to focus on the noise transmission, and especially at high (>10Hz) frequencies. In that case, it is important to look directly at what we are interested in for LIGO: which is the bottom mass. This is a new challenge, measuring the bottom mass motion is not as easy as measuring the top mass, especially above 10Hz as we will see below.

The first problem is the sensitivity required to measure the signal. The pendulum response to sensor noise falls as $1/f^6$ at the bottom mass. This means that between 10Hz and 100Hz, the signal you measure has been reduced by 1 million.

The second issue is related to our sensors. The pendulum is instrumented with OSEMS (see section 0) which have a sensitivity of $5e^{-11} m/\sqrt{Hz}$ above 10Hz and increase slightly with low frequencies. Those sensors are position sensors and measure the relative distance between the frame and the masses. These sensors work perfectly for the top mass and the low frequencies, because the pendulum moves a lot more than the frame. However, as the frequency increases and as the filtering increases at the bottom mass, the frame's motion becomes much bigger than the mass motion. In this regime, we aren't measuring the pendulum motion anymore, but the frame itself. The plot in figure 6.4 is a good example of this phenomenon, we are plotting the transfer function between M1 actuators in X and M3 position in X measured by the OSEMS.

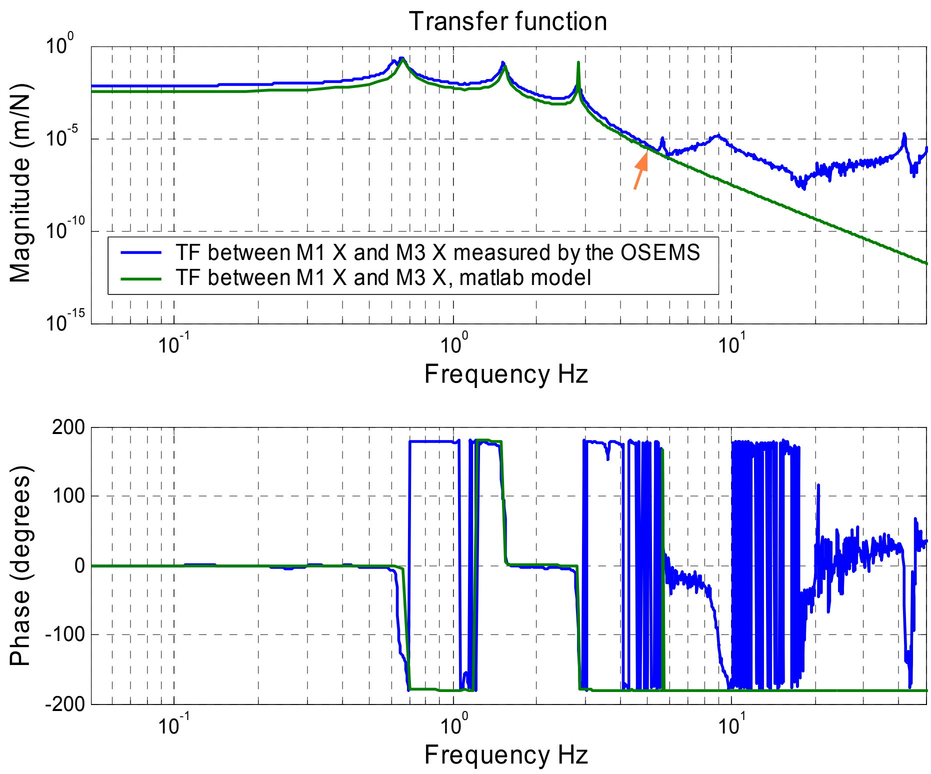

Figure 6.4: Transfer function from Mass1 to Mass3 using the OSEMS

As we can see, above 5Hz, the OSEMS aren't measuring the pendulum anymore, this is due to the fact that the frame of the pendulum moves more than the bottom mass of the pendulum.

The force that our drive can supply is limited because of electronics limitations. In addition to this, the filtering at the first mass is “only” 1/f^2, if we drive too hard, the first mass will move too much and we might break the pendulum.

We need to find a sensor to solve these problems:

1. Find a sensitive enough sensor to compensate for the 1/f^6 pendulum filtering
2. Find an inertial sensor or a relative sensor with a reference that is quieter than what we want to measure

The second problem is what will mostly drive our choice. It is not easy or nearly impossible to get an inertial instrument that would be small and light enough to be placed on the bottom mass without disturbing its dynamics. Moreover, it would be really hard to find one sensitive enough to get this measurement done.

The only way is to use a relative measurement, using a reference that is quieter than the elevated sensor noise driven pendulum. A good reference is actually very easy to think about: another triple pendulum will filter as much noise as the first one, and be an excellent reference. If we can put 2 triple pendulums face to face and measure the distance between the bottom mass of 2 pendulums, we can measure the motion of the bottom mass.

We can measure the distance between 2 mirrors with an excellent sensitivity using interferometry techniques. The vast majority of interferometric displacement measurements are carried out with two-beam splitting interferometers. Other types of interferometer may be used as well. The Fabry-Perot cavity is an attractive way to measure small displacements because it directly measure the distance between 2 parallel mirrors, and doesn’t require an external reference such as a classic Michelson interferometer arm.

In 1983, RWP Drever et al. invented a technique to stabilize the frequency of a laser by locking it to a Fabry-Perot reference cavity [46], this technique is based on an earlier microwave technique invented by RV Pound, and much of the implementation was worked out at JH Hall’s group. The technique can also be worked the other way around, to lock a cavity to a laser, when you do this, you can measure the length of the cavity with a very high sensitivity.

We will explain this technique in detail later, but for now, let’s explain the measurement strategy in few words: The measurement involves building up an optical field in a cavity formed between two mirrors. The phase and amplitude of the optical field that is reflected off the resonant cavity strongly depends on the microscopic separation of the mirrors. As one of the mirror moves, the PDH technique detects this phase shift and will give us a very accurate measurement of the length between the 2 masses, we will then apply a feedback force to the first pendulum to keep this length constant and keep the cavity at resonance. By knowing the force we have to apply on the first pendulum, we know how much our second pendulum moved.

Let’s come back and focus on the goal of the experiment. We want to verify our noise model, and check the transmission between the sensor noise and the bottom mass of the pendulum.

Below 5Hz, the measurement can be done with the OSEMS, these sensors work well at low frequencies and are easy to use and reliable.

Above 5Hz, we will use the optical cavity measurement. The cavity will be used to measure 3 important transfer functions:

1. The transfer function from sensor noise to mass3 using the classic damping
2. The transfer function from sensor noise to mass3 using the modal damping

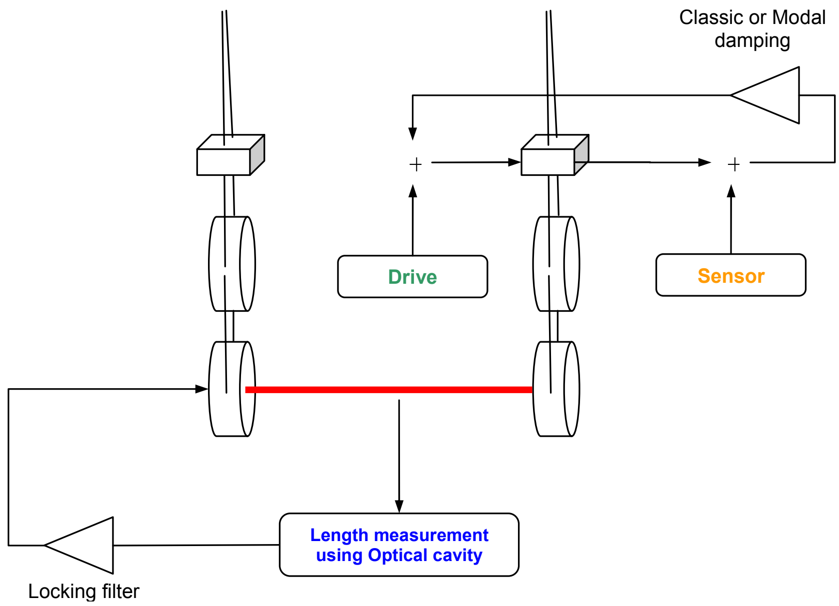

Figure 6.5: experiment diagram

The OSEMS and cavity measurements will then be merged to obtain the transfer function at both low and high frequencies on the same plot. We'll then be able to compare the results with our model.

6.4 LOCKING A CAVITY USING THE POUND-DREVER-HALL TECHNIQUE

6.4.1 Qualitative model

We have mentioned above that we have chosen to use a Fabry-Perrot cavity to measure the displacement of the pendulum, this method consists of having a laser beam boucing between 2 partially reflective mirrors. Because the mirrors are not 100% reflective, a small part of the light escape the cavity, this light is the key to know how the mirrors move.

In the following paragraphs we will explain how to extract a displacement signal out of a light intensity measurement. Because it is not possible to measure the electric field of an optical beam directly, we will use the Pound-Drever-Hall technique to extract the phase information from the intensity measurement. However, we will see that this technique only provides a linear output when the cavity is close to resonance (+/- few nanometers around resonance). To perform the measurement, it is necessary to add a control loop to lock the cavity at resonance.

Below is the complete diagram of our optical experiment. It shows what we call a Pound-Drever-Hall setup.

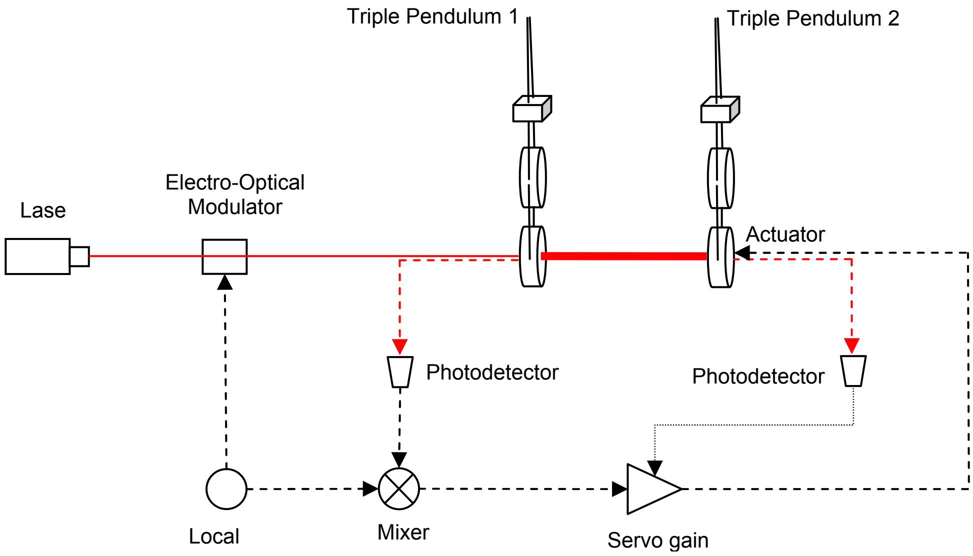

Figure 6.6: Pound-Drever-Hall Layout with 2 triple pendulums

The arrangement shown above is used to measure the spacing between the 2 pendulums.

We send the beam into the cavity formed by the 2 triple pendulums. If the length between the 2 pendulum's mirrors is equal to a finite number of the laser wavelength, the power between the 2 mirrors builds up and the reflective beam cancels with the incident beam (they both have the same amplitude and opposite phase). By placing a photo detector looking at the reflected beam, we can measure the spacing between the 2 triple pendulums. In the case where the cavity resonates, the photo detector measuring the reflecting beam measures zero.

If we look at the amplitude measured by the photo-detector on the reflected beam around this resonance, we get the following plot:

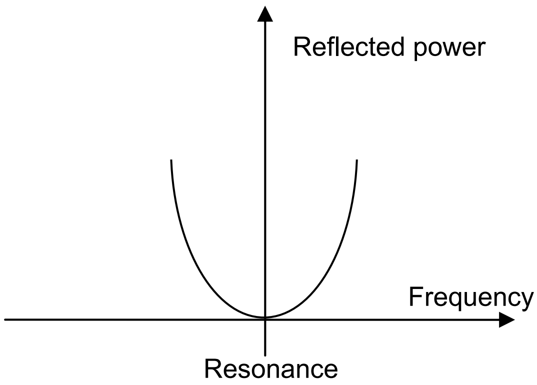

Figure 6.7: power measured by the photo-detector on the reflected beam around the resonance

Looking at this amplitude, we see that it is impossible to know on which side of the resonance we are at because the plot is symmetrical on both side. A way to know on which side of the resonance we are at would be to get the derivative of this amplitude according to the frequency. For a conceptual understanding, it is interesting to imagine that we can modulate the laser frequency.

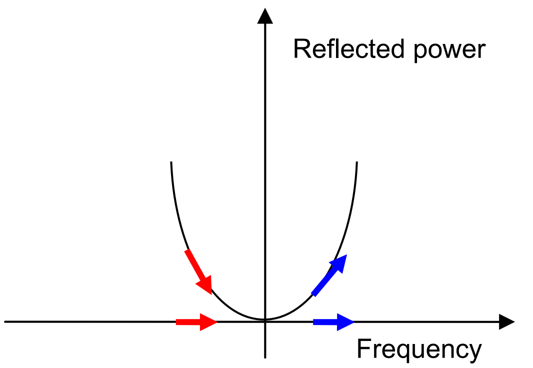

Figure 6.8: Power measured by the photo-detector on the reflected beam around the resonance

If we are above the resonance, increasing the laser frequency increases the power in the reflected beam (blue). If we are below the resonance, increasing the laser frequency decreases the power in the reflected beam (red). If we modulate the laser beam frequency, we can now tell on which side of the resonance we are on by knowing if the reflected power varies in phase or 180 degrees out of phase with the modulation. This modulation is done with the optical modulator before the beam is injected into the cavity

The next step is to compare the modulation signal (produced by the local oscillator) with the output of the photo-detector, and to extract only what is happening at the modulation signal, this is the role of the mixer. The sign of the mixer's output is different on either side of the resonance, and is zero when the cavity resonates. This is exactly the kind of signal we need to measure the spacing between the 2 pendulums. This signal is called the error signal because it reaches 0 at resonance and increase or decrease when we are moving away from the resonance.

However, as we will see below in the mathematical model, this error signal is only linear when the cavity is close to resonance. In order to perform the measurement, it is necessary to lock the cavity at resonance. This is the role of the servo control that actuates one of the pendulum to keep the cavity "locked".

The transmitted beam isn't necessary to lock the cavity and make the measurement, however, by measuring the intensity going trough the cavity with this sensor, we can normalize the other measurements in case the laser beam intensity changes or if the alignment of the optical elements change a little bit, it makes the measurement easier.

6.4.2 Quantitative model

In practice, it is actually easier and more desirable to modulate the phase of the laser beam instead of its frequency. It is a lot easier to resort to a quantitative model to understand how this works, and we will give a short description of the mathematics used for the cavity.

A laser beam has an electric field that can be approximated in one point by

- $E = E_0 e^{i\omega t}$ *6.1*

In the qualitative description, we talked about dithering the frequency, in practice, this is easier to dither the phase using an Electro-Optical Modulator. After the beam has passed trough this EOM, its electric field becomes:

- $E_{inc} = E_0 e^{i(\omega t + \beta \sin \Omega t)}$ *6.2*
- $E_{inc} \approx E_0 \left[J_0(\beta) e^{i\omega t} + J_1(\beta) e^{i(\omega+\Omega)t} - J_1(\beta) e^{i(\omega-\Omega)t} \right]$ *6.3*

Where Ω is the modulation frequency and β is called the modulation depth. This electric field shows 3 terms, like 3 incident beams entering the cavity, one carrier at the laser frequency, and 2 sidebands.

Let's now calculate the reflected beam, we just multiply each of the incident beams by the reflection coefficient at the appropriate frequency:

- $$E_{ref} = E_0\left[F(\omega)J_0(\beta)e^{i\omega t} + F(\omega+\Omega)J_1(\beta)e^{i(\omega+\Omega)t} - F(\omega-\Omega)J_1(\beta)e^{i(\omega-\Omega)t}\right] \quad 6.4$$

Where F is the reflection coefficient that varies with the frequency. F is a complex coefficient that depends on properties of both the beam and the cavity. For a symmetric cavity with no losses like ours, it is equals to:

- $$F(\omega) = \frac{r\left(e^{i\phi}-1\right)}{1-r^2 e^{i\phi}} \quad 6.5$$

Where r is the amplitude reflection coefficient of each mirror (they are both the same in a symmetrical cavity like ours) and

- $$\phi = \frac{2\omega L}{c} = \frac{4\pi L}{\lambda} \quad 6.6$$

The photodetector is only able to measure the power in the reflected beam :

- $$P_{ref} = \left|E_{ref}\right|^2 \quad 6.7$$

- $$\begin{aligned} P_{ref} &= P_c\left|F(\omega)\right|^2 + P_s\left\{\left|F(\omega+\Omega)\right|^2 + \left|F(\omega-\Omega)\right|^2\right\}\ldots \\ &+ 2\sqrt{P_c P_s}\,\mathrm{Re}\left[F(\omega)F^*(\omega+\Omega) - F^*(\omega)F(\omega-\Omega)\right]\cos\Omega t\ldots \\ &+ 2\sqrt{P_c P_s}\,\mathrm{Im}\left[F(\omega)F^*(\omega+\Omega) - F^*(\omega)F(\omega-\Omega)\right]\sin\Omega t\ldots \\ &+ (2\Omega\, terms) \end{aligned} \quad 6.8$$

The mixer pulls out the term that is proportional to the local oscillator signal (or modulation signal) in $\sin \Omega t$, every other terms vanish.

- $\varepsilon = 2\sqrt{P_c P_s}\ \mathrm{Im}\left[F(\omega)F^*(\omega+\Omega) - F^*(\omega)F(\omega-\Omega)\right]$ 6.9

It is important to note that the frequency ω or the length of the cavity L play the same role in this equation, the technique can either be used to measure the laser frequency or to measure the length of the cavity. The error signal can now be plotted against the variation of the length of the cavity

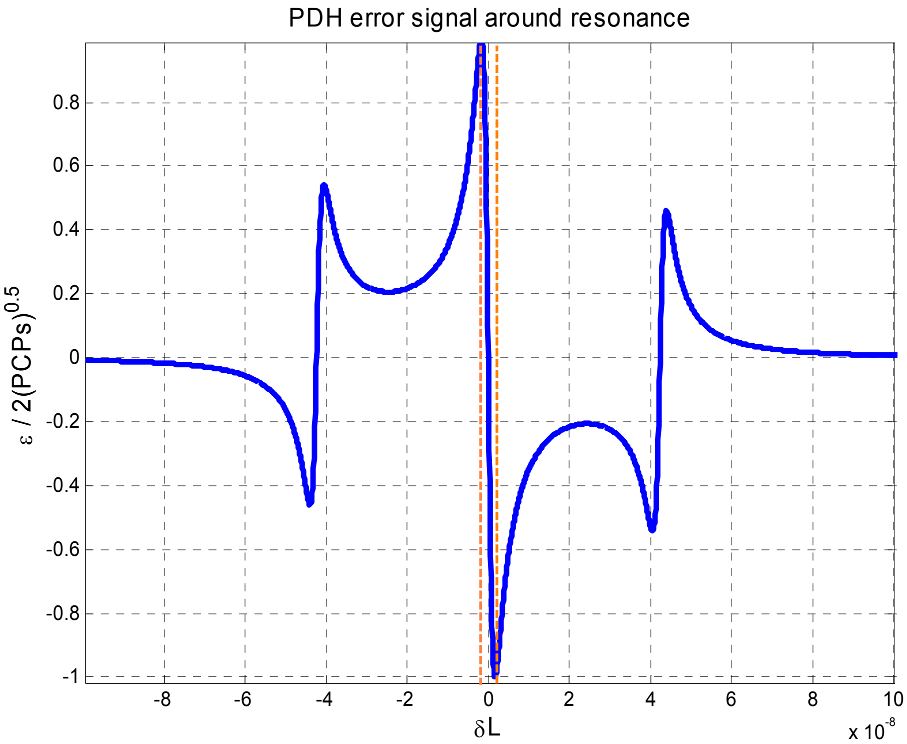

Figure 6.9: PDH error signal around the cavity resonance

We see that we get a very useful signal close to the resonance: The error signal is 0 when the cavity is exactly on resonance and linearly goes up or down whether we are moving on one side or the other side of the resonance. However, it is necessary to keep the cavity between the 2 orange lines (+/- 2 nanometers in our case) to get a linear measurement. This is why we use this signal to lock the cavity on resonance.

The 2 other peaks correspond to the modulation frequencies, and aren't used for our experiment. In the linear area (between the orange lines), the error signal can be approximated by a linear function.

Near resonance, we can assume that the sidebands are completely reflected, which leads to

- $$F(\omega \pm \Omega) \approx -1 \tag{6.10}$$

In this condition, the error signal can be written as a linear function directly proportional to the change of length of the cavity:

- $$\varepsilon = -16\pi\sqrt{P_c P_s}\,\frac{r}{\lambda(1-r^2)}\delta L \tag{6.11}$$

6.4.3 Locking loop

An important step is to design a control loop to keep this cavity on resonance. Because we can't measure the transfer function until we have designed this control loop, we will use the model of the pendulum. We then design a very simple filter to cross the upper unity frequency with a slope of 1/f and gain some phase in the high frequencies to compensate for some electronics and digitization delay. The plant, filter and open loop are plotted below:

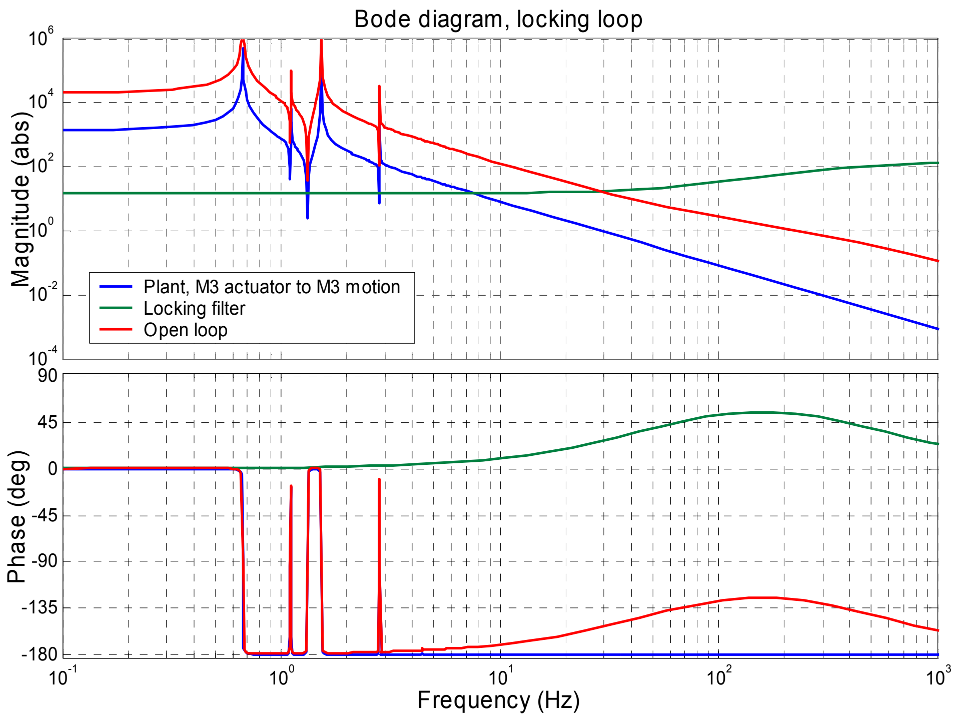

Figure 6.10: plant, filter and open loop transfer functions for the locking loop

The main limit for the upper unity frequency and the loop gain is the digitization phase loss. Using our Dspace system and the computation load we have (due to our input/outputs, calculation and filters), we can't get a sampling time smaller than 3.10^{-4} seconds. We can plot the phase loss due to this digitization:

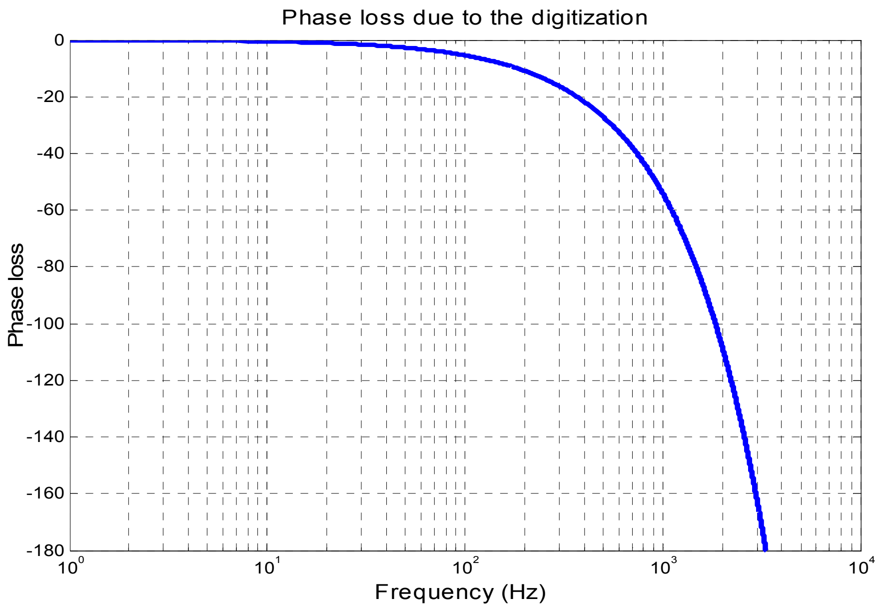

Figure 6.11: Digitization phase loss, Ts=3e-4 sec

We can see that it would become really hard to compensate for the phase loss above 500Hz. To keep a decent phase margin, we decided to choose an upper unity frequency of 300Hz, which explains the open loop shown above.

6.4.4 Installation and pictures

A second triple pendulum is installed in the vacuum chamber to create the cavity with the first pendulum. Several optical elements are added too. A small optical table, outside the chamber, will be used for the instruments (photo detectors, EOM, camera). The laser beam is brought to this table from the main LASTI laser (Infrared $\lambda = 1064nm$) through an optical fiber. This experiment is also a good test for LASTI to see the effects of a long optical fiber on the beam, especially how much acoustic noise couple to the fiber and the optical beam.

The picture below shows the inside of the vacuum chamber, the 2 triple pendulums and the optical elements:

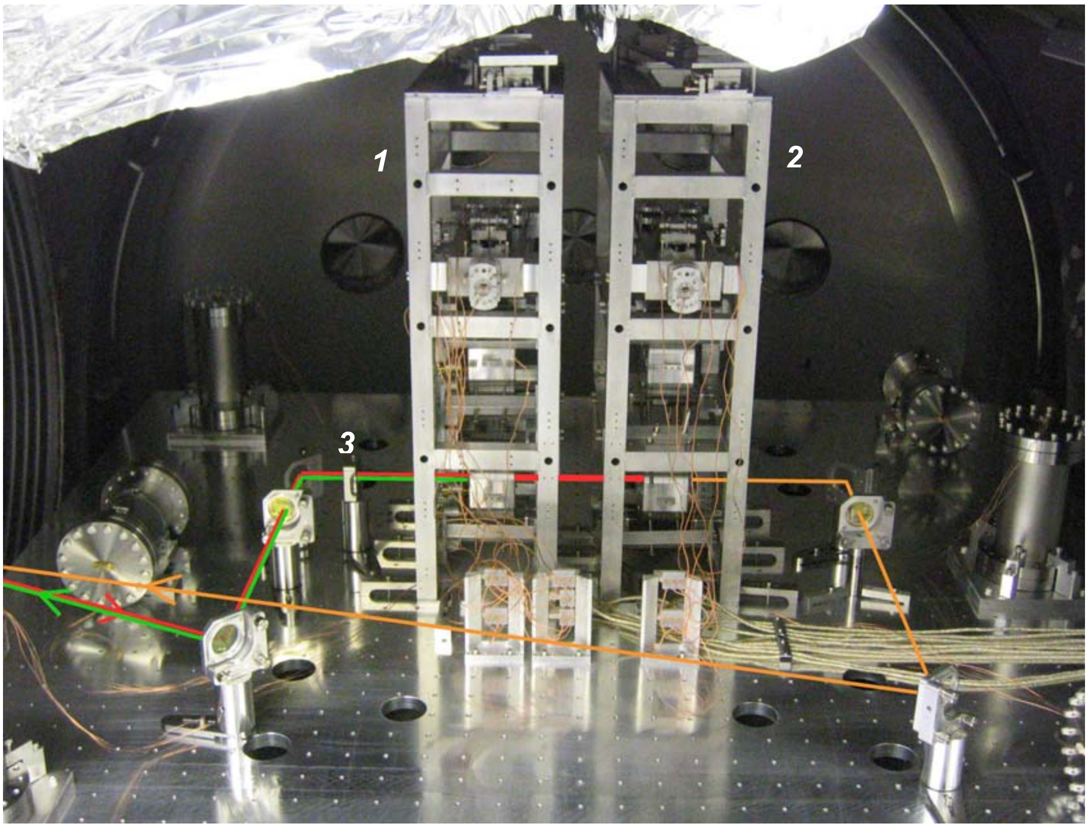

Figure 6.12: In vacuum optical table picture

- Incident beam in red
- Reflected beam in green
- Transmitted beam in orange

1. Triple pendulum 1, this pendulum will keep the cavity locked
2. Triple pendulum 2, this pendulum will run the damping loop we want to test
3. Quarter Wave Plate, This device changes the polarity of the beam that double passes through it by 90 degrees, so that the reflected beam polarization is rotated by 90 degrees with respect to the incident beam, it enables us to separate the incident beam and the reflected beam with a polarizing beam splitter located on the outside optics table.

This picture below shows the optical table outside the chamber:

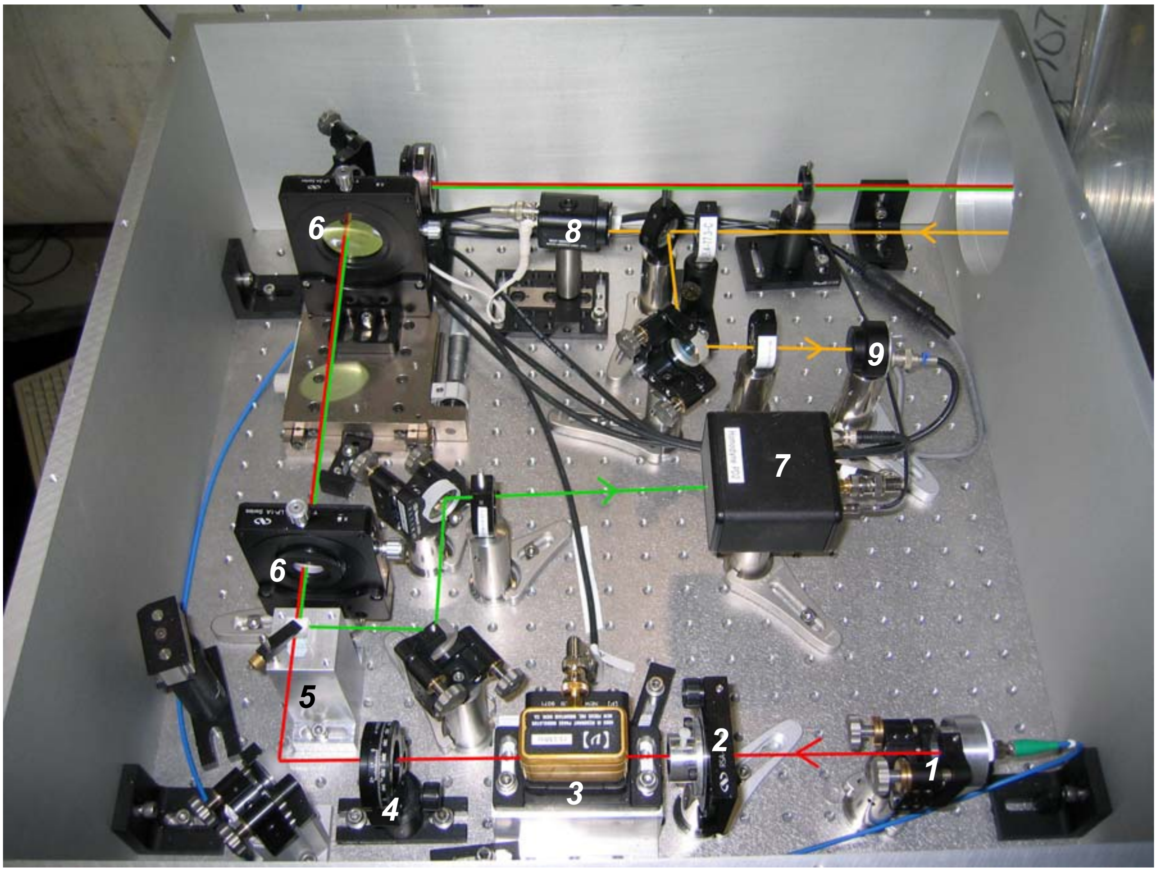

Figure 6.13: outside optical breadboard picture

- Incident beam in red
- Reflected beam in green
- Transmitted beam in orange

1. Optical fiber output
2. Polarizer, cleans up the polarization from the fiber for accurate alignment with the EOM
3. Electro-Optical Modulator, modulates the phase of the laser beam with a 13,3 Mhz sine
4. Half way plate, used to rotate polarization and hence change the transmitted power through 5
5. Polarizing Beam Splitter Cube
6. Mode matching lenses
7. Reflected beam photo-detector, this is the sensor we use to create the PDH error signal
8. Camera, monitors the transmitted beam to tell us how the cavity is locked, and to which optical mode the cavity is locked to.
9. Transmitted beam photo-detector, we use this sensor to track the power built up in the cavity. This power level is proportional to the gain of the PDH signal. We can use this to make sure that the control loop gain is constant.

6.5 RESULTS

6.5.1 The loop gain

The first important measurement is the open loop measurement. Every measurement made using the cavity will be suppressed by the open loop gain of the locking loop. Let's take the diagram example below. Our goal is to measure the transfer function H on the second pendulum, this transfer function can be the transmission from sensor noise to bottom mass for example. However, as we can see on the diagram, we can't measure H directly, because the sensor we use is in loop and the only measurement we have is x. In order to retrieve H, we must know P and F. PF is the open loop transfer function of the cavity.

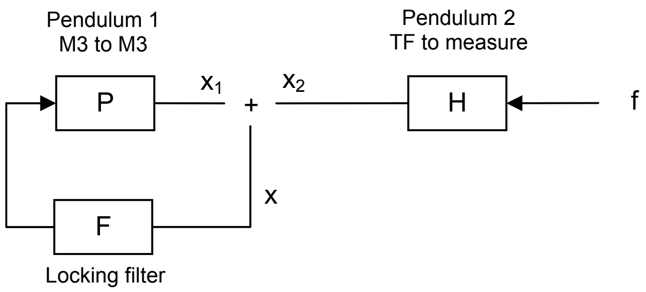

$$H = \frac{x_2}{f}$$

$$x_2 = x - PFx$$

$$H = \frac{x}{f}(1 - PF)$$

$$H = \frac{x}{f}(1 - open\ loop)$$

Figure 6.14: Transfer functions diagram

The first step is to measure PF. Because the cavity has to be locked (feedback must be on) to use it, the measurement of the open loop is done by injecting some noise and measuring the signal before and after the sum. The transfer function between the post sum signal and the pre sum signal is the open loop:

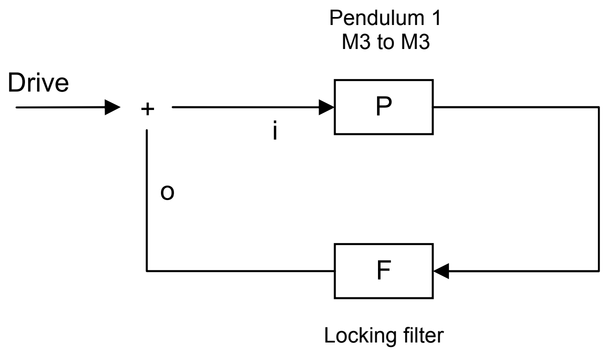

$$PF = \frac{i}{o} = open\ loop$$

Figure 6.15: Open loop measurement diagram

The measured open loop is then compared to our model. On the plot below, you can see the result of the open loop measurement.

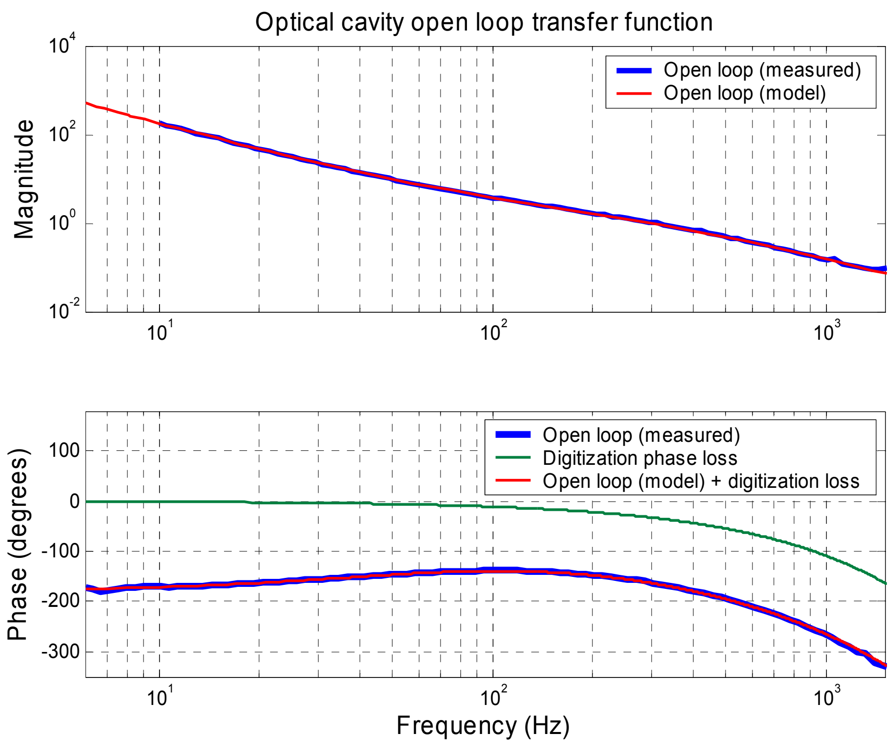

Figure 6.16: Open loop, model and measurement

The model and the data are plotted; we see that they agree very well, this is not surprising, because the behavior of the pendulum at these frequencies is very well known. We also see the effect of the digitization on the phase. If there wasn't any digitization, the blue phase should match the red one. The expected phase loss due to the digitization is plotted in green.

6.5.2 Sensor noise to M3 transfer functions

The final step is to measure the transfer function we are interested in: the transmission between the sensor noise and the motion of the bottom mass.
The low frequencies are measured using the osems and the high frequencies are measured using the optical cavity. Data are then merged to one plot and compared to the model.
We also compare 2 different types of damping loop:

1. The "classic" filtering feedback, as seen in section 2.5.2
2. The modal damping and MIMO estimator, as seen in section 5.3

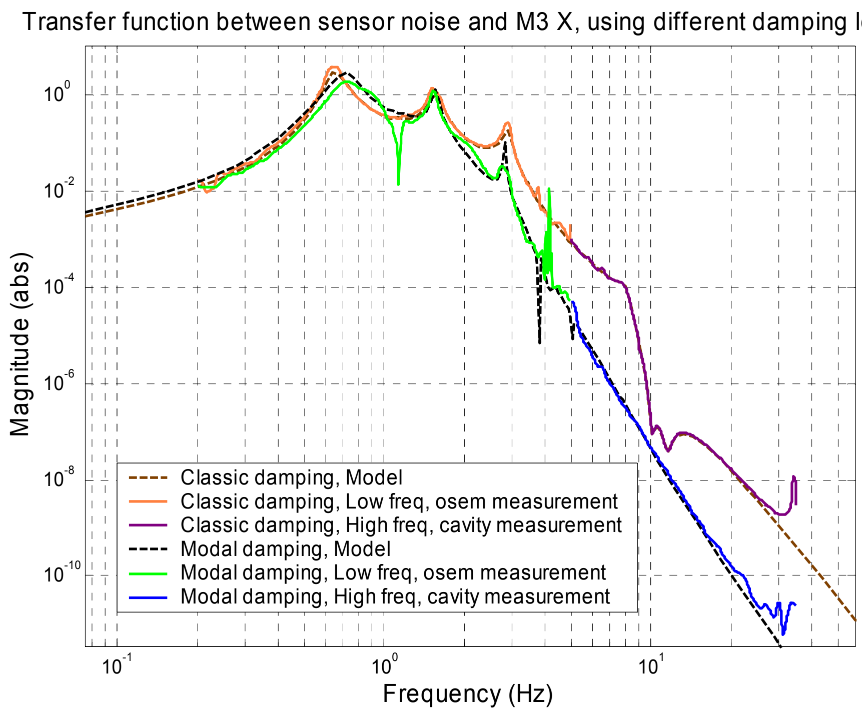

Figure 6.17: Transfer functions from sensor noise to the bottom mass

The high frequencies agree very well, between 5Hz and 25Hz, the data are clean and match the model almost perfectly. This is a very good result; it verifies our noise model at high frequencies, which is the most important part for sensor noise transmission.

The low frequencies agree well for the classic feedback too. For the modal damping, the data are slightly different than the model at some frequencies (dip at 1.1 Hz and slightly different bump for the first mode), this difference is not very significant, and most likely due to some mismatch between the model and the real plant, or some cross coupling that would be more important than expected.

Overall, the measurement is a very important step, it is the last and definitive verification for our noise model, and this proved that our model can be trusted.

6.6 LOCKING AND DAMPING ON THE SAME PENDULUM

The experiment using the optical cavity was more than just a vibration measurement. In the future, the triple pendulum will be used in the LIGO interferometers and will lock some more complicated optical cavities. The experiment we have is also very important to test the behavior of the triple pendulum and the damping loops during the cavity lock.

Because our modal control loop is very dependant of the dynamics of the pendulum to work properly, we noticed that if we use this loop on the 2 pendulums, then the system becomes unstable. By studying the problem more carefully, we noticed that our damping loop turns unstable on the pendulum that locks the cavity once the cavity is locked. This is something that had never been noticed before because classic feedback loops aren’t as dependant on the plant dynamics. This following section will describe the experiments and simulations we made to understand this phenomenon, and give some ideas of solutions to fix it.

In this experiment, we are going to focus on the pendulum that we use to keep the cavity locked. The goal is to characterize this pendulum during the lock, and when the cavity is unlocked, and to compare both systems.

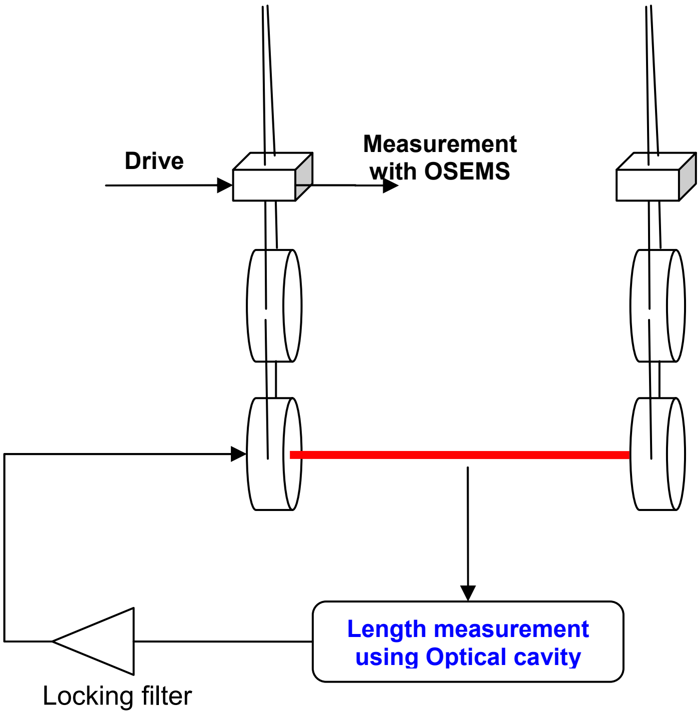

Figure 6.18: Experiment diagram

The characterization of the pendulum is done with the cavity locked and with the cavity unlocked, and the results are compared. The biggest difference, as expected, shows on the direction controlled by the cavity, the longitudinal (or X).

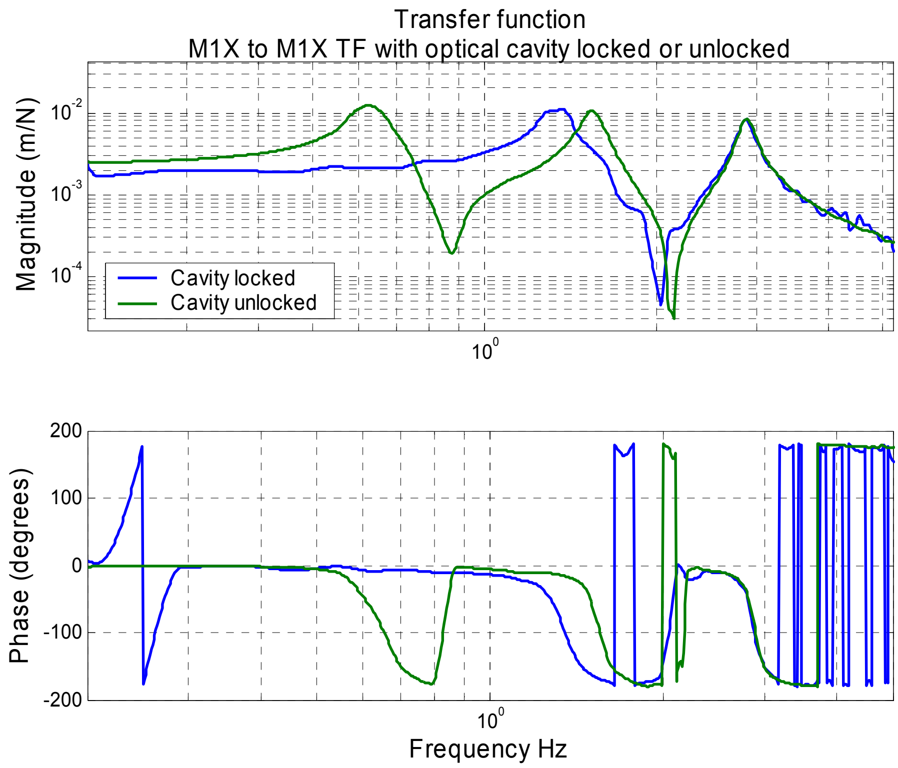

Figure 6.19: Transfer function from M1X to M1X while the cavity is locked and unlocked

As we can see on the plot, the difference is very significant. One of the X mode completely disappear when the cavity is locked. The second mode frequency moves from 1.55Hz unlocked to 1.35Hz locked. The last resonance in X doesn't move at all.

There is a very significant change in the dynamics of the pendulum when we use this pendulum to lock a cavity. If we try to use the modal damping on this pendulum, the damping will go unstable when the cavity gets locked because the model and the real pendulum aren't the same anymore. It is necessary to understand this phenomenon to try to find a solution and adapt the modal damping.

By building a Simulink model of the whole experiment, with the 2 pendulums and the optical cavity loop, we have been able to understand this problem. The model we made and the experiment agree very well, so this problem is something we can predict. An interesting test is to modify the loop gain on the cavity loop, and see how the pendulum behaves by plotting this same transfer function:

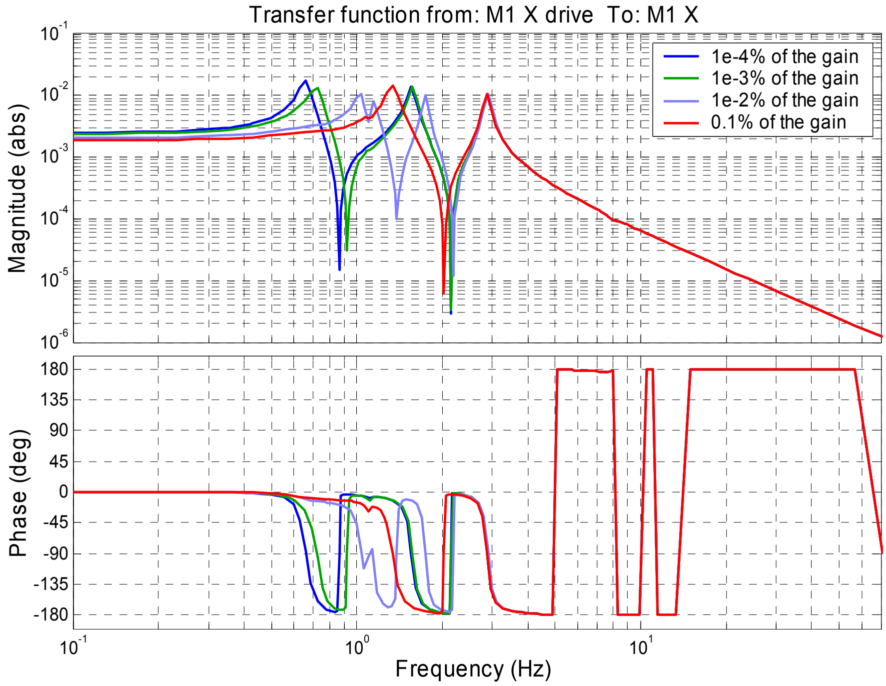

Figure 6.20: change in the pendulum dynamics when the cavity loop gain increases

We see that as the gain increases, the resonance frequency of the first mode moves and the 1st and 2nd mode collapse into 1. We also noticed that the gain doesn't have to be very high to reach the final state where only 2 modes exist, only 0.1% of the loop gain we use is enough to produce this phenomenon.

There is a very simple hypothesis that we can check with our model. The idea is that the loop on the cavity actually clamps the bottom mass in X in inertial space. The loop gain acts like a physical clamp on it, maintaining the mass at a given position. Therefore, our pendulum doesn't behave like 3 suspended masses in the X direction, the pendulum now only has 2 degrees of freedom in X and one mode completely vanishes.

An easy way to check this hypothesis is to build the model of the pendulum considering the bottom mass is now clamped, this is very easy in state space formulation, we simply remove the degree of freedom corresponding to M3 X, since this degree of freedom is now clamped and can't move anymore. Then, we can compare the dynamics of our new model of the pendulum with the experiment we have done above:

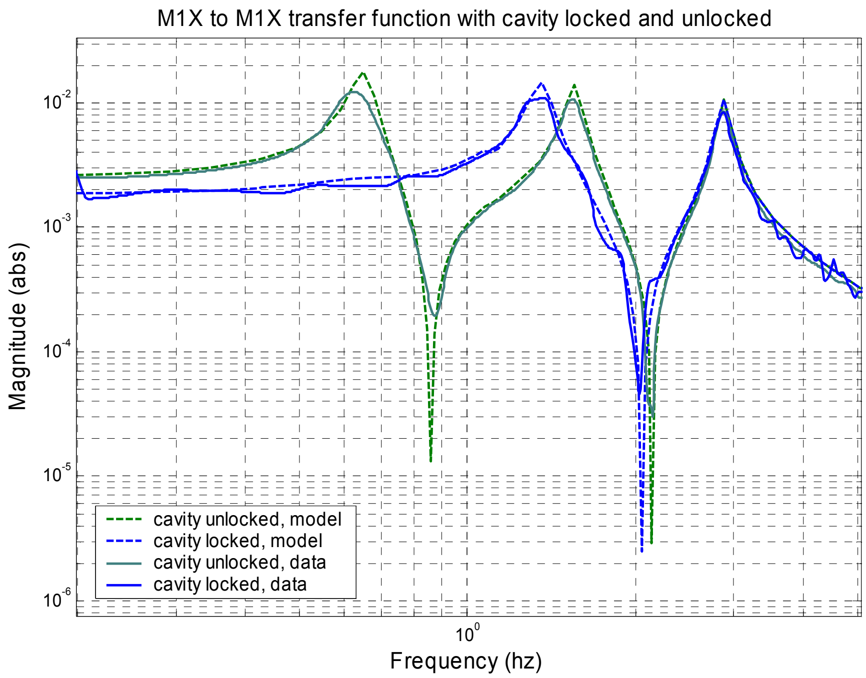

Figure 6.21: Transfer function from M1X to M1X while the cavity is locked and unlocked

We see that the new model with a reduced number of DoF match the experiment perfectly. The pendulum behaves exactly like a 2DoF system in X during the lock. This explains why the damping loop and the cavity locking loop can't run on the same pendulum at the same time. Few solutions to solve this problem are suggested in the following section.

6.7 FUTURE WORK

This cavity experiment is important for advanced LIGO. It first enabled us to validate our noise models for the new damping loop, but it also provided useful information about the behavior of the triple pendulum in a locked cavity. In Advanced LIGO, the triple pendulum and mostly the quadruple pendulums will be used in locked cavities and the change in the dynamics that we have noticed when the cavity locks will be a significant change to take into account. Two solutions have been partially studied and several simulations have been made to check their feasibility and efficiency. More work could be carried out in future studies to optimize these methods and apply them to the working cavity.

The first suggested solution is to use the modified pendulum mode (with the bottom mass locked) in the damping loop. In that case, the model and the lock pendulum will match very well and the damping loop will be able to run in parallel with the locking loop. However, the transition from the unlocked cavity to the locked cavity can still be a significant problem.

The second suggested solution is to get rid of the damping loop in the X direction, and replace it by a hierarchical control for the cavity. In that case, the cavity sense the motion of the bottom mass, and the cavity control loop actuate on the 3 masses to hold them all in place. Although the design of such a control loop is complicated, it is possible and provides very good results on simulations.

7 CONCLUSION

The goal of this thesis was to design, optimize and validate new control schemes to minimize the sensor noise injection induced by an active control loop. The use of modal decomposition and estimation has been studied and optimized to provide acceptable damping performances while minimizing sensor noise transmission in the loop.

The method studied in this thesis has been applied to solve the control challenges related to Advanced LIGO suspensions. The seismic isolation of Advanced LIGO is made of 3 different stages; the last stage is the suspension which can be a triple or a quadruple pendulum. The suspensions provide the high frequencies passive isolation and enable to reduce the thermal noise effect by using high Q materials. The rigid-body resonances of these pendulums need to be damped by using active control. However, the isolation provided by the first 2 stages of seismic isolation is so effective that the sensor noise introduced by the pendulum's sensors is not negligible and needs to be taken into account.

If standard active control techniques were used, this sensor noise would be re-injected into the pendulum and increase the displacement noise. The goal was to design a control loop that would the resonances while minimizing the sensor noise re-injection into the pendulum.

Several methods have been studied in LIGO or VIRGO before this thesis, including improving the sensitivity of the sensors or using a hybrid active/passive damping loop. Unfortunately, these methods have drawbacks and a better alternative remained to be found.

In order to use the control methods used in this thesis, it was first necessary to know the system we want to control very well. In section 2, the characterization of the pendulum has been made and results showed a very good match between the physical system and the numerical models.

For each direction, an independent modal control has been designed. The gain of each controller has been balanced to reduce the sensor noise. The first modes got a large control gain while the highest modes which carry most of the sensor noise got a smaller control gain.

In order to use the modal decomposition and increase the noise filtering, two different kinds of estimators have been studied in section 3. The SIMO disturbance estimator has been used for simple systems while a MIMO modal estimator was developed for more complicated and heavily coupled systems.

In section 4, tools have been designed to optimize the estimator and the modal control loop. The damping performances and the sensor noise filtering have been balanced using these tools. The stability of the loop has also been checked in case the numerical model and the plant don't match perfectly.

The method has then been applied to 2 different systems in section 5. The SIMO estimator has been used for the Yaw direction of the triple pendulum while the MIMO modal estimator has been used for the X/Pitch direction. Excellent results have been obtained in simulation, in both case, the sensor noise transmission has been reduced by a factor of about 100 compared to a classic control approach, while keeping the same damping performances.

The simulation has been validated and confirmed with the experiment in section 6. In order to measure such small displacements, an optical cavity has been formed between 2 identical triple pendulums. This technique enabled us to measure displacements to the order of the nanometer.

After the loop model got validated with the measurement, the experiment led us to another important observation: the dynamics of the pendulum got significantly changed by the locking loop of the cavity. This issue, never observed before, is now understood and several suggestions have been made to solve it.

This control loop method was specifically designed and studied for Advanced LIGO triple pendulum but it also concerns any well modeled system where the sensor noise injection due to the control loop is an issue.

In general, the modal decomposition enables the designer to identify which mode carries the most sensor noise and then reduce the sensor noise transmission by reducing the control gain on this mode. The estimator is also very efficient to reduce the sensor noise transmission, instead of designing fast estimators with high gains; the estimator is purposely made slower to filter the sensor noise, at the cost of the damping performances. With the tools developed in this thesis, it is possible to balance both the damping performances and the sensor noise transmission, and optimize the loop.

Most of the applications for this technique can be found in very sensitive instruments where the performances of the system are so great that the sensor noise needs to be taken into account when control loops are designed. It is especially useful in the field of gravitational waves detection such as LIGO or VIRGO where the mechanical isolation performances of the systems are so high. For example, this control method could be applied to the quadruple pendulums and other suspensions of Advanced LIGO.

Future work

This thesis focused on the sensor noise filtering aspect of the method, how to design and optimize the loop to reduce the sensor noise injection is now well understood and improvements are not really necessary on that way. However, in the future, it will be necessary to study some other aspects such as the robustness or the cross couplings.

The method currently uses independent modal control, but some directions like X/Pitch or Y/roll don't naturally generates decoupled and independent modes. The coupling between modes reduces the stability margin of the loop. Two approaches could be used to improve the situation, it is possible to use global modal control by keeping the coupled modes and design a MIMO (for example optimized with LQ) controller, another approach could be to force the modes to be decoupled.

The method developed in this thesis can also be extended to improve the behavior of the loop when the plant and the model don't match very well. In Advanced LIGO, several dozens of these pendulums will be used, and having to characterize all of them could be time consuming. A possible solution would be to design an adaptive estimator that slightly modifies the parameters of the model to optimize the modal decomposition and the decoupling of the modes.

Last, but not least, we have seen previously that this control scheme can't be used with a locked optical cavity on the pendulum running the locking loop. Thanks to numerical simulations, we now understand the problem and have studied several solutions like hierarchical control or a modified model of the locked pendulum. These solutions work in simulations, but more work need to be done to optimize and validate these on a working pendulum.

Appendix A Matching the model with gradient minimization

A very important thing for the modal control is to have a good model that matches the plant as well as possible (~5%). Differences in the model, especially for the resonance frequencies, can make the system less stable and if those differences are too large, can turn the loop unstable. It is especially true if several resonances are really close to each other (for example the last 2 pitch resonances).

Our experience with the triple pendulum tells us that the models is good and complete enough for our purposes. We are also able to improve the match between the model and the plant by tweaking its parameters by few percents.

The solution we found to make the model more accurate was to use the characterization of the real plant to get the resonances frequencies, and then use a mathematical method to adjust the parameters of the model so that it gives us the same frequencies.

(See chart on next page)

The Matlab function used for the gradient minimization is called fminimax.

We use a gradient minimization to find the best inputs (parameters) that minimize the error. We limit the parameter's change to be +/-5% of the initial parameter.

At the end, we have a slightly different new model; we check the new resonances and the new modal basis (which shouldn't change too much).

This model can be used in the estimator loop to improve performances.

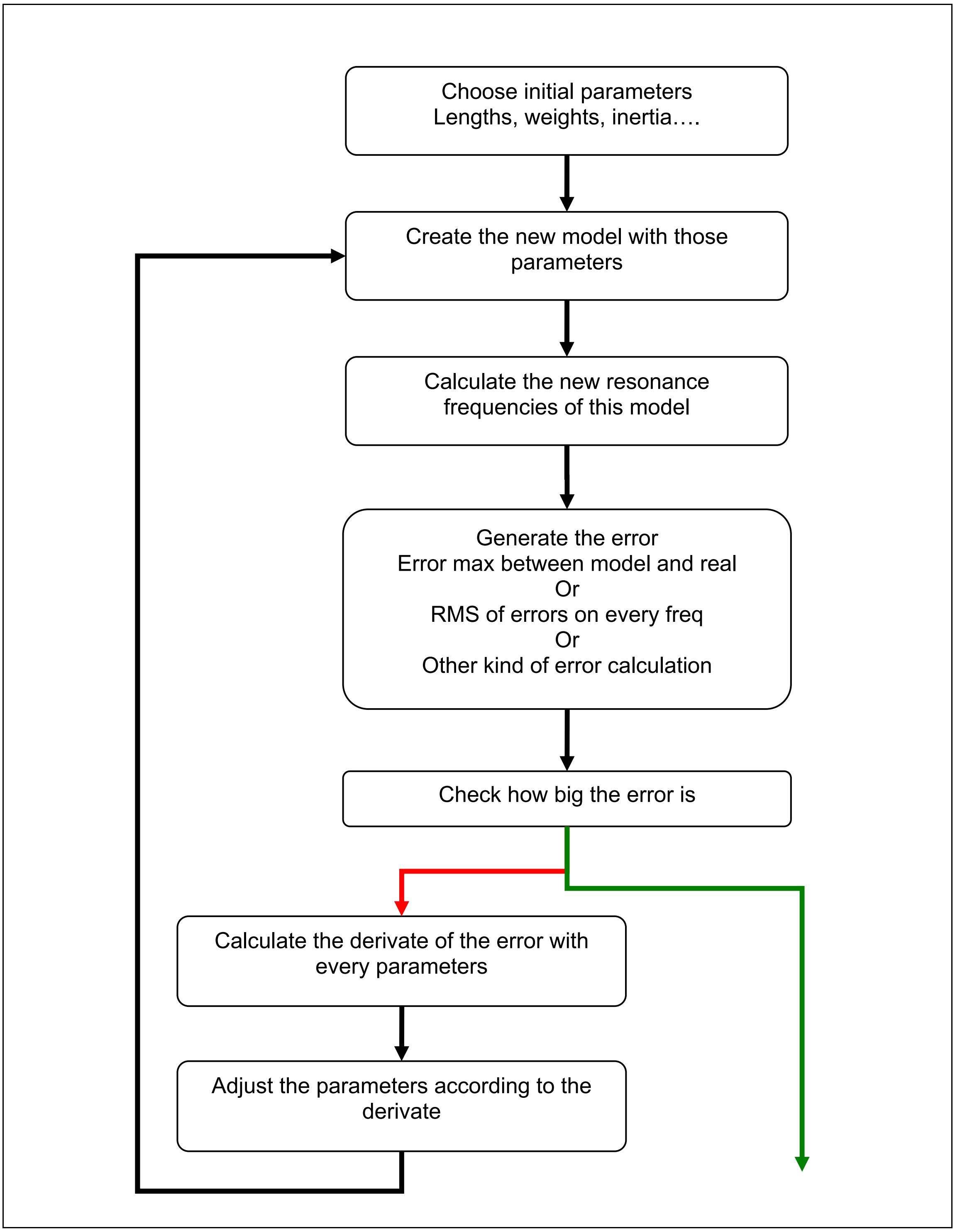
Choose initial parameters
Lengths, weights, inertia….
Create the new model with those parameters
Calculate the new resonance frequencies of this model
Generate the error
Error max between model and real
Or
RMS of errors on every freq
Or
Other kind of error calculation
Check how big the error is
Calculate the derivate of the error with every parameters
Adjust the parameters according to the derivate

Appendix B Noise reduction for white noise drive

Based on paper [47]

The goal of this method is to calculate the transfer function between the drive D and the sensors without being affected by the noise N coming from the ground. In order to do that, we will measure the motion on the floor N during the acquisition. Then we can

- Calculate the transfer function by removing the part of S that is coherent with the noise (N) measurement
- Calculate the "total coherence", a combination of the coherence between D to S and N to S (this is not a simple addition, you can't sum coherence). If the "total coherence" is 1, that means the other sources don't exist and you know everything about your system.

We will only show the main step in this annex.

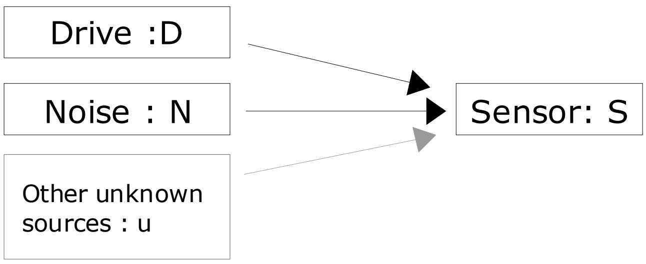

We first introduce a cartesian inner product, it is useful to express the correlation between 2 channels:

$$(X_1, X_2) = \sum_{1<k<k\max} X_1(k).\overline{X_2(k)}$$ (where the bar means complex conjugate)

We start by calculating FFT of the 3 channels and we split these FFT into many parts, gathering points of each parts into vectors (each vector correspond to a frequency range). We will calculate the coherence for each vector.

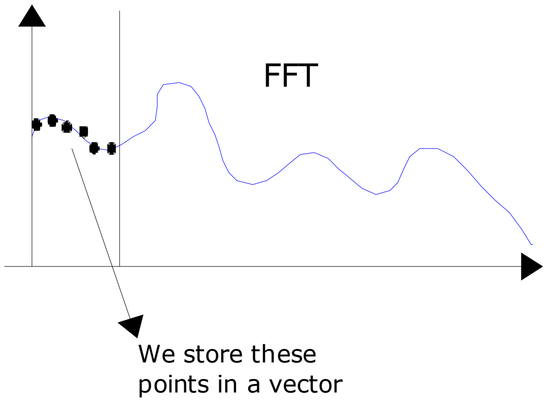

For each vector (each vector correspond to a frequency band), we want to write the vector S as :

$$S = Tf_d.D + Tf_n N + u$$

Where Tf_d and Tf_n are scalar and correspond to the transfer function and where u (a vector) is unknown and is an indication of the coherence (u is 0 if the "total coherence" is 1).

The goal is to find Tf_d and Tf_n so that we minimize u. Which means that we assume the best transfer functions are the one that minimize the norm $N = (u,u)$

This leads to

$$(D,u) = \left(D, S - \overline{Tf_d}D - \overline{T_{fn}}N\right) = 0$$
$$(N,u) = \left(N, S - \overline{Tf_d}D - \overline{T_{fn}}N\right) = 0$$

With the properties of the dot product :

$$(D,S) - \overline{Tf_d}.(D,D) - \overline{Tf_n}.(D,N) = 0$$
$$(N,S) - \overline{Tf_d}.(N,D) - \overline{Tf_n}.(N,N) = 0$$

$$\begin{bmatrix} Tf_d \\ Tf_n \end{bmatrix} = \begin{bmatrix} (D,D) & (D,N) \\ (N,D) & (N,N) \end{bmatrix}^{-1} \begin{bmatrix} (D,S) \\ (N,S) \end{bmatrix}$$

And you can also calculate u with $S = Tf_d.D + Tf_n N + u$ and get the total coherence:

$$\rho = \sqrt{1 - \frac{(u,u)}{(S,S)}}$$

BIBLIOGRAPHY

[1] **EINSTEIN A.,** *The meaning of relativity,* 5th edition, Princeton University Press, (1922), 192p.

[2] **WEBER J.,** *Detection and Generation of Gravitational Waves*, Physical Review, (1960), Vol. 117, Nº 1, pp. 306-313.

[3] **HULSE R. TAYLOR J.,** *Discovery of a pulsar in a binary system*, Astrophysical Journal, (1975), Vol. 195, pp. 51-53.

[4] **THORNE K.S.,** *Gravitational Waves*, **In:** KOLD E.W., PECCEI R. eds, Proceedings of the 1994 Snowmass Summer Study on Particle and Nuclear Astrophysics and Cosmology, World Scientific Singapore, (1995), pp.160-184.

[5] **SCHUTZ B.F.,** *Determining the Hubble constant from gravitational wave observations*, Nature, (1986), Vol. 323, pp. 310-311.

[6] **THORNE K.S.,** *300 years of Gravitation*, chapter 9, Cambridge: Cambridge University press, (1987), pp. 390.

[7] **WEBER J.,** *Detection and generation of gravitational waves*, Physical Review, (1960), Vol. 117, pp. 306-313

[8] **BARISH B. WEISS R**., *LIGO and the Detection of Gravitational Waves*, Physics Today, (1999), Vol. 52, no 10, pp. 44-50.

[9] **WEISS R.,** *Quarterly Progress Report*, MIT Research Lab of Electronics, (1972), Vol. 105, pp.54.

[10] **SMITH J.R. and the GEO600 Collaboration,** *Commissioning, characterization and operation of the dual-recycled GEO 600*, Classical and. Quantum Gravity, (2004), Vol.21, pp. 1737-1745.

[11] **TSUBONO K. and the TAMA collaboration**, *TAMA Project*, **In:** TSUBONO K., FUJIMOTOT M.K. & KURODA K. eds, Proceedings of Conference on Gravitational Wave Detection, Universal Academy Press Inc Tokyo, (1997), pp. 183-191.

[12] **VINET J.Y. and the VIRGO collaboration**, Proceedings of Gravitation and Cosmology, ICGC-95 Conference, Astrophysics and Space Library, Kluwer Academic Publishers (1997), Vol. 211, pp. 89-93.

[13] **MACDONALD D.K.C.,** *Noise and fluctuations: An introduction*, New York: Wiley, (1962)

[14] **EINSTEIN A.,** *Investigations on the theory of the Brownian Movement*, New York: Dover, (1956)

[15] **CALLEN H.B., WELTON T.A,** *Fluctuation-Dissipation Theorem*, Physical Review, (1951), Vol. 83, pp. 34.

[16] **FRITSCHEL P., COYNE D., GIAIME J., LANTZ B., SHOEMAKER D.,** *Seismic Isolation Subsystem Design Requirements Document*, **[en ligne]**, (2001), disponible sur http://www.ligo.caltech.edu/docs/E/E990303-03.pdf, (consulté le 01/06/2006)

[17] **FRITSCHEL P.,** *Second generation instruments for the Laser Interferometer Gravitational Wave Observatory (LIGO)*, **In:** CRUISE M., SAULSON P. eds, Proceedings of SPIE Gravitational Wave Detection, Bellingham, WA, 2003, Vol. 4856, (2003), pp. 282-291.

[18] **GUSTAFSON E., SHOEMAKER D., STRAIN K., WEISS R.,** *LSC White Paper on Detector Research and Development*, **[en ligne]**, (1999), disponible sur http://www.ligo.caltech.edu/docs/T/T990080-00.pdf, (consulté le 01/06/2006)

[19] **ROBERTSON N.A. and LIGO collaboration**, *Seismic isolation and suspension systems for Advanced, Gravitational Wave and Particle Astrophysics Detectors*, **In:** HOUGH J., SANDERS G. EDS, proceedings of SPIE, (2004) vol. 5500, pp. 81-91.

[20] **HARDHAM C. and LIGO seismic group**, *Multi-DOF Isolation and Alignment with Quiet Hydraulic Actuators*, Proceedings of ASPE Spring Topical Meeting on Control of Precision Systems, (2004), pp. 127-132.

[21] **HARDHAM C.,** *Quiet Hydraulic actuators for LIGO*, PhD Thesis, (2005), Stanford University.

[22] **HUA W., DEBRA D., HARDHAM C., LANTZ B., GIAIME J.,** *Polyphase FIR Complementary Filters for Control Systems,* Proceedings of ASPE Spring Topical Meeting on Control of Precision Systems, (2004), pp. 109-114.

[23] **GIAIME J. and the LIGO seismic group**, *Seismic isolation for Advanced LIGO*, Classical and. Quantum Gravity, (2002), Vol. 19, pp. 1591-1597.

[24] **ROBERTSON N. and the LIGO collaboration**, *Seismic isolation enhancements for initial and advanced LIGO*, Classical and Quantum Gravity (2004), Vol. 21, pp. 915-921.

[25] **HUA W. and the LIGO collaboration**, *Low frequency isolation for Advanced LIGO*, Gravitational Wave and Particle Astrophysics Detectors, **In:** ATAD-ETTEDGUI E., DIERICKX P. eds, Proceedings of SPIE, (2004), vol. 5500, pp. 194-205.

[26] **ROBERTSON N. and the LIGO collaboration**, *Advanced LIGO suspension system conceptual design*, **[en ligne]**, (2001), disponible sur http://www.ligo.caltech.edu/docs/T/T010103-04.pdf, (consulté le 01/07/2006)

[27] **QIPIANI K. and the Virgo Collaboration,** *The Inertial Damping of the VIRGO suparattenuator and the residual motion of the mirror*, Classical and Quantum Gravity, (2002), Vol. 19, pp.1631-1637.

[28] **PLISSI M.V., TORRIE C.I., HUSMAN M.E., ROBERTSON N.A., STRAIN K.A., WARD H., LUCK H., HOUGH J.,** *GEO 600 triple pendulum suspension system : Seismic isolation and control*, Review of scientific instruments, (2000), Vol. 71, Nº 6, pp. 2539-2545.

[29] **ASTON S., SPEAKE C.,** *Geometric OSEM Sensor development*, **[en ligne]**, (2004), disponible sur http://www.ligo.caltech.edu/docs/T/T040043-01-K.pdf, (consulté le 01/03/2005)

[30] **STRAIN K.A.,** *Input to the OSEM selection review decision*, **[en ligne]**, (2004), disponible sur http://www.ligo.caltech.edu/docs/T/T040110-01-K.pdf, (consulté le 01/03/2005)

[31] **ASTON S., SPEAKE C.,** *Interferometric OSEM Sensor development*, **[en ligne]**, (2004), disponible sur http://www.ligo.caltech.edu/docs/T/T040044-01-K.pdf, (consulté le 01/03/2005)

[32] **PLISSI M.V., TORRIE C.I., BARTON M., ROBERTSON N.A., GRANT A., CANTLEY C.A., STRAIN K. A., WILLEMS P.A.., ROMIE J.H., SKELDON K.D., PERREUR-LLOYD M.M., JONES R.A., HOUGH J.,** *An investigation of eddy-current damping of multi-stage pendulum suspensions for use in interferometric gravitational wave detectors*, Review of scientific instruments, (2004), Vol. 75, no 11, pp. 4516-4522.

[33] **STRAIN K.A,** *Discussion document for Advanced LIGO suspension ECD requirements*, **[en ligne]**, (2005), disponible sur http://www.ligo.caltech.edu/docs/T/T050093-00-K.pdf, (consulté le 01/10/2005)

[34] **LOSURDO G., PASSUELLO D.**, *Noisy sensors in control loops: an idea to reduce re-injected noise (Part I)*, **[en ligne]**, (2003), VIRGO document VIR-NOT-FIR-1390-256, disponible sur http://wwwcascina.virgo.infn.it/suspcon/MSCdocs/notes/doppioloop.pdf (consulté le 01/05/2005)

[35] **MEIROVITCH L.,** *Dynamics and control of structures*, New York: Wiley, (1992), 448p.

[36] **MEIROVITCH L., BARUH H., OZ H.,** *A comparison of control techniques for large flexible systems*, Journal of guidance and control, (1987), Vol. 4, Nº 2, pp. 157-163

[37] **GAWRONSKI W.K.,** *Dynamics and control of structures: A modal approach*, New York: Springer, (1998), 231p.

[38] **BAZ A., POH S., FEDOR J.,** *Independent modal space control with positive position feedback*, ASME journal, (1992), Vol. 14, pp. 96-103.

[39] **LUENBERGER D.G.,** *Observing the state of a linear system*, IEEE Transactions on Military Electronics (1964), Vol. 8, Nº 2, pp. 74-80.

[40] **LUENBERGER D.G.,** *Observers for Multivariable Systems*, IEEE Transactions on Automatic Control, (1966), Vol.11, Nº 2, pp. 190-197.

[41] **FRANKLIN G.F., POWELL J.D., WORKMAN M.,** *Digital control of dynamic systems*, 3rd edition, Prentice Hall, (1997), 850p.

[42] **MEIROVITCH L., BARUH H.,** *The implementation of modal filters for control of structures, Journal of guidance and control*, (1985), Vol. 8, No 6.

[43] **KALMAN R.E.,** *A new approach to linear filtering and prediction problems*, ASME, journal of Basic Engineering, (1960), Vol. 82 , pp. 35-45

[44] **TORRIE C.I.,** *Development of the suspensions for the GEO 600 gravitational wave detector*, PhD thesis, (2000), University of Glasgow.

[45] **SIMON D.,** *Optimal State Estimation: Kalman, H Infinity, and Nonlinear Approaches*, New York: Wiley, (2006), 552 p.

[46] **DREVER R.W.P., HALL J.L., KOWALSKI F.V., HOUGH JFORD., G.M., J.MUNLEY A., WARD H.,** *Laser Phase and Frequency Stabilization Using an Optical Resonator,* Applied Physics, (1983), Vol. 31 B, pp. 97-105

[47] **ALLEN B., HUA W., OTTEWILL A.C.**, *Automatic cross-talk removal from multi-channel data*, **[en ligne]**, (1999), disponible sur http://www.ligo.caltech.edu/docs/P/P990002-00.pdf (consulté le 01/05/2004)

FOLIO ADMINISTRATIF

THESE SOUTENUE DEVANT L'INSTITUT NATIONAL DES SCIENCES APPLIQUEES DE LYON

NOM : RUET DATE de SOUTENANCE : 11 Janvier 2007

Prénoms : Laurent

TITRE :

Active control and sensor noise filtering duality

Application to Advanced LIGO suspensions

NATURE : Doctorat Numéro d'ordre :

Ecole doctorale : MEGA

Spécialité : Génie Mécanique

RESUME :

L'étude présentée porte sur le contrôle actif des suspensions pour Advanced LIGO. LIGO est un projet américain ayant pour but la détection d'ondes gravitationnelles, prédites par Einstein. Afin de mesurer ces ondes, le bruit sismique doit être atténué par un facteur de plusieurs milliards. Le dernier étage du système d'isolation sismique est un pendule filtrant le bruit sismique à hautes fréquences. Ce pendule presente d'importantes résonances à basses fréquences qui sont amorties par contrôle actif. Toutefois, ce controle re-injecte le bruit de mesure et deteriore les performances d'isolation du pendule. La problématique est donc de concevoir une boucle de contrôle qui amortie les résonances tout en minimisant la réinjection du bruit de mesure à hautes fréquences. L'association d'un contrôle modal et d'un estimateur d'état est étudiée dans ce but. Les simulations sont vérifies expérimentalement en utilisant une méthode permettant de mesurer des vibrations de l'ordre de 10^{-9}m.

MOTS-CLES : Contrôle actif, bruit de mesure, LIGO, suspension

Laboratoire (s) de recherche : INSA LAMCOS, MIT LIGO

Directeur de thèse: Docteur HDR Johan DER HAGOPIAN, Professeur Luc GAUDILLER

Professeur Willy CHARON	Rapporteur	L3M, UTBM, Belfort
Docteur HDR Johan DER HAGOPIAN	Co-Directeur de thèse	LAMCOS-DCS, INSA de Lyon
Professeur Régis DUFOUR	Examinateur	LAMCOS-DCS, INSA de Lyon
Professeur Luc GAUDILLER	Co-Directeur de thèse	LAMCOS-DCS, INSA de Lyon
Professeur Jean-Claude GOLINVAL	Rapporteur	LTAS-VIS, Université Liège, Belgique
Docteur HDR Jean-Marie MACKOWSKI	Examinateur	LMA, Université Lyon I
Docteur Richard MITTLEMAN	Examinateur	MIT Cambridge USA, LIGO